UNICA

UNIVERSITÀ
DEGLI STUDI
DI CAGLIARI

Ph.D. DEGREE IN

Earth and Environmental Sciences and Technologies

Cycle XXXVI

EXPLORING INNOVATIVE TECHNOLOGIES FOR NUTRIENT REMOVAL AND RECOVERY FROM AGRO-INDUSTRIAL WASTEWATER: ANAMMOX AND ELECTROCHEMICAL PROCESSES

Scientific Disciplinary Sector(s)

ICAR/03

Ph.D. Student:	Emma Dessì
Supervisor:	Alessandra Carucci
Co-Supervisor:	Stefano Milia

Final exam. Academic Year 2022/2023
Thesis defence: February 2024 Session

Table of contents

Summary

The present thesis is framed within the wastewater treatment field, and specifically in the topic of nutrient removal and recovery from nutrient-rich wastewater generated from the management of agro-industrial residues (i.e., anaerobic digestion supernatant and swine manure denitrified effluent).

Agro-industrial residues production is increasing due to the growing global population and the rise of industrialization. Due to the high eutrophic and polluting potential, these wastes require proper treatment (i.e., chemical, physical, or biological) to avoid environmental pollution. Besides, the high levels of nitrogen, phosphorus and potassium pose the opportunity of applying nutrient recovery techniques to integrate their management with waste valorisation. Since actual chemical fertilisers derive from finite natural resources (e.g., phosphate rock, potash deposits) and through energy-intensive processes (e.g., Haber Bosh), the recovery of bio-fertilisers (e.g., struvite, calcium phosphate) from agro-industrial residues is gaining increasing attention as a sustainable and cost-efficient alternative. Moreover, this approach would allow to close the nutrient loop in agriculture and to limit pollution through slow-release fertiliser application on fields.

The single-step Partial Nitritation/Anammox (PN/A) process allows for achieving fully autotrophic nitrogen removal in a single reactor: ammonium can be partially oxidised to nitrite by aerobic oxidising bacteria and the remaining ammonium is oxidised by anammox metabolism using nitrite as final electron acceptor. This process increases the sustainability of biological nitrogen removal in wastewater treatment as the need for carbon addition (and concomitant increased sludge production) is avoided and oxygen consumption is reduced, as well as the emission of nitrous oxide, which has become a significant factor in the greenhouse gas footprint of the total water chain. Anammox-based treatments were applied to different influent streams, usually characterised by high ammonium content and low biodegradable organic matter concentration such as supernatant from anaerobic digestion of waste sludge.

Recently, the combination of nitrogen removal with phosphorus recovery has received increased attention due to the promotion of a circular strategy in wastewater management. With this aim, upstream and downstream chemical precipitation of phosphorus has been tested in combination with biological nitrogen removal, but few cases of application with PN/A were studied. Downstream precipitation is typically reported as more advantageous since the biological pretreatment decreases the buffer capacity of the wastewater through ammonium nitrogen and concomitant bicarbonates removal. Thus, lower volumes of alkali are needed to increase the pH up to the targeted value for minerals precipitation. In alternative to downstream precipitation, concomitant P removal has been recently proven feasible in PN/A process. Calcium phosphate precipitates, and particularly hydroxyapatite, can be subjected to biomineralisation in supersaturated conditions generating

a granule with a mineral core which can be extracted.

Electrochemical systems are emerging as sustainable alternatives to conventional methods in wastewater treatment. In electrochemical mediated precipitation, water electrolysis is achieved through current application promoting hydroxyls production. The controlled increase in pH allows mineral precipitation and thus nutrient recovery from wastewater with limited or zero-chemicals addition. Different minerals, such as struvite, can be obtained depending on the wastewater composition.

Firstly, the feasibility and performances of single-stage PN/A process combined with downstream chemical precipitation were evaluated for calcium phosphate recovery from agro-industrial anaerobic digestion supernatant. Increasing nitrogen loading rate strategy promoted biomass growth and activity (from 0.21 ± 0.04 up to 0.40 ± 0.07 gN_2 $(gVSS \cdot d)^{-1}$) which was not affected by the treated wastewaters. PN/A efficiently removed ammonium nitrogen and alkalinity (removal efficiency ≥ 80%) achieving effluent concentrations of 13 ± 2 and 15 ± 3 $mgNH_4^+$-N L^{-1}, and 125 ± 11 and 120 ± 7 $mgCaCO_3$ L^{-1}, in phase I and phase II, respectively. Titration test results suggested that downstream P chemical precipitation is more cost-effective than upstream treatment (ca. 90% reduction of NaOH (5M) dosing costs). Calcium phosphate precipitation (mixture of amorphous calcium phosphate and hydroxyapatite) was achieved through batch precipitation experiment reaching higher removal efficiency for pH≥10 at 2.00 calcium/phosphate ratio and 25ºC. The results of this research are described and discussed in Chapter 2.

Then, concomitant phosphorus removal was explored in PN/A process treating agro-industrial anaerobic digestion supernatant (Chapter 3). Moreover, a non-damaging separation method to recover the mineral from the sludge was tested on biomass granules. Process start-up was obtained within about seven months of operation in a 3L-SBR and stable simultaneous nitrogen and phosphorus removal (ammonium conversion rate up to 0.28 $kgNH_4^+$-N $(m^3 \cdot d)^{-1}$ and phosphorus removal efficiency of ca. 34%) were reached from agro-industrial wastewater in phase IV, without external calcium addition. Ultrasonic treatment was identified as a promising method for mineral-from-biomass separation limiting the loss of anammox activity (activity reduction limited to 15% when exposition time was 15 min) while disassembling the multi-layered biomass granule structure. To the best of the author knowledge, no previous study was performed concerning the application of a separation method for calcium phosphate recovery from PN/A granular sludge. Thus, this work findings can pave the way for the development of a separation protocol which would be critical for the future scale-up of the system.

A double-compartment electrochemical system was operated to explore reagent-free phosphorus

precipitation from swine manure denitrified effluent through the application of low current density (≤1.2 A m^{-2}). The electrochemical system was shown as a promising alternative to NaOH dosage for pH adjustment when targeting P recovery allowing for economical savings (cost for raising the pH at 11.5 was estimated as 0.57 € m^{-3} or 14.77 € kg^{-1} P when dosing NaOH vs. 0.31 € m^{-3} or 13.81 € kg^{-1} P in the electrochemical treatment). Moreover, the feasibility of catholyte neutralisation (final pH of 6.43 ± 0.05) through anode compartment was proven with an associated economic benefit (0.26 € m^{-3} when dosing H_2SO_4 for catholyte neutralization). Efficient phosphorus removal (72 ± 2% for 1x and 4x diluted effluent, respectively) was achieved when applying 1.2 A m^{-2} to reach pH 11.5 with a specific energy consumption which behaved inversely to the effluent strength, accounting for 69.07 ± 1.84 (1x) and 118.71 ± 8.22 kWh kg^{-1} P (4x). Precipitates (magnesium phosphate) mostly remained suspended in the bulk liquid and limited deposition of solids was detected into the electrochemical system also by electrochemical spectroscopy tests (0.79 Ω m^2 increase of the ohmic resistance in the two-electrode configuration test). The results of this research are described and discussed in Chapter 4.

Finally, chemical-free K-struvite recovery (richness on dry weight was above 10% for phosphorus, potassium, and magnesium) from a swine denitrified effluent at pH 11.5 was successfully achieved using a crystalliser combined with a two-chambered electrochemical system (Chapter 5). Three different cell configurations were tested in batch and Cell 3 was selected as the optimal configuration as the corresponding specific energy consumption and ohmic resistance increases (134 ± 22 kWh kg^{-1} P and 28 ± 1 Ω m^2, respectively) were the lowest. The combined system was then operated in continuous-flow mode using the selected electrochemical cell achieving high ion removal efficiencies (85 ± 3% for PO_4^{3-}-P, 81± 8% for Mg^{2+} and 16 ± 2% for K^+) and through the power supply on/off control, the targeted pH (11.5) was successfully maintained in the crystalliser. Catholyte neutralization in the anodic compartment was proven feasible, leading to a decline in the pH-value down to 6.05 ± 0.71 when current was applied. Promising levels of chlorine (44 mgCl_2 L^{-1}) were measured in the outlet, which opens the door to combining MPP recovery with production of value-added chemicals such as free chlorine.

The results presented in this PhD thesis support the application of partial nitritation/anammox and electrochemical mediated precipitation as promising and cost-effective alternative technologies for the treatment of nutrient-rich wastewater.

CHAPTER 1: General introduction

1.1 Agro-industrial wastes: production and management

Food waste is a major issue in the European Union (EU), with over 58 million tons being produced annually corresponding to ca. 131 kg per inhabitant (1). Particularly, the primary production sector generates 34% of food waste, accounting for 11 kg per inhabitant. However, when taking into account agro-industrial waste, these numbers increase significantly. According to Bedoić et al. (2), agricultural waste production (including co-products and by-products) in the EU reached 2.6 billion tons per year based on data available from 2010 and 2016. Such amounts of residual organic matter represent both massive resource opportunities and potential risks for the environment and human health if not managed properly. Due to the high eutrophic and polluting potential, agro-industrial wastes require proper treatment (i.e., chemical, physical, or biological) to minimize the environmental hazard and for simultaneous nutrient removal or recovery. Among the different techniques, biological treatment typically presents lower cost, fewer risks of secondary pollution and simple operation (3). Processes such as composting and anaerobic digestion (AD) are commonly adopted for biowaste stabilisation and to recover by-products, namely compost, digestate and biogas. Compost is obtained by the organic matter aerobic bioconversion into a stable form of organic carbon (i.e., humus). This bio-product is typically used as a soil conditioner or fertiliser in gardening and agriculture to enhance soil structure, moisture retention, and nutrient content. Digestate is the organic by-product of AD process which enables the organic matter bioconversion into biogas for electricity or biomethane production. The residual complex organic compounds and the inorganic elements, involving nitrogen (N), phosphorus (P) and potassium (K) are retained in the digestate. It was estimated that ca. 80–90% of the AD feedstock introduced is converted into digestate (4). In the digestion process, a significant fraction of the organic N and P are released in the corresponding soluble form (i.e., ammonium (NH_4) and phosphate (PO_4)), while the residual part enriches the particulate fraction. This same process applies also to K. However, most of released PO_4 tends to directly precipitate reacting with soluble cations, such as calcium (Ca^{2+}) and magnesium (Mg^{2+}). Due to its high-nutrient content, digestate has been mainly applied directly on soil as the most economical practice to implement (5). Nevertheless, direct field inappropriate application can lead to pollution, as nutrient excess on soil can be transferred to water resources and cause soil deterioration. It was assessed that 30–50% of fertiliser nutrients are lost due to leaching into groundwater or volatilisation into air (6). Moreover, water contamination due to excessive fertilisation of the crops is generating high costs related to the need for remediation. For instance, Sutton et al. (7) estimated that nitrogen pollution costs amounted to 70-100 billion euros

per year for the EU. To prevent water contamination and protect water quality, the Nitrates Directive (Council Directive 91/676/EEC) fixed the amount of N from manure and organic residues that can be applied to the land (i.e., 170 kgN per hectare per year), further limiting the direct application of digestate and manure. When contemplating both basic agronomic principles and legal limitations, the prevailing criterion in the strategic application of agro-industrial residues (e.g., manure) to soil is typically N content (8). Biological N removal (BNR) based on aeration (e.g., through nitrification-denitrification, NDN) is commonly applied for the effective onsite liquid fraction treatment of manure produced by farms or digestate generated from AD (3). NDN process is the most widespread method to remove N as a robust and cost-effective technique. Nitrification consists in the conversion of ammonium to nitrate through a two-step oxidation, while denitrification allows a stepwise nitrate to dinitrogen gas (N_2) anoxic reduction. When the wastewater is supposed to be applied to the soil, BNR can be useful for lowering N levels below the legislation limits. Beyond N, agro-industrial residues are typically rich in P and K being essential macro-nutrients for crops. As the need for food production is raising, a growing interest is directed to the implementation and promotion of efficient and economic strategies to recover and re-use nutrients from raw or digested wastes reducing the need for fossil-fuel based fertilisers and thus limiting EU's dependency on nutrients from third countries (9). With this aim, EC (European Commission) recently facilitated the use of recovered materials, listing animal by-products, compost, digestates, struvite, biochar and sewage sludge among the allowed materials for being used as fertiliser or for fertilising products (10). When their compliance with requirements outlined in the Fertilising Products Regulation (Regulation (EU) 2019/1009) is provided, these materials are no longer considered waste, and they acquire the product status. Particularly, circular economy strategy promotes using by-products as secondary raw materials in a different process. However, this is limited by stricter regulations applied in some of the Member States and by high costs related to recovery techniques (11). Recovered products present still lower economic competitiveness compared to primary resources raising a critical issue to be addressed (10). Thus, lowering operative costs and improving product quality while preserving high recovery efficiency, are key drivers for introducing the recovery materials in the market. Nevertheless, a fairer economical balance should also consider environmental costs related to nutrients disposal impact by recognising recycling materials as value added products (5). Moreover, fertilisers derived from recovered by-products showed interesting characteristics. Minerals derived from residues, such struvite or calcium phosphate, are slow-release fertilisers which are preferable to their highly soluble mined counterparts as they allow limiting groundwater pollution due to leaching (12). Fertilisers produced from residues typically showed also advantages in terms of potentially harmful or polluting composition. Particularly, these advantages would be boosted by the introduction of legislation limits

on such compounds. As higher levels of heavy metals are typically associated to the virgin mined mineral, recycled materials might be favoured over their counterpart due to more stringent requirements for heavy metals content on fertilisers (i.e., for cadmium (Cd) ≤ 60 mg Cd per kg P_2O_5) (13). Besides, since the use of chemical fertiliser is banned in organic farming, the interest on bio-based fertiliser production is recently increasing (10). Nevertheless, important limitations are still related to the reputation of product derived from residues recycling activities among the users. To date farmers have been hesitant to adopt them due to a lack of confidence on recovered materials (10). For this reason, educational activities aiming to raise customers awareness play an important role in by-products management.

Operational challenges, regulatory limitations, and the volatility of market prices related to fertiliser production, encompassing considerations of both quality and quantity, pose obstacles to formulating a comprehensive global strategy for valorisation of residues into bio-fertiliser. Thus, the primary objective would be to identify suitable technologies or a combination thereof to enhance the treatment of agro-industrial waste, creating recycled, value-added materials within a genuine circular economy framework (9). Finally, an interplay between legislation, stakeholders and recovery technologies is needed to promote an effective and sustainable management of by-product with the outlook of circular economy strategy implementation (10).

1.1.1 Current fertiliser trends

The global population has doubled to 8.1 billion in the last 40 years following a continuous upward trajectory which is challenging for granting food-security (9). According to a medium-variant forecast, it is expected to surpass 10 billion people by 2050, exceeding the capacity of the planet to feed all the human-beings (6). Consequently, the demand for increased food production becomes critical and as agriculture represents the primary source of food, boosting crop yields is a paramount challenge. In the last decades, agricultural productivity has primarily advanced through the application of fossil-fuel based fertilisers. Chemical fertiliser uses in the EU was 186.6 and 194.4 Mt in 2016 and 2018 respectively (9) and forecasts indicate that global demand for main nutrient such as N, P, and K for fertiliser production would rise by 10% at least (14). Although, numerous issues are connected to actual industrial production of fertilisers being highly energy demanding and mainly based on fossil fuels (N-fertilisers on Haber–Bosch process) or natural reserves such as phosphate rock and potash rock (6,8). P and K are non-renewable resources typically extracted from phosphate and potash rocks, respectively, mainly for the fertiliser production. Thus, these mineral deposits are essential in supporting food production and are becoming increasingly scarce due to intense mining

activity. Economically mined phosphate rock reserves have been estimated at 7 billion tons (Figure 1.1), and annual consumption is expected to grow to 49 million tons in 2024 according to the United States Geological Survey report (15). Recent studies reported that the K requirement is steadily raising at a rate of 9–10% over the years, reaching a potash production of 42 million tons in 2018 (16,17). Consequently, it is predicted that P consumption peak would occur in the next 10 to 30 years (15,18), while the peak potash is expected to be achieved in 2057 (17) (Figure 1.1). Due to the uneven distribution of mineral deposits around the Earth, many countries are depending on import which, combined with high economic volatility, can lead to political tensions in the future (10). Large sedimentary deposits of phosphate rock are found in Africa (Jordan, Morocco, and Western Sahara), China, the Middle East and USA (18), while leading potash producers are Canada, Russia, Belarus, Germany, Israel, and Jordan (16). These resources are only finitely available or inaccessible to many countries due to the non-availability of profitable commercial deposits. For these reasons, EU has included phosphate rock and P in the critical raw material list (10).

Due to fast depleting reserves, the future stability of nutrient dependent sectors, such as agriculture, is uncertain. Moreover, evidences from many studies clearly indicates that the intense application of chemical fertilisers on fields causes serious environmental problems such as groundwater pollution and soil quality deterioration. In such framework, the implementation a virtuous cycle of nutrients to reduce the use of natural resources while also avoiding pollution needs is a key challenge. Thus, nutrient recovery from residues might become soon an essential practice with raising attention in closing nutrient loops. In this, agro-industry residues are receiving growing attentions as they are rich in nutrients. According to Kok et al. (19), if all the P was recovered from urban wastewaters in 2015, 20% (3.7 Mt P year^{-1}) of the agricultural demand (19.1 Mt year^{-1}) could have been satisfied, while when considering livestock manure alone this value increases up to 90% (17.39 Mt P year^{-1}). In average the total P content in livestock manure ranges from 9.3 to 39 gP kg^{-1} depending on the specific animals, with highest levels contained in swine manure (18).

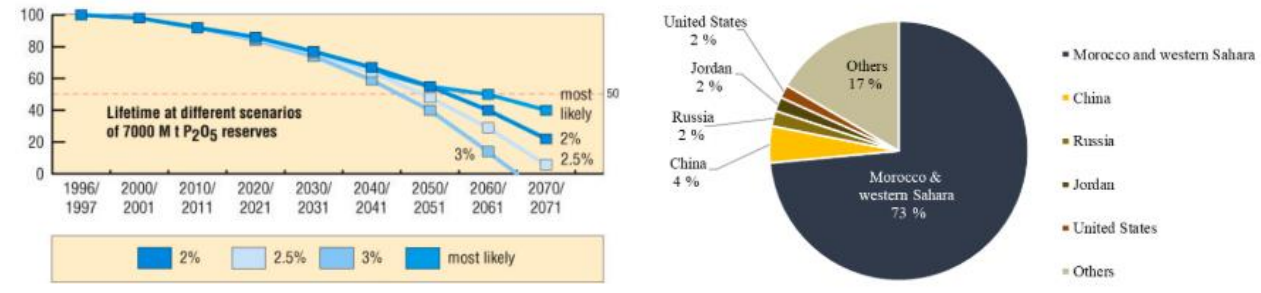

(a) (b)

Figure 1.1 – (a) Prediction of global phosphorus lifetime reserves (P_2O_5) under different consumption growth scenarios (15); Estimated global phosphate rock deposits distribution (19).

1.1.2 Nutrients recovery from agro-industrial wastes

Growing population worldwide and increasing industrialisation leads to intensive agriculture and animal production, generating large quantities of residues such as livestock manure which pose a serious global environmental issue; animal manure management presents an estimated pollution cost over 12300 million euros per year in Europe (9). Therefore, suitable treatment and disposal of livestock manure is required for minimizing the environmental hazard (i.e., leaching to groundwater, eutrophication, greenhouse gases and odours emission) and simultaneous nutrient recovery (3). The high moisture content (around 95–98%) of this residue negatively affects direct application in the surrounding areas and hinders transportation due to large volumes. Thus, solid-liquid separation is typically applied as up-front in a treatment train to broaden the opportunities of organic compounds and nutrient recovery, which can be used for producing compost materials and other value-added products or energy through AD application. As resulting liquid stream is rich in soluble nutrients (i.e., NH_4, PO_4), biological process such as BNR and a variety of physical or chemical precipitation techniques can be effectively applied to remove and/or recover them achieving environmental standards including application to field and water reuse (20) (Figure 1.2).

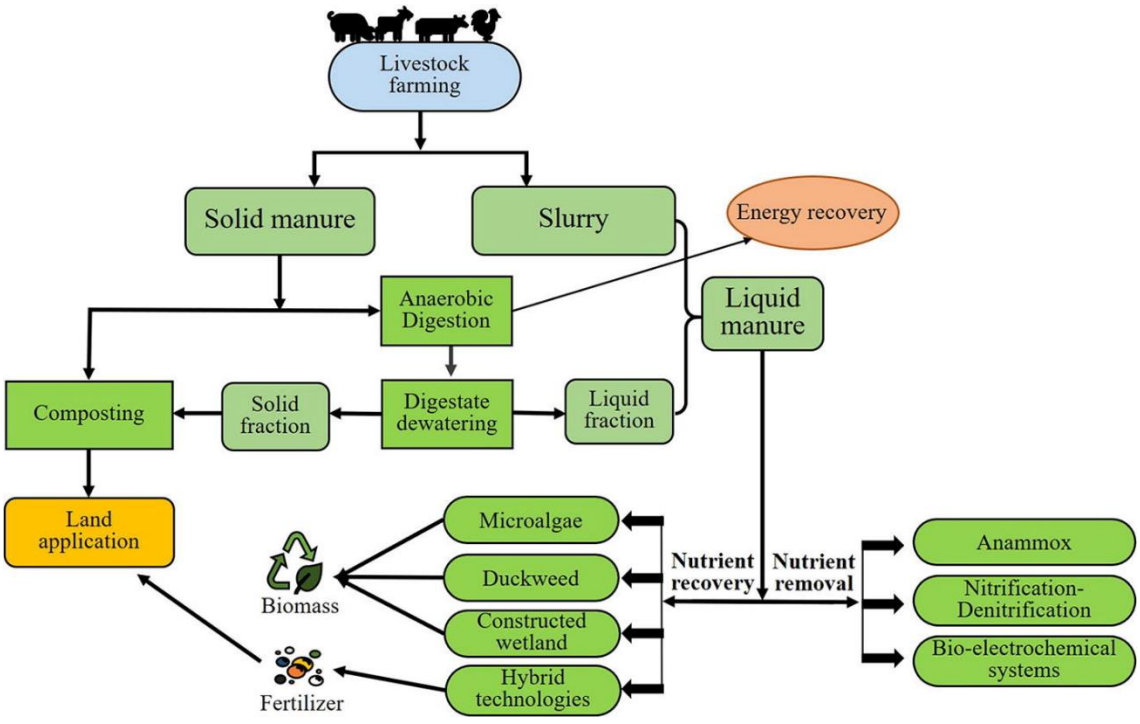

Figure 1.2 - Management options for livestock manure valorisation (3).

As an alternative, manure and other kinds of agro-industrial residues (e.g., crop residues), due to high organic content, can be effectively used for biogas production through AD generating a nutrient-rich by-product, namely digestate. In the last decades, AD technology widespread due to the benefit associated with the process. Currently, there are more than 14000 plants running across Europe, with 80% of them being operated in the agricultural sector and farm based (21). As European production of digestate accounts for 56 million tons per year (3), researchers are exploring different alternatives to direct soil application, identifying the most promising pathways to valorise this nutrient-rich by-product. Particularly, digestate has gained particular interest in fertiliser production due to its high nutrient content. In the new sustainable development model, digestate can be considered as a new mine for fertilisers recovery (21). Digestate valorisation for fertiliser production is a revenue opportunity as it is particularly rich in essential nutrients for agriculture such as N, P, and K (22). Hence, decentralized AD of agricultural residues and digestate in-direct application in the agricultural sector can help closing the nutrient loop (23). This would prevent mined fertiliser nutrients from being dissipated in the environment and becoming pollutants (24). In fact, the most of recovery products obtained from digestate are slow-release fertilisers such as struvite-type minerals, ensuring a proper uptake for the soil. The possible recovered product depends mainly on the digestate composition. Physicochemical characteristics of this residue is highly variable, and it is regulated by AD feedstock and operative conditions, determining its agronomic value and the nutrient recovery potential. When agricultural feedstock is used, digestate typically presents high dry matter content (6.41–24%) due to limited digestibility of lignin (4). As initial stage of digestate valorisation scheme, liquid-solid separation is commonly applied to reduce management costs (4,5). Presenting a reduced volume, the solid fraction can be more easily transported for long distance to produce compost or to be converted into concentrated fertiliser. While the solid fraction typically contains 40–80% dry matter, 40–90% of P, the liquid fraction is richer in NH_4-N and K (4). Digestate liquid fraction usually presents lower nutrient content but with levels precluding the direct discharge, thus, proper treatment is required. Since the paradigm shifted from nutrient removal to recovery, this liquid stream has recently gained attention to explore its conversion into value-added products. Different technologies based on chemical, physical and biological processes for nutrient recovery from liquid fraction have been recently explored but few applications to agro-industrial effluent were reported (5) (Figure 1.3). Bolzonella et al. (21) reported that physical methods, such as stripping, evaporation and membranes technologies are typically applied in full-scale plants treating agro-industrial digestate in Italy. These methods basically allow concentrating the nutrients in the liquid stream to reduce transportation costs. However, the high inputs of energy and material required by these techniques lead to high operational costs (5.4–7.0 € m^{-3} digestate) and collaterally generates negative impacts (5). Thus, biological

technology, also in combination with chemical precipitation appears appealing to reduce economic and environmental costs. Many different biological processes have been applied to the liquid stream from digestate but, as digestate usually presents low COD levels, autotrophic processes are more suitable. For instance, microalgae can successfully be harvested from digestate liquid fraction. Particularly, they are able to remove both N and P from digestate via assimilation for biomass growth while capturing atmospheric CO_2 and producing renewable biomass for biorefinery (22). Microalgae treatment is typically carried out in open raceway ponds or photobioreactors with a competitive cost compared to other physical or chemical technologies (25). Moreover, harvested microalgae can be used as AD complement feedstock to improve biogas quality or sold as high-protein animal feed (5). The main drawbacks related to this technology are the large footprint requirement and the need for digestate dilution due to the negative effects of high turbidity and ammonia (22).

Chemical processes are mainly applied for P recovery through magnesium phosphate (MgP) and calcium phosphate (CaP) precipitation. pH values of anaerobic digestates streams generally range between 7.0-8.2 (5), thus an alkali source must be added to increase the pH to the optimal range for such phosphate minerals formation. MgP is most frequently precipitated as struvite, a multi-nutrient fertiliser which requires equimolar amounts of Mg, P, NH_4 or K and a suitable pH ranging from 7.5 to 11.0 depending on the struvite-type mineral to precipitate (8,26). As digestate liquid fraction usually presents limited levels of Mg, an external dosage is often required. Thus, struvite precipitation costs are strongly related to the quantity and quality of Mg and alkali sources added and contributing to up to 75% of overall production costs (5). In general, the precipitated phosphate mineral mainly depends on operational pH and digestate characteristics (26). When Ca levels are significant, struvite precipitation might be affected. It is reported that at lower P concentrations (<40 mg PO_4^{3-}-P L^{-1}) the negative impact on precipitation is more intense than at higher concentrations (>60 mg PO_4^{3-}-P L^{-1}) and, particularly, when Ca/PO_4 ratio is higher than 0.5 CaP over MgP formation is promoted (5). Depending on digestate characteristics, different Ca/P forms such as octacalcium phosphate, or amorphous calcium phosphate can be precipitated being often a metastable precursor of hydroxyapatite, which is a more thermodynamically stable phase (25). To obtain the optimal Ca/P ratio for hydroxyapatite formation (i.e., typically 1.67), Ca is frequently supplied through soluble compounds such as $CaCl_2$, $Ca(OH)_2$, or CaO (27). As pH of 9 or higher is typically required for efficient precipitation, large quantities of alkali lead to high costs, especially for highly buffered liquid fractions (5). To reduce excessive chemical input costs and sludge production, biological processes can be used in combination with chemical precipitation. Particularly, autotropic processes such as nitrification and anammox which use bicarbonate as inorganic carbon source can consequently decrease the buffer capacity of the wastewater (26). In alternative, techniques such as CO_2 stripping

can also be utilized to simultaneously increase pH and reduce dissolved inorganic compounds concentration. Struvite and hydroxyapatite are both suitable to be applied to crop production as slow-release fertilisers, or as raw material for synthetic fertiliser production.

When nutrient recovery technologies cannot be applied to the digestate liquid fraction, its valorisation through energy production can be considered as an alternative. As the liquid fraction is usually characterized by high levels of N, the energy offered by ammonia (NH_3) chemical bonds can be exploited through hydrolysation or thermal oxidation process. After stripping, NH_3 can be converted into N_2 and H_2 by a catalytic reaction in gas phase, or it can be burned together with methane to generate renewable energy (5). However, the high energy required for NH_3 stripping which is not generally balanced by recovered energy, and increased NO_x production during thermal process, are the major disadvantages dampening the actual application of these methods.

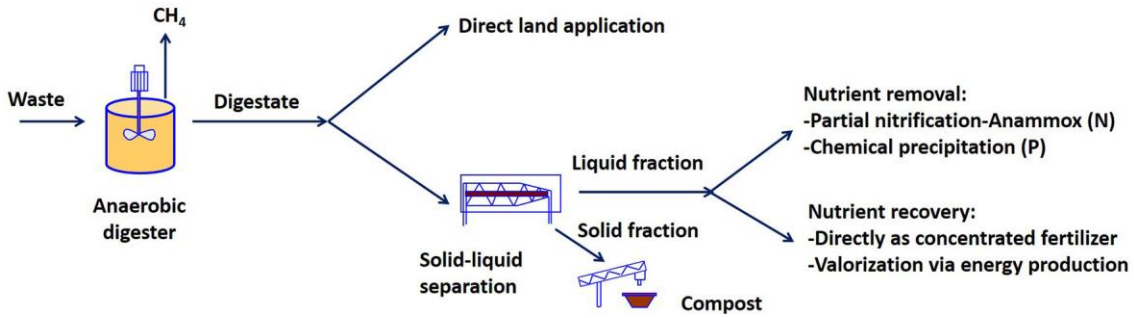

Figure 1.3 - Management options for digestate generated by waste anaerobic digestion (5).

1.2 Anammox-based technologies for nutrient-rich wastewater treatment

Anaerobic ammonia oxidation (Anammox) is a biological process that has gained attention as an effective and environmentally sustainable method to remove NH_4 from wastewater (29). Since its unveiling in the 1900s, this promising process has been applied on a wide variety of wastewater with 66 full-scale plants running worldwide for an overall treatment capacity close to 150 tN d^{-1} (30). Anammox bacteria are autotrophic and carry out an anaerobic oxidation of NH_4-N to N_2 using nitrite (NO_2) as the electron acceptor (Re. 1, (31)) while producing nitrate (NO_3) as a by-product. Anammox process is considered a 'shortcut' in the biogeochemical N cycle which can contribute to the carbon footprint of wastewater treatment (29). Combining partial nitritation (PN) with anammox process was adopted to broaden the direct applicability to wastewater treatment. Through the first aerobic step of PN ammonium-oxidizing bacteria (AOB) carry out the conversion of NH_4 to NO_2 being available to anammox bacteria (Re. 2, (30)). In 1997 Jetten et al. (32) studied for the first time this process combination using two different reactors, while in 2002 Sliekers et al. (33) explored the one-stage

completely autotrophic nitrogen removal over nitrite (i.e., CANON) system (Re. 3, (30)). Since then, one-stage and two-stage partial nitritation/anammox (PN/A) process has been applied at different scales becoming the mainstream methodology (34). Compared to the conventional biological nitrogen removal involving full nitrification ($NH_4 + O_2 \rightarrow NO_2 + O_2 \rightarrow NO_3$) and denitrification ($NO_3 + COD \rightarrow N_2$), the PN/A process provides several advantages corresponding to the main purposes of modern wastewater treatment. In fact, the need for carbon addition is omitted, oxygen demand (i.e., energy requirement) is reduced by 60%, the sludge production is limited by 80%, and finally, it is characterised by lower greenhouse gases (e.g., N_2O) emissions (34–36). As PN/A is a more energy-efficient and environmentally sustainable technology, the number of operating facilities is increasing worldwide (26). So far, 80% of the world's full-scale PN/A processes are designed in one-stage, and it is not vague to see that one-stage process is dominant (37).

$$Nitritation: 1.32\ NH_4^+ + 1.98\ O_2 \rightarrow 1.32\ NO_2^- + 1.4\ H_2O + 2.64\ H^+ \quad (Re.1)$$

$$Anammox: 1\ NH_4^+ + 1.32\ NO_2^- + 0.13\ H^+ \rightarrow 1.02\ N_2 + 0.26\ NO_3 + 2.03\ H_2O \quad (Re.2)$$

$$Overall\ (PN/A): 1\ NH_4^+ + 0.85\ O_2 \rightarrow 0.45\ N_2 + 0.11\ NO_3 + 1.08\ H^+ + 1.44\ H_2O \quad (Re.3)$$

Since anammox bacteria are autotrophic, their growth rate is quite slow, with the exponential phase being 10–22 days or within 10–12 days when cultured at 35ºC (5). Thus, ammonium-rich wastewater is recommended for anammox-based technologies operated in continuous (34). Particularly, N-rich effluent from AD typically presenting low carbon to nitrogen (C/N) ratio are suited to anammox process since carbon source is not required. Decoupling of carbon and nutrient removal allows maximizing the production of renewable energy by converting all carbon sources in the AD and removing N through anammox process (26,29,30,38). Moreover, digestate liquid fraction often presents temperature around 15-35ºC which is a favourable condition for the following autotrophic processes (26). Thus, AD integration with PN/A process is promising. Several studies have investigated full-scale side-stream anammox installations for the treatment of digested sewage, landfill leachate, and rejected water (39).

Anaerobic treatment such as AD has been applied increasingly in treating organic residues to generate renewable energy (methane-rich biogas). Although anaerobic digestion (AD) is an effective method to remove organic compounds (measured as chemical oxygen demand: COD), the removal of nutrients (N, P) is fairly limited (30). To enhance nutrient recovery from digestate, P recovery combined with Anammox-based technologies has been explored as downstream chemical precipitation and as concomitant CaP biomineralization.

1.2.1 Anammox combined to downstream chemical precipitation

Chemical precipitation for P recovery presents simple operation and high removal efficiency. However, the main drawback is the high costs of chemicals needed to increase the bulk liquid pH for minerals precipitation (5). The alkali demand increases with the wastewater alkalinity which is related to the buffer capacity. High strength wastewaters such as AD effluents are characterised by high buffer capacity due to NH_3/NH_4^+ and $H_2CO_3/HCO_3^-/CO_2^{-3}$ equilibria. Thus, different processes such as CO_2 stripping through aeration were applied as pretreatment to decrease the alkali dosing. Since CO_2 stripping is an energy-demanding process, biological processes involving bicarbonate and ammonium consumption have been explored. Particularly, nitrification and anammox have been reported as effective and low-cost pretreatment to reduce the consumption of reagents (40). As autotrophic processes, nitrogen removal entails alkalinity consumption with a consequent decline of bulk liquid buffer capacity mostly due to total inorganic carbon content decrease. Moreover, NH_4^+conversion into N_2 by anammox bacteria implies a decrease in the medium ionic strength (i.e., loss of salinity) which further favours mineral precipitation due to a higher effective concentration of involved ions (26). As P precipitation typically requires increasing pH, the biological process enables to reduce the chemical dosage involving significant cost savings for downstream precipitation. Since reduced aeration is needed, PN/A technologies allow to further reduce operative costs compared to conventional nitrification. Previous application of nitrification or PN/A process showed that it is possible to decrease the amount of NaOH required up to 50 and 89%, respectively, while achieving an economically profitable struvite recovery (5). Moreover, a recent study reported that PN/A enables alkalinity removal efficiency up to 90%, surpassing CO_2 stripping performance (41). The remaining $NH_4^+$from the biological removal can be precipitated as struvite, or in case of higher Ca levels, CaP precipitation can be achieved. Concerning the liquid effluent, beyond satisfactory discharge into water bodies, ion precipitation can also help adjusting water quality in terms of the N-P-K content to match specific requirements according to the final use (e.g., reuse for crop fertigation).

1.2.2 HAP-Anammox for simultaneous ammonium-nitrogen removal and phosphorus recovery

Concomitant P precipitation in anammox-based technology is an emerging process that has recently gained attention due to the opportunity of simultaneous N removal and P recovery, while enhancing anammox sludge settleability and increasing biomass concentration in the bioreactor (42). It has been reported that CaP precipitation can potentially occur in anammox granular sludge and hydroxyapatite (HAP, $Ca_{10}(PO4)_6(OH)_2$) recovery can be eventually achieved (Re. 4 (43)). As minerals are mainly found inside anammox granules, P mineralization is considered being biologically induced rather than

a simple chemical crystallization (41). Particularly, the anammox process supplies alkalinity, providing the essential conditions for P crystallisation and mineral growth.

$$10Ca^{2+} + 6PO_4^{3-} + 2OH^- \rightarrow Ca_{10}(PO_4)_6(OH)_2 \qquad (Re.4)$$

The granulation process has been studied by many authors allowing to understand the main factors involved (Fig. 1.4). When Ca^{2+} and PO_4^{3-} are present in sufficient levels in the bulk liquid, the high pH generated by anammox reactions near the cell can lead to supersaturation conditions consequently inducing the crystal nuclei formation and mineral growth (43). Then, the heterogeneous growth of biofilm and HAP crystals allows anammox (A)-HAP flocs to expand forming microbe-crystal consortia, while hydraulic shear force leads to the HAP core encapsulation by the anammox biofilm (44). The resulting A-HAP granules structure can be theoretically divided in three layers (Figure 1.4): an outer biofilm involved in anammox reaction, a middle layer for biomineralization, and an inner HAP mineral core (37). In one-stage PN/A configurations, the granular structure may exhibit increased complexity, as variations in bacterial metabolism contribute to diverse distributions of dissolved oxygen (DO), pH, and substrate concentration leading to a stratified configuration of aerobic and anaerobic zones (AOB-AnAOB and eventually DNB) on the surface of the HAP core (42,43). AnAOB are more sensitive to external environment, so they are likely distributed in the inner layer enhancing their resilience against possible inhibition. Different hypotheses have been raised by authors to explain this granulation phenomenon. Heterotrophic filamentous bacteria could play a key role as linking agents while the microorganisms secrete extracellular polymeric substances (EPS) facilitating granule formation (AnAOB showing elevated EPS production) and Ca^{2+} ions are suggested to significantly contribute to granulation and biomass accumulation through adsorption and adhesion (45). Still, the granulation process of A-HAP-based granules demonstrates variability across different applications, emphasizing the need for further investigation into the mechanisms of granulation and the overall cycle (37).

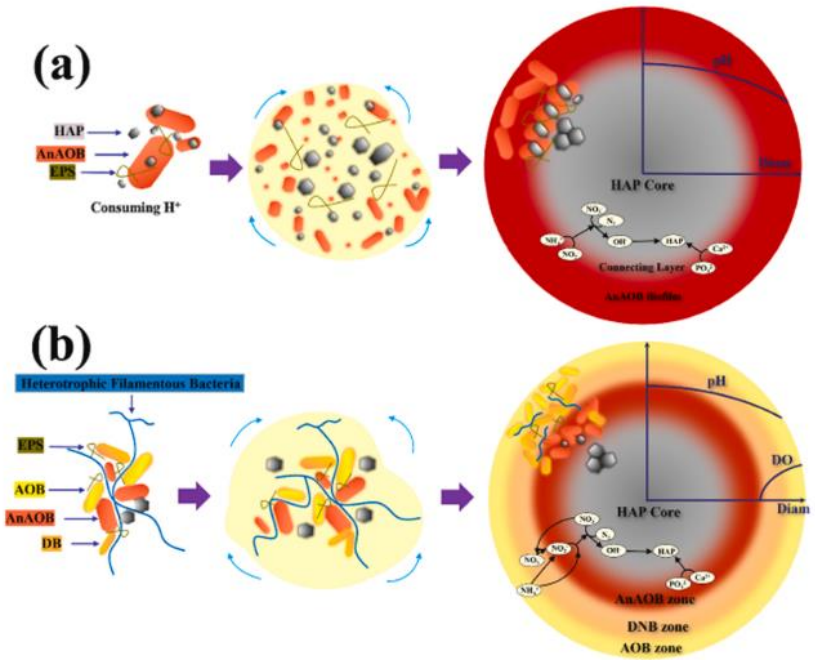

Figure 1.4 - Structure and granulation mechanism of (a) anammox (A)-hydroxyapatite (HAP) granule; (b) one-stage A-HAP based granule presenting a stratified biofilm with aerobic and anaerobic zones (37).

Because of the slow growth of the anammox bacteria, it is crucial to enhance the granules physical strength and settling velocity to obtain sufficient biomass retention even at a high flow rate (46). The introduction of carriers and biofilm reactors can be used for this purpose. HAP can be considered as biocarrier allowing for granule immobilisation by mineral cores turning into an economical and convenient way to improve anammox processes while removing P from the wastewater (37). Cultivated anammox granules with a HAP core have been shown to have excellent settleability, a large granule diameter, superior mechanical strength, and biomass attachment (42,47). Particularly, it has been reported that maintaining an appropriate influent P concentration is critical to preserve high biomass retention within the system and high removal efficiencies (37). Li et al. (48) reported that when influent P level is increased in the range from 40 to 250 mg L^{-1}, the recovery efficiency increases with the influent concentration and high NRE can be achieved (i.e. 88.5%). Xue et al. (49) observed consistent performance when the influent P concentration was higher than 11.4 mg L^{-1} but when it dropped to 5.7 mg L^{-1}, granular sludge experienced flotation. Constituent ion concentration is a driving force for CaP precipitation and, particularly, Ca/P ratio is a critical factor for HAP crystallization. The stochiometric Ca/P value for HAP precipitation is typically 1.67, thus wastewater characterised by at least this value can favour the mineralisation. However, Ca/P variability especially in practical applications can affect the coupling process's stability. Ca addition generally enhances

the system performance as higher influent Ca/P ratios promote CaP mineralisation and consequently phosphorus recovery. When the influent Ca/P ratio decreases, the efficiency of HAP crystallization is hindered, and the lack of supersaturated conditions can eventually lead to dissolution of already-formed crystals consequently affecting granular sludge stability due to expansion and flotation (47). Oppositely, excessive Ca/P ratios can lead to an overabundance of free HAP, hindering substrate-biomass contact, impacting mass transfer efficiency, and inhibiting the anammox process (48). Moreover, high Ca/P reached by chemical addition can generate pollution problems due to high levels on Ca being expulsed with the effluent. Thus, finding a balance on the HAP constituent ion levels is critical to achieve superior process performance and to avoid environmental problems. In this context, Lin et al. (48) proposed a model to help regulating Ca dosage in function of influent P concentration. This finding would allow also to eventually minimize chemical dosage in actual wastewater, lacking Ca, and thus to reduce operational costs.

As constituent ion concentration is a limiting factor for microbe-HAP granule formation, low-strength wastewater (20-50 mgNH_4-N L^{-1}), typically presenting low P concentrations, can hinder the cultivation process. Thus, high-strength wastewaters (500-1500 mg NH_4-N L^{-1}) are more suitable for the start-up and stable operation for HAP strategy (37). The liquid fraction of anaerobic digestate is a high-strength wastewater typically abundant in inorganic nutrients like N and P. The combination of upstream AD and the one-stage PN/A process was proposed as a low-energy consuming and environmentally sustainable method for maximizing the energy recovery from organic carbon compounds, while allowing a more compact infrastructure for both processes (42,43). Anammox based-technology has been extensively studied for treating such high-strength wastewater, but challenges related to P recovery and inhibition due to high substrate concentrations persist. However, the introduction of the HAP strategy presents a novel approach to address these challenges. Airlift reactor configurations have shown promising performance in the combined PN/A-HAP process achieving higher performance than conventional SBR operation (44) (Figure 1.5). Laboratory-scale experiments using synthetic wastewater showed high (i.e., ≥77%) simultaneous N and P removal efficiency (NRE, PRE) (50,51). Moreover, as HAP granules can prevent inhibition by high concentrations of FA and FNA, a higher nitrate loading rate (NLR) can be adopted (37). Chen et al. achieved exceptionally high nitrate removal rate (NRR) of 4.5 gN $(L \cdot d)^{-1}$ and NRE of 77.5% with an NLR of 6 gN $(L \cdot d)^{-1}$ and an operative temperature of 25ºC, displaying remarkable performance not reported previously (52). However, experience with real wastewater is still limited. Johanson et al. (41) and Magrí et al. (43) worked with urban side-stream centrate proving the feasibility of HAP mineralisation with simultaneous N removal in one-stage PN/A process, while Chen et al. (47,53) did not detect any P removal while working with HAP-sludge to treat fish processing water and pretreated

municipal wastewater. These experiences showed that there is a limited experience on one-stage process treating actual wastewater and on strategies to implement effective P recovery. Particularly, PN/A-HAP long-term operation testing and comparing different type of wastewaters under seasonal temperatures is still needed to be explored (54).

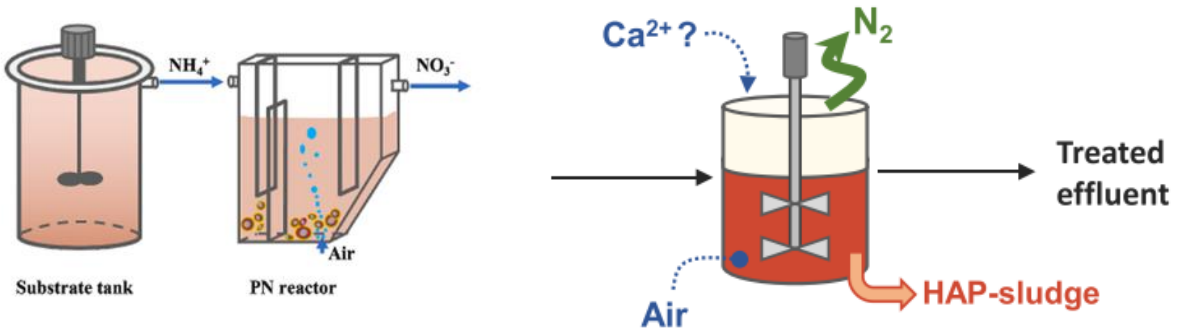

(a) (b)

Figure 1.5 – Single-stage Partial Nitritation/Anammox process with concomitant hydroxyapatite (HAP) precipitation operated in air-lift reactor (left) (37) and sequencing batch reactor (right) (43).

HAP biomineralization can be easily integrated into the existing anammox-based granular sludge system without the need for extra devices representing a remarkable advantage of this strategy for P recovery. In fact, the operation costs are minimized by using the current infrastructure while allowing to recover a value-added product. During stable operation, highly mineralized sludge can be produced within the bioreactor. As mineral accumulates on granules, gravity increases leading them to settle at bottom of the reactor from which they can be easily harvested (41). Once this sludge is harvested, the high P content (i.e., 10−16%) makes it an interesting resource for subsequent valorisation (43). CaP compounds are well suited for use in food and energy crop production due to their potential value as a slow-release fertiliser or as a raw material for synthetic fertiliser production (25). Comparable performance to traditional phosphate fertilisers were achieved in a greenhouse study on ryegrass cultivation, but further study of the fertiliser value of CaP recovered from different processes is needed as the low solubility of most of these compounds may limit their potential for reuse directly as fertiliser (55). In alternative, CaP can be industrially processed into traditional inorganic fertilisers due to their similar composition with natural PR. Recovered CaP contains lower levels of toxic or radioactive contaminants than natural phosphate minerals, making them attractive feedstocks for the fertiliser industry (56). However, there is still a lack of research related to the actual HAP recovery from the sludge. Johanson et al. (41) suggested direct sludge spreading on field or for using it as raw material in industry combustion is a possible strategy to get rid of the organic fraction. In both cases, HAP recovery would lead to the loss of anammox which is slow-growth bacteria potentially hindering the long-term stability of the process. Besides, Magrí et al. (43) experience pointed out the need of

finding an operational compromise between microbial activity long-term optimization and the interest in extracting P-rich granules from the system. To date, the research has not been focused on testing an efficient separation method that will allow effective P-recovery from sludge without damaging the slow-growth biomass. Hence, exploring a non-damaging method for biomass-from-mineral separation is a critical challenge to evaluate the effective HAP recovery from anammox-based process especially when considering future scale-up of the technique.

1.3 Electrochemical systems applied to nutrient recovery

Nutrient recovery from wastewaters typically involves their conversion from soluble into solid form by increasing pH which conventionally is achieved through alkali dosage (57). Chemical precipitation is considered an efficient and stable process, but presenting high operative costs related to reagents addition and sludge production. While electrochemical technologies (ETs) have been extensively studied for wastewater decontamination over the last thirty years, their operation for resource recovery only recently has garnered attention (58). ETs have demonstrated to be promising methods for P, N and K recovery with multiple factors affecting the system's performance, including pH, current density (CD), electrode configuration, and water matrix. Main advantages over chemical precipitation methods include cost efficiency, great flexibility, and low maintenance, increased environmental sustainability, limited or zero chemical demand and potential energy production (57). Moreover, ETs allow precise manipulation of electrode reactions by adjusting current or voltage to minimize side reactions, enhancing product purity and technical feasibility for practical application (58).

1.3.1 Electrocoagulation and electromediated precipitation processes

Electrochemical nutrient recovery techniques can be divided basing on the anode function, specifically sacrificial anodes and dimensionally stable anodes processes (59). The first method relies on electrocoagulation process in which metal oxides are electrochemically produced in-situ to form precipitates and adsorb dissolved compounds. Through current application, cations such as Fe^{2+}, Mg^{2+}, and Al^{3+}, are released from a sacrificial anode improving phosphate salts precipitation (58,60,61). Particularly, Mg-sacrificial anodes has gained popularity due to higher cost-effectiveness compared to chemically induced struvite precipitation (62). Moreover, authors reported that electrochemical Mg continuous dosing allows limiting or completely avoiding the cost of chemicals while improving crystal growth (59). Although, the most limiting drawback of this technique lies in the inevitable recurring anode replacement, which is depleted due to oxidation, leading to an increase in the long-term operational costs (63). In dimensionally stable anode process the electrode is inert

and nutrients removal is driven by hydroxyls (OH^-) production and high pH at the cathode which drives electrochemically mediated precipitation (EMP). EMP has been applied by many authors as a clean method to achieve on-site OH^- production driven by water electrolysis with a limited or zero-chemical input (64–66). When an electric current is supplied, water molecules undergo a reduction and are converted into hydrogen (H_2) at the cathode. This process causes the simultaneous production of OH^- (Re. 5) which increases the local pH. At the anode, water molecules are oxidized generating oxygen (O_2) and protons (H^+) (Eq. 6), thus neutralizing the OH^- produced at the cathode. In certain ETs, ion exchange membranes find application to prevent cross-neutralization of the low-pH anolyte with the high-pH catholyte. In such case, membranes are separating the system into two, or multiple compartments generating a pH gradient between the anode and cathode.

Cathode: $2H_2O + 2e^- \rightarrow H_2 + 2OH^-$ *(Re. 5)*

Anode: $2H_2O \rightarrow O_2 + 4H^+ + 4e^-$ *(Re. 6)*

Due to electro-migration, counter cations in wastewater move towards the cathode and get attached to its surface from which they can be periodically collected as precipitates. However, process optimisation and sustainable mineral recovery strategies are still necessary to make the EMP method economically viable as the precipitation on the electrode surface can hinder the process stability. Excessive electrode's coating typically increases ohmic resistances along the operation eventually leading to cathode deactivation (67). Moreover, precipitates collection implies the need for arresting the treatment which is a limiting factor for the long-term operational feasibility. To ease the mineral recovery some authors suggested implementing automatic scraping methods (68,69), while Takabe et al. (70) successfully tested polarity inversion to detach the solids from the cathode. Furthermore, the adoption of the electrochemical process is limited by its high energy consumption. High values of CD (up to 300 A m^{-2} (70,71)) are commonly applied to improve P removal rates leading to increased operational costs (72) (Figure 1.5). With the aim of contributing to the development of an energy-efficient electrochemical process and limiting the precipitation in the electrode surface, the application of a low CD in the electrochemical system could be a viable option. As an example, Lei et al. (73) achieved 70% P removal efficiency from acidic cheese wastewater by applying extremely low CD (0.2 A m^{-2}) reaching a specific energy consumption of 26.4 kWh kg^{-1} P, which was two orders of magnitude lower than their previous system operated with a high CD. Under these conditions the co-precipitation of calcium carbonate ($CaCO_3$) and brucite ($Mg(OH)_2$) was also reduced. Moreover, recent studies reported that high overall energy efficiency is achievable when H_2 is produced in the cathode compartment, balancing the energy required for electrochemical nutrient removal (59). As an alternative to reduce the applied CD, combining bio-electrochemical system with

EMP, can significantly reduce energy demand (57). As exoelectrogenic microbes can generate electrons, bio-electrochemical system requires less energy input than abiotic electrochemical system. Lei et al. (74,75) used bio-electrochemical and abiotic electrochemical systems to treat domestic wastewater, respectively, and the specific energy consumption of the bio-system (69 kWh kg^{-1} P) was lower than for the abiotic system (110 kWh kg^{-1} P). Although bio-electrochemical systems hold great potential in reducing energy consumption, it often requires additional carbon sources, and its working conditions are stricter than abiotic systems (63).

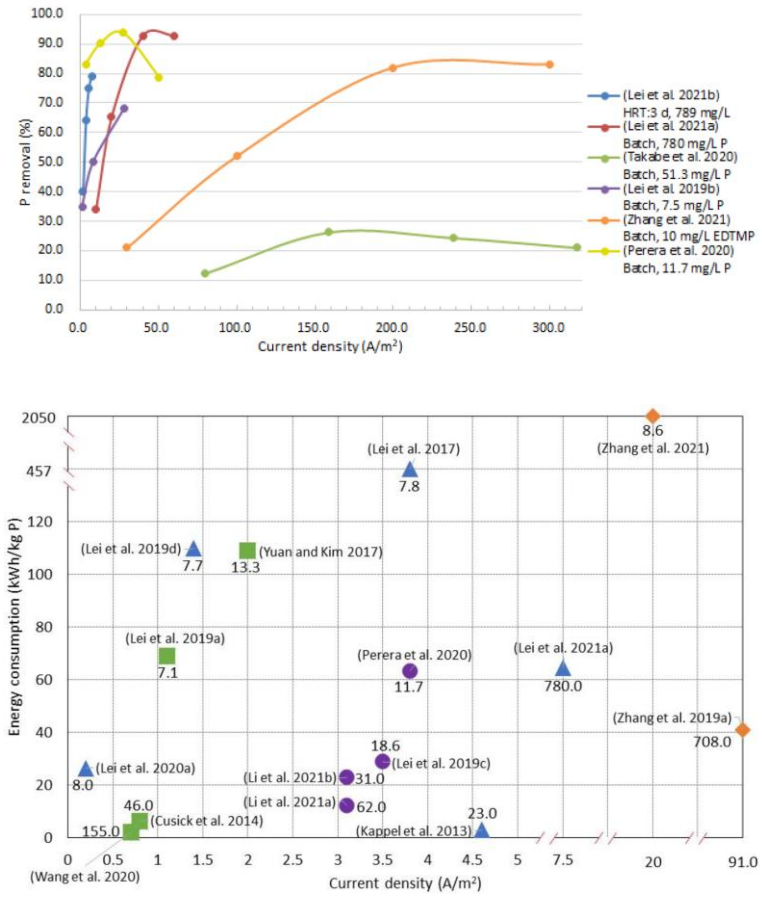

Figure 1.5 – *Top:* Phosphorus removal as a function of applied current density (63); *Bottom:* energy consumption of (bio)electrochemical system under various conditions based on literature data (triangles represent electrochemical cells; squares represent bioelectrochemical cells; circles represent (bio)electrochemical cells with membranes or packed with ores; diamonds represent non-ortho P treatment) (numbers by the symbols are initial P concentration [mg L^{-1}]) (63).

Further work is needed to increase cost-efficiency of ETs in nutrient recovery, improving quality of products and developing ease and automatised precipitate recovery systems. Overall, ETs can potentially play a critical role in remote areas and in decentralized wastewater treatment as self-sustainable, cost-effective, versatile, and robust systems (58). Recovering nutrient from wastewaters

not only attains the pollution abatement goal but can also offers an alternative sustainable source of fertilisers for agricultural activities (57).

1.3.2 Electrochemical struvite recovery

Struvite and CaP are the two typical recovery products in electrochemical system treating nutrient-rich wastewater. Particularly, struvite holds the advantage of simultaneously recovering P and N or K. When NH_4 is abundant in the wastewater, NH_4-struvite ($MgNH_4PO_4$, magnesium-ammonium-phosphate hexahydrate, MAP) is favourably precipitated in the mole ratio of $Mg:NH_4:PO_4$ of 1:1:1 by adjusting the bulk liquid pH (Re. 7, (15)).

$$Mg^{2+} + NH_4^+ + H_nPO_4^{n-3} + 6H_2O \rightarrow MgNH_4PO_4 \cdot 6H_2O + nH \qquad n = 0,1,2 \qquad (Re.7)$$

When K concentration is high, and NH_4 is limited or absent, K-struvite ($MgKPO_4$; magnesium-potassium-phosphate hexahydrate, MPP) is the final product which forms according to a $Mg:K:PO_4$ molar ratio of 1:1:1, under supersaturation and alkaline conditions (Re. 8, (8)).

$$Mg^{2+} + K^+ + H_nPO_4^{n-3} + 6H_2O \rightarrow MgKPO_4 \cdot 6H_2O + nH \qquad n = 0,1,2 \qquad (Re.8)$$

As waste valorisation product, the precipitated phosphate salt struvite-type materials have received great attention as they can be applied to crops as a slow-release fertiliser simultaneously providing P, Mg and N or K (15,76). Particularly, MPP precipitation looks interesting being the only method to selectively remove, recover, and reuse potassium from wastewaters (77). Struvite crystallisation is affected by a combination of factors including pH, temperature, constituent ion activities, and the coexistence of other ions. Research findings showed that MPP precipitation normally occurs at pH between 9.0 and 12.0, which is above the optimal values (pH 8.5–9.5) for the precipitation of its analogue NH_4-struvite ($MgNH_4PO_4 \cdot 6H_2O$;) (78). The precipitation of MPP is notably more complex, primarily influenced by the solubility product and inhibitory compounds. MPP solubility product constant is significantly higher compared to MAP (12.6-13.4 and 10.8-12.2, respectively), playing a crucial role in precipitation efficiency (77). Additionally, inhibiting substances such as ammonia and calcium, can hinder MPP formation based on their concentrations in the treated wastewater. Electrochemical treatment has been reported as an efficient and sustainable method for struvite precipitation from different wastewater with several studies on MAP, but still limited applications on MPP.

Mg is typically the limiting constituent ion in struvite precipitation, thus magnesium sources such as $MgCl_2$, $MgSO_4$, $Mg(OH)_2$, MgO are commonly used to increase its concentration. As an alternative to chemical dosing, Mg-sacrificial anode can be used in electrochemical treatment for this purpose. MAP precipitation through electrochemical treatment is mainly achieved through electrocoagulation

(62,79,80) (Figure 1.6). Current studies have demonstrated a high P removal (>90%) and MAP with purity above 95% can be obtained using Mg-sacrificial anode corresponding to a total cost ranging between 31.27 and 81.57 \$ kg^{-1}P or 5.26 \$ kg^{-1} struvite, depending on the local market magnesium price (77). Particularly, Hug et al. (62) reported that, considering material costs, dissolution of a Mg sacrificial anode can compete when easily soluble magnesium salts ($MgCl_2$ and $MgSO_4$) are considered, but MgO dosage is still cheaper than the electrochemical process. MPP recovery using a sacrificial Mg-anode was achieved by Shan et al. (81). With an optimal CD of 3.5 mA cm^{-1}, K and P removal efficiency of 35.4% and 88.5%, respectively, were achieved in one-compartment system treating simulated urine. Recovered product was mainly formed by MPP, but some impurities such as $MgNaPO_4$ and $Ca_3(PO_4)_2$ were identified through solid analysis. Li et al. (82) explored MPP recovery from landfill leachate through EMP using a double-compartment system equipped with a cation-exchange membrane and working with an applied CD of 40 mA cm^{-2} (Figure 1.6). This study demonstrated the feasibility of a combined process achieving remarkable removal efficiency for organic matter and NH_3-N (i.e., 82%, and 99% respectively) with simultaneous chloride and MPP recovery. Particularly, the recovered gaseous chlorine was used for on-site decolorization for allowing a complete removal of synthetic dye contained in the wastewater. Moreover, the combined process allowed to produce hydrogen as a valuable electrolysis by-product.

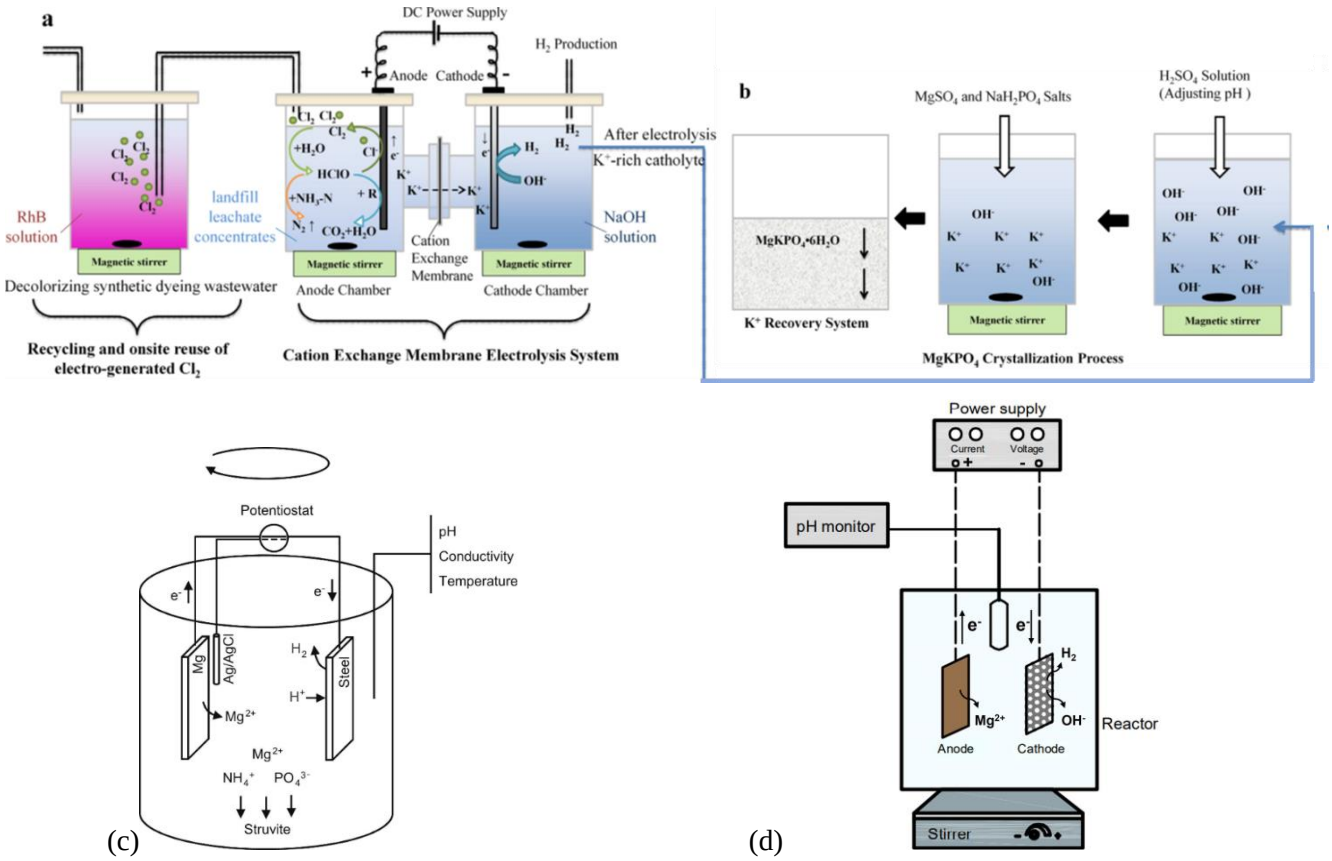

Figure 1.6 – *Top:* Double-compartment electrolysis cell equipped with a cation-exchange membrane system (a) and the three reactors used for potassium struvite recovery (b) (82). *Bottom:* Single-compartment with a sacrificial magnesium electrode used for ammonium struvite recovery (c) (62); single-compartment system with a sacrificial magnesium electrode used for potassium struvite recovery (d) (81).

However, the economic benefit potentially achieved by MPP recovery and hydrogen generation (841586 \$ $year^{-1}$ and 538880\$ $year^{-1}$, respectively) could not offset energy consumption cost (i.e., 6227563 \$ $year^{-1}$) (82). Such high energy consumption was primarily attributed to the large distance within the electrodes (i.e., 10 cm). Nevertheless, the MPP economic benefit was remarkably higher compared to struvite recovery from reverse osmosis concentrates in wastewater treatment plants (7000 \$ $year^{-1}$). These findings suggest that MPP recovery through EMP is promising but further work is needed to improve the cost-effectiveness of MPP by optimising the applied CD and improving the system configuration and dimensional features to limit energy consumption.

1.4 Scope and outline of this thesis

This Ph.D. thesis aimed to explore and optimise innovative technologies (i.e., PN/A and EMP) for the treatment of agro-industrial wastewaters. As already mentioned in paragraph 1.1, such wastewaters are characterised by high levels of nutrients (N, P, and K) and negligible organic matter

content due to specific pretreatment. This Ph.D. thesis has reached its aim through the following specific goals:

- To evaluate the feasibility and performances of single-stage PN/A process combined with downstream chemical precipitation for CaP recovery from agro-industrial anaerobic digestion supernatant (Chapter 2).
- To test single-stage PN/A process operated in a 3L SBR for concomitant nitrogen removal and CaP precipitation treating agro-industrial anaerobic digestion supernatant. In this step, a mineral-from-biomass, non-damaging separation method was explored (Chapter 3).
- To evaluate the feasibility and performances of EMP process and catholyte neutralisation based on a double-compartment electrochemical system to precipitate P from swine manure denitrified effluent (Chapter 4).
- To test EMP process for K-struvite recovery through a double-compartment electrochemical system combined with a 14.6L crystalliser treating swine manure denitrified effluent. In this step, the optimal electrochemical system configuration was evaluated through batch experiment, while P recovery, catholyte neutralisation and chlorine production performances were further explored during continuous operation (Chapter 5).

References

1. Eurostat. *Food Waste and Food Waste Prevention - Estimates*. 2023; 1–7. https://ec.europa.eu/eurostat/statistics-explained/index.php?title=Food_waste_and_food_waste_prevention_-_estimates.

2. Bedoić R, Ćosić B, Duić N. *Technical potential and geographic distribution of agricultural residues, co-products and by-products in the European Union*. Sci Total Environ. 2019; 686: 568–79. https://doi.org/10.1016/j.scitotenv.2019.05.219.

3. Zubair M, Wang S, Zhang P, Ye J, Liang J, Nabi M. *Biological nutrient removal and recovery from solid and liquid livestock manure: Recent advance and perspective.* Bioresour Technol. 2020; 301: 122823. https://doi.org/10.1016/j.biortech.2020.122823.

4. Barampouti EM, Mai S, Malamis D, Moustakas K, Loizidou M. *Exploring technological alternatives of nutrient recovery from digestate as a secondary resource.* Renew Sustain Energy Rev. 2020; 134: 110379. https://doi.org/10.1016/j.rser.2020.110379.

5. Campos JL, Crutchik D, Franchi Ó, Pavissich JP, Belmonte M, Pedrouso A. *Nitrogen and*

Phosphorus Recovery From Anaerobically Pretreated Agro-Food Wastes: A Review. Front Sustain Food Syst. 2019; 2: 1–11. https://doi.org/10.3389/fsufs.2018.00091.

6. Chojnacka K, Moustakas K, Witek-Krowiak A. *Bio-based fertilisers: A practical approach towards circular economy.* Bioresour Technol. 2020; 295: 122223. https://doi.org/10.1016/j.biortech.2019.122223.

7. Sohal VS. *Too much of a good thing?* Sci Transl Med. 2013; 5 (213): 5–7. https://doi.org/10.1126/scitranslmed.3008071.

8. Company E, Farrés M, Colprim J, Magrí A. *Exploring the recovery of potassium-rich struvite after a nitrification-denitrification process in pig slurry treatment.* Sci Total Environ. 2022; 847: 157574. https://doi.org/10.1016/j.scitotenv.2022.157574.

9. Dadrasnia A, de Bona Muñoz I, Yáñez EH, Lamkaddam IU, Mora M, Ponsá S, et al. *Sustainable nutrient recovery from animal manure: A review of current best practice technology and the potential for freeze concentration.* J Clean Prod. 2021; 315. https://doi.org/10.1016/j.jclepro.2021.128106.

10. Jupp AR, Beijer S, Narain GC, Schipper W, Slootweg JC. *Phosphorus recovery and recycling-closing the loop.* Chem Soc Rev. 2021; 50 (1): 87–101. https://dx.doi.org/10.1039/D0CS01150A.

11. Duquennoi C, Martinez J. *European Union's policymaking on sustainable waste management and circularity in agroecosystems: The potential for innovative interactions between science and decision-making.* Front Sustain Food Syst. 2022; 6. https://doi.org/10.3389/fsufs.2022.937802.

12. Law KP, Pagilla KR. *Phosphorus Recovery by Methods Beyond Struvite Precipitation.* Water Environ Res. 2018; 90 (9): 840–50. https://doi.org/10.2175/106143017X15131012188006.

13. Garske B, Stubenrauch J, Ekardt F. *Sustainable phosphorus management in European agricultural and environmental law.* Rev Eur Comp Int Environ Law. 2020; 29 (1): 107–17. https://org.doi/10.1111/reel.12318.

14. FAO 2019. *World fertiliser trends and outlook to 2022*. Rome. https://doi.org/10.4060/ca6746en.

15. Yesigat A, Worku A, Mekonnen A, Bae W, Feyisa GL, Gatew S. *Phosphorus recovery as K-struvite from a waste stream: A review of influencing factors, advantages, disadvantages and*

challenges. Environ Res. 2022; 214: 114086. https://doi.org/10.1016/j.envres.2022.114086.

16. Jena SK. *A Review on Potash Recovery from Different Rock and Mineral Sources.* Mining, Metall Explor. 2021; 38 (1): 47–68. https://doi.org/10.1007/s42461-020-00286-7.

17. Al Rawashdeh R. *World peak potash: An analytical study.* Resour Policy. 2020; 69: 101834. https://doi.org/10.1016/j.resourpol.2020.101834.

18. Vučić V, Müller S. *New developments in biological phosphorus accessibility and recovery approaches from soil and waste streams*. Eng Life Sci. 2021; 21 (3–4): 77–86. https://doi.org/10.1002/elsc.202000076.

19. Kok DJD, Pande S, Van Lier JB, Ortigara ARC, Savenije H, Uhlenbrook S. *Global phosphorus recovery from wastewater for agricultural reuse.* Hydrol Earth Syst Sci. 2018; 22 (11): 5781–99. https://doi.org/10.1016/j.cej.2018.02.088.

20. Vanotti MB, García-González MC, Szögi AA, Harrison JH, Smith WB, Moral R. *Removing and Recovering Nitrogen and Phosphorus from Animal Manure*. Anim Manure Prod Charact Environ Concerns, Manag. 2020; 275–321. https://doi.org/10.2134/asaspecpub67.c22.

21. Bolzonella D, Fatone F, Gottardo M, Frison N. *Nutrients recovery from anaerobic digestate of agro-waste: Techno-economic assessment of full scale applications.* J Environ Manage. 2018; 216: 111–9. https://doi.org/10.1016/j.jenvman.2017.08.026.

22. Guilayn F, Rouez M, Crest M, Patureau D, Jimenez J. *Valorization of digestates from urban or centralized biogas plants: a critical review*. Vol. 19, Reviews in Environmental Science and Biotechnology. Springer Netherlands; 2020. 419–462. https://doi.org/10.1007/s11157-020-09531-3.

23. Vaneeckhaute C, Styles D, Prade T, Adams P, Thelin G, Rodhe L. *Closing nutrient loops through decentralized anaerobic digestion of organic residues in agricultural regions: A multi-dimensional sustainability assessment.* Resour Conserv Recycl. 2018; 136: 110–7. https://doi.org/10.1016/j.resconrec.2018.03.027.

24. Scholz M. *Creating a circular economy for phosphorus fertilisers.* Fertil Focus. 2017; 36–41.

25. Xu F, Khalaf A, Sheets J, Ge X, Keener H, Li Y. *Phosphorus Removal and Recovery From Anaerobic Digestion Residues*. 1st ed. Vol. 3, Advances in Bioenergy. Elsevier Inc.; 2018. 77–136 p. http://dx.doi.org/10.1016/bs.aibe.2018.02.003.

26. Magrí A, Carreras-Sempere M, Biel C, Colprim J. *Recovery of phosphorus from waste water*

profiting from biological nitrogen treatment: Upstream, concomitant or downstream precipitation alternatives. Agronomy. 2020; 10 (7). https://doi.org/10.3390/agronomy10071039.

27. Peng L, Dai H, Wu Y, Peng Y, Lu X. *A comprehensive review of phosphorus recovery from wastewater by crystallization processes.* Chemosphere. 2018; 197: 768–81. https://doi.org/10.1016/j.chemosphere.2018.01.098.

29. Weralupitiya C, Wanigatunge R, Joseph S, Athapattu BCL, Lee TH, Kumar Biswas J. *Anammox bacteria in treating ammonium rich wastewater: Recent perspective and appraisal.* Bioresour Technol. 2021; 334: 125240. https://doi.org/10.1016/j.biortech.2021.125240.

30. Driessen W, Hendrickx T. *Two decades of experience with the granular sludge-based anammox® process treating municipal and industrial effluents.* Processes. 2021; 9 (7): 1–15. https://doi.org/10.3390/pr9071207.

31. Strous M, Van Gerven E, Zheng P, Kuenen JG, Jetten MSM. *Ammonium removal from concentrated waste streams with the anaerobic ammonium oxidation (anammox) process in different reactor configurations.* Vol. 31, Water Research. 1997. p. 1955–62. https://doi.org/10.1016/S0043-1354(97)00055-9.

32. Jetten MSM, Horn SJ, Van Loosdrecht MCM. *Towards a more sustainable municipal wastewater treatment system.* Water Sci Technol. 1997; 35 (9): 171–80. https://doi.org/10.1016/S0273-1223(97)00195-9.

33. Sliekers AO, Derwort N, Gomez JLC, Strous M, Kuenen JG, Jetten MSM. *Completely autotrophic nitrogen removal over nitrite in one single reactor.* Water Res. 2002; 36 (10): 2475–82. https://doi.org/10.1016/S0043-1354(01)00476-6.

34. Choi D, Cho K, Jung J. *Optimization of nitrogen removal performance in a single-stage SBR based on partial nitritation and ANAMMOX.* Water Res. 2019; 162: 105–14. https://doi.org/10.1016/j.watres.2019.06.044.

35. Chen G, Zhang Y, Wang X, Chen F, Lin L, Ruan Q. *Optimizing of operation strategies of the single-stage partial nitrification-anammox process.* J Clean Prod. 2020; 256: 120667. https://doi.org/10.1016/j.jclepro.2020.120667.

36. Cao Y, van Loosdrecht MCM, Daigger GT. *Mainstream partial nitritation–anammox in municipal wastewater treatment: status, bottlenecks, and further studies.* Appl Microbiol Biotechnol. 2017; 101 (4): 1365–83. http://dx.doi.org/10.1007/s00253-016-8058-7.

37. Cao L, Yang Y, Xue Y, Ma H, Li YY, Hu Y. *A review of efficient nitrogen removal and phosphorus recovery by anammox-hydroxyapatite based processes: Challenges and opportunities.* J Environ Chem Eng. 2023; 11 (5): 111103. https://doi.org/10.1016/j.jece.2023.111103.

38. Cao S, Zhou Y. *New direction in biological nitrogen removal from industrial nitrate wastewater via anammox.* Appl Microbiol Biotechnol. 2019; 103 (18): 7459–66. https://doi.org/10.1007/s00253-019-10070-3.

39. Cho S, Kambey C, Nguyen VK. *Performance of anammox processes for wastewater treatment: A critical review on effects of operational conditions and environmental stresses.* Water. 2020; 12 (1). https://doi.org/10.3390/w12010020.

40. Johansson S, Ruscalleda M, Saerens B, Colprim J. *Potassium recovery from centrate: taking advantage of autotrophic nitrogen removal for multi-nutrient recovery.* J Chem Technol Biotechnol. 2019; 94 (3): 819–28. https://doi.org/10.1002/jctb.5828.

41. Johansson S, Ruscalleda M, Colprim J. *Phosphorus recovery through biologically induced precipitation by partial nitritation-anammox granular biomass.* Chem Eng J. 2017;327:881–8. http://dx.doi.org/10.1016/j.cej.2017.06.129.

42. Guo Y, Chen Y, Webeck E, Li YY. *Towards more efficient nitrogen removal and phosphorus recovery from digestion effluent: Latest developments in the anammox-based process from the application perspective.* Bioresour Technol. 2020; 299. https://doi.org/10.1016/j.biortech.2019.122560.

43. Magrí A, Company E, Gich F, Colprim J. *Hydroxyapatite Formation in a Single-Stage Anammox-Based Batch Treatment System: Reactor Performance, Phosphorus Recovery, and Microbial Community.* ACS Sustain Chem Eng. 2021; 9 (7): 2745–61. https://dx.doi.org/10.1021/acssuschemeng.0c08036.

44. Guo Y, Li YY. *Hydroxyapatite crystallization-based phosphorus recovery coupling with the nitrogen removal through partial nitritation/anammox in a single reactor.* Water Res. 2020; 187: 116444. https://doi.org/10.1016/j.watres.2020.116444.

45. Xue Y, Ma H, Kong Z, Li YY. *Formation Mechanism of hydroxyapatite encapsulation in Anammox-HAP Coupled Granular Sludge.* Water Res. 2021;193. https://doi.org/10.1016/j.watres.2021.116861.

46. Ma H, Zhang Y, Xue Y, Li YY. *A new process for simultaneous nitrogen removal and*

phosphorus recovery using an anammox expanded bed reactor. Bioresour Technol. 2018; 267 : 201–8. https://doi.org/10.1016/j.biortech.2018.07.044.

47. Chen Y, Sanjaya EH, Guo G, Li YY. *High nitrogen removal performance of anaerobically treated fish processing wastewater by one-stage partial nitritation and anammox process with hydroxyapatite (HAP)-based syntrophic granules and granule structure.* Bioresour Technol. 2021; 338: 125526. https://doi.org/10.1016/j.biortech.2021.125526.

48. Lin L, Zhang Y, Beckman M, Cao W, Ouyang T, Wang S. *Process optimization of anammox-driven hydroxyapatite crystallization for simultaneous nitrogen removal and phosphorus recovery.* Bioresour Technol. 2019; 290: 121779. https://doi.org/10.1016/j.biortech.2019.121779.

49. Xue Y, Ma H, Kong Z, Guo Y, Li YY. *Bulking and floatation of the anammox-HAP granule caused by low phosphate concentration in the anammox reactor of expanded granular sludge bed (EGSB).* Bioresour Technol. 2020; 310: 123421. https://doi.org/10.1016/j.biortech.2020.123421.

50. Guo Y, Li YY. *Hydroxyapatite crystallization-based phosphorus recovery coupling with the nitrogen removal through partial nitritation/anammox in a single reactor.* Water Res. 2020; 187. https://doi.org/10.1016/j.watres.2020.116444.

51. Chen Y, Guo Y, Feng G, Urasaki K, Guo G, Qin Y, et al. *Key factors improving the stability and the loading capacity of nitrogen removal in a hydroxyapatite (HAP)-enhanced one-stage partial nitritation/anammox process.* Chem Eng J. 2023; 452 (P4): 139589. https://doi.org/10.1016/j.cej.2022.139589.

52. Chen Y, Feng G, Guo G, Urasaki K, Kubota K, Li YY. *Improved Properties and Enhancement Strategies of Hydroxyapatite-Based Functional Granular Sludge for a High-Rate Partial Nitritation/Anammox System.* Environ Sci Technol. 2023; 57 (19): 7624–33. https://doi.org/10.1021/acs.est.3c00491.

53. Chen Y, Feng G, Guo G, Luo Z, Rong C, Wang T. *Nitrogen removal by a Hydroxyapatite-enhanced Micro-granule type One-stage partial Nitritation/anammox process following anaerobic membrane bioreactor treating municipal wastewater.* Bioresour Technol. 2022; 348: 126740. https://doi.org/10.1016/j.biortech.2022.126740.

54. Chen Y, Guo G, Li YY. *A review on upgrading of the anammox-based nitrogen removal processes: Performance, stability, and control strategies.* Bioresour Technol. 2022; 364:

127992. https://doi.org/10.1016/j.biortech.2022.127992.

55. Bauer PJ, Szogi AA, Vanotti MB. *Agronomic effectiveness of calcium phosphate recovered from liquid swine manure.* Agron J. 2007; 99 (5): 1352–6. https://doi.org/10.2134/agronj2006.0354.

56. Hao X, Wang C, Van Loosdrecht MCM, Hu Y. *Looking beyond struvite for P-recovery.* Environ Sci Technol. 2013; 47 (10): 4965–6. https://dx.doi.org/10.1021/es401140s.

57. Du J, Waite TD, Feng J, Lei Y, Tang W. Coupled electrochemical methods for nitrogen and phosphorus recovery from wastewater: a review. Environ Chem Lett [Internet]. 2023;21(2):885–909. Available from: https://doi.org/10.1007/s10311-023-01561-x

58. Liu Y, Deng YY, Zhang Q, Liu H. *Overview of recent developments of resource recovery from wastewater via electrochemistry-based technologies.* Sci Total Environ. 2021; 757: 143901. https://doi.org/10.1016/j.scitotenv.2020.143901.

59. Perera MK, Englehardt JD, Dvorak AC. *Technologies for Recovering Nutrients from Wastewater: A Critical Review.* Environ Eng Sci. 2019; 36 (5): 511–29. https://doi.org/10.1089/ees.2018.0436.

60. Devlin TR, Kowalski MS, Pagaduan E, Zhang X, Wei V, Oleszkiewicz JA. Electrocoagulation of wastewater using aluminum, iron, and magnesium electrodes. J Hazard Mater. 2019; 368: 862–8. https://doi.org/10.1016/j.jhazmat.2018.10.017.

61. Xie S, Bai Z, Shao W, Wang C, Qin J, Liu Z. *Phosphate removal by ex situ generated Fe (hydr)oxides from scrap iron electrocoagulation: the critical role of coprecipitation.* Environ Sci Adv. 2023; 2 (6): 898–907. https://doi.org/10.1039/d3va00024a.

62. Hug A, Udert KM. *Struvite precipitation from urine with electrochemical magnesium dosage.* Water Res. 2013; 47 (1): 289–99. http://dx.doi.org/10.1016/j.watres.2012.09.036.

63. Wang Y, Kuntke P, Saakes M, van der Weijden RD, Buisman CJN, Lei Y. *Electrochemically mediated precipitation of phosphate minerals for phosphorus removal and recovery: Progress and perspective.* Water Res. 2022; 209: 117891. https://doi.org/10.1016/j.watres.2021.117891.

64. Saha J, Kumar Gupta S. *The production and quantification of hydroxyl radicals at economically feasible tin-chloride modified graphite electrodes.* J Environ Chem Eng. 2018; 6 (4): 3991–8. https://doi.org/10.1016/j.jece.2018.05.049.

65. Clauwaert P, De Paepe J, Jiang F, Alonso-Fariñas B, Vaiopoulou E, Verliefde A.

Electrochemical tap water softening: A zero chemical input approach. Water Res. 2020; 169. https://doi.org/10.1016/j.watres.2019.115263.

66. De Paepe J, De Pryck L, Verliefde ARD, Rabaey K, Clauwaert P. *Electrochemically Induced Precipitation Enables Fresh Urine Stabilization and Facilitates Source Separation.* Environ Sci Technol. 2020; 54 (6): 3618–27. https://dx.doi.org/10.1021/acs.est.9b06804.

67. Ceballos-Escalera A, Pous N, Balaguer MD, Puig S. *Electrochemical water softening as pretreatment for nitrate electro bioremediation.* Sci Total Environ. 2022; 806. https://doi.org/10.1016/j.scitotenv.2021.150433.

68. Lei Y, Zhan Z, Saakes M, van der Weijden RD, Buisman CJN. *Electrochemical recovery of phosphorus from wastewater using tubular stainless-steel cathode for a scalable long-term operation.* Water Res. 2021; 199: 117199. https://doi.org/10.1016/j.watres.2021.117199.

69. Cid CA, Jasper JT, Hoffmann MR. *Phosphate Recovery from Human Waste via the Formation of Hydroxyapatite during Electrochemical Wastewater Treatment.* ACS Sustain Chem Eng. 2018; 6 (3): 3135–42. https://doi.org/10.1021/acssuschemeng.7b03155.

70. Takabe Y, Ota N, Fujiyama M, Okayasu Y, Yamasaki Y, Minamiyama M. *Utilisation of polarity inversion for phosphorus recovery in electrochemical precipitation with anaerobic digestion effluent.* Sci Total Environ. 2020; 706: 136090. https://doi.org/10.1016/j.scitotenv.2019.136090.

71. Zhang Q, Ba X, Liu S, Li Y, Cai L, Sun H. *Synchronous anodic oxidation-cathodic precipitation strategy for efficient phosphonate wastes mineralization and recovery of phosphorus in the form of hydroxyapatite.* Sep Purif Technol. 2021; 272 :118895. https://doi.org/10.1016/j.seppur.2021.118895.

72. Jin H, Yu Y, Zhang L, Yan R, Chen X. *Polarity reversal electrochemical process for water softening.* Sep Purif Technol. 2019; 210: 943–9. https://doi.org/10.1016/j.seppur.2018.09.009.

73. Lei Y, Geraets E, Saakes M, van der Weijden RD, Buisman CJN. *Electrochemical removal of phosphate in the presence of calcium at low current density: Precipitation or adsorption ?*. Water Res. 2020; 169: 115207. https://doi.org/10.1016/j.watres.2019.115207.

74. Lei Y, Du M, Kuntke P, Saakes M, Van Der Weijden R, Buisman CJN. *Energy Efficient Phosphorus Recovery by Microbial Electrolysis Cell Induced Calcium Phosphate Precipitation.* ACS Sustain Chem Eng. 2019; 7 (9): 8860–7.

https://doi.org/10.1021/acssuschemeng.9b00867.

75. Lei Y, Remmers JC, Saakes M, Van Der Weijden RD, Buisman CJN. *Influence of Cell Configuration and Long-Term Operation on Electrochemical Phosphorus Recovery from Domestic Wastewater*. ACS Sustain Chem Eng. 2019; 7 (7): 7362–8. https://doi.or/10.1021/acssuschemeng.9b00563.

76. Kabdaşlı I, Siciliano A, Limonti C, Tünay O. *Is K-Struvite Precipitation a Plausible Nutrient Recovery Method from Potassium-Containing Wastes?—A Review*. Sustain. 2022; 14 (18). https://doi.org/10.3390/su141811680.

77. Bagastyo AY, Anggrainy AD, Khoiruddin K, Ursada R, Warmadewanthi IDAA, Wenten IG. *Electrochemically-driven struvite recovery: Prospect and challenges for the application of magnesium sacrificial anode.* Sep Purif Technol. 2022; 288: 120653. https://doi.org/10.1016/j.seppur.2022.120653.

78. Shih K, Yan H. *The Crystallization of Struvite and Its Analog (K-Struvite) From Waste Streams for Nutrient Recycling*. Environmental Materials and Waste: Resource Recovery and Pollution Prevention. Elsevier Inc.; 2016. 665–686 p. http://dx.doi.org/10.1016/B978-0-12-803837-6.00026-3.

79. Govindan K, Im SJ, Muthuraj V, Jang A. *Electrochemical recovery of H2 and nutrients (N, P) from synthetic source separate urine water.* Chemosphere. 2021; 269: 129361. https://doi.org/10.1016/j.chemosphere.2020.129361.

80. Tan X, Yu R, Yang G, Wei F, Long L, Shen F. *Phosphate recovery and simultaneous nitrogen removal from urine by electrochemically induced struvite precipitation.* Environ Sci Pollut Res. 2021; 28 (5): 5625–36. https://doi.org/10.1007/s11356-020-10924-8.

81. Shan J, Liu H, Long S, Zhang H, Lichtfouse E. *Electrochemical crystallization for recovery of phosphorus and potassium from urine as K-struvite with a sacrificial magnesium anode.* Environ Chem Lett. 2022; 20 (1): 27–33. https://doi.org/10.1007/s10311-021-01333-5.

82. Li X, Zhu W, Wu Y, Wang C, Zheng J, Xu K. *Recovery of potassium from landfill leachate concentrates using a combination of cation-exchange membrane electrolysis and magnesium potassium phosphate crystallization.* Sep Purif Technol. 2015; 144: 1–7. http://dx.doi.org/10.1016/j.seppur.2015.01.035.

CHAPTER 2: Nutrient removal and recovery from agro-industrial wastewater through Partial Nitritation/Anammox process combined with downstream chemical phosphorus removal

Abstract

In conventional wastewater treatment plants, the soluble phosphorus (P) is recovered mainly through chemical crystallisation, with abundant use of chemicals and high production of sludge increasing the operational costs. Recently, many attempts were carried out to effectively combine P removal with biological nitrogen removal from nutrient-rich wastewater using downstream and upstream configurations. In this work, the feasibility of Partial Nitritation/Anammox process (PN/A) treating agro-industrial anaerobic digestion supernatant was assessed and the possible advantages of P removal from its effluent were explored through chemical precipitation tests. PN/A process was operated according to a single-stage configuration in a 3L sequencing batch reactor operated for 118 days achieving over 80% as nitrogen and alkalinity removal while specific anammox activity increased up to 0.40 ± 0.07 gN_2 $(gMLVSS \cdot d)^{-1}$. The biological process effectively decreased the effluent buffer capacity leading to a reduction of ca. 90% NaOH (5M) in dosing costs when pH was increased at 10.5 (i.e., 0.71 € m^{-3} vs 0.03 € m^{-3} considering influent and effluent, respectively), confirming downstream advantages over upstream process. A set of batch precipitation experiments was performed on the PN/A to investigate the influence of operational parameters such as pH (i.e., from 7.5 to 10.5), calcium (Ca)/P ratio (i.e., 1.64; 2.00), and temperature (i.e., 25°C; 35°C) on P and cations removal from PN/A effluent. pH increase and Ca/P increase favoured calcium phosphate (CaP) precipitation achieving a complete P removal and Ca^{2+} removal up to 75% when pH≥10 and 2.00 Ca/P ratio were tested. Magnesium (Mg^{2+}) removal was limited but enhanced by pH rising, and, consistently, was more effective for lower Ca/P. The rise in temperature from 25°C to 35°C did not negatively affect P and Ca removal, suggesting that the operative bioreactor temperature would not represent a limiting factor for concomitant P precipitation. CaP minerals are the main product resulting from batch precipitation tests. Hydroxyapatite presence was detected in the precipitated product through Fourier Transform Infrared analysis as the main characterising chemical groups were identified (i.e., PO_4^{3-} at ca. 550 cm^{-1} and. 1000 cm^{-1}; CO_3^{2-} at 1400-1580 cm^{-1}; OH^- at 3500-3800 cm^-

[1]), while X-ray powder diffraction patterns evidenced the low crystallinity of the solids as the product was likely formed by a mixture of amorphous calcium phosphate and hydroxyapatite.

2.1 Introduction

In the last decades, the global P demand has been increasing mainly due to food production which is supported by the intense use of fertilisers on crop cultures and phosphate-based feed for livestock. These are responsible for about 82% and 7%, respectively (1), of P industrial natural deposits exploitation, namely phosphate rock (PR). The mining of PR is a very topical issue since these are dwindling resources, unevenly distributed around the globe. Annually, around 50 Mt of P is extracted from the earth (2), mainly in China (1), which makes European agriculture reliant on imported PR (3). Thus, since 2014, PR and P have been identified by the European Union as 2 of the 27 critical raw materials (4). Such conditions, combined with the PR economic volatility could create vulnerability to the food industry and future political tensions (1,2,5). On the other hand, there are environmental concerns regarding phosphate overabundance in soils for the risk of P leaching into water bodies possibly leading to eutrophication. This twofold problem points out the compelling need for sustainable P management and efficient recovery and recycling systems. Many physical/chemical approaches have been developed to recover P from wastewater liquid phase, sludge, and ashes. A lower recovery rate is usually associated with the liquid phase (50–60% vs 90% considering recovery from sludge and its ashes) but with minor energy demand and generating fewer emissions (2). In conventional wastewater treatment plants (WWTPs), the soluble P is recovered mainly through chemical crystallisation, with abundant use of reagents and high production of sludge increasing the operational costs. Recently, many attempts to efficiently combine multi-nutrient treatment, such as nitrogen (N) and P removal have been carried out. Biological N removal (BNR) is commonly used to reduce ammonium nitrogen (NH_4^+-N) content in wastewater. The conventional approach involves autotrophic nitrification (conversion of ammonium to nitrite and nitrate) and heterotrophic denitrification (conversion of nitrate to nitrogen gas), but increasing interest is given to the PN/A process. This fully autotrophic method presents several advantages when compared to the conventional Nitrification/Denitrification process. In fact, the need for carbon addition (and concomitant increased sludge production) is omitted, the oxygen consumption (i.e., energy requirement) is reduced by 60%, the excess sludge production is limited by 80%, and finally, it is characterised by lower greenhouse gases (e.g., nitrous oxide) emissions (6,7). Particularly, PN/A process integration with anaerobic digestion for biogas production is advantageous as it does not require organic C source. From a P recovery perspective, biological treatment based on nitrification

involves a reduction in the buffering capacity of the process effluent. Thus, particular interest was devoted to downstream precipitation taking advantage of the intense alkalinity consumed related to biological treatment. The lower buffer capacity of wastewater treated with biological N removal results in a limited chemicals consumption for pH increasing. Additionally, the alkaline environment achieved during precipitation may enhance water sanitation by promoting pathogen destruction (8). To the author knowledge a limited number of studies were performed on PN/A downstream P chemical precipitation (9–11).

In this work, the feasibility of PN/A process treating agro-waste anaerobic digestion supernatant was assessed and P removal from its effluent was explored through batch chemical precipitation tests. PN/A process was operated according to a single-stage configuration in a 3L sequencing batch reactor (SBR). Removal performance and biomass activity were monitored during 118 days of operation. PN/A influent and effluent were characterised through titration tests with NaOH (5M) demonstrating the advantages related to the downstream process. For the same purpose, saturation indexes (SIs) of possible mineral phases were calculated by Visual MINTEQ for PN/A influent and effluent. A set of batch precipitation experiments was performed to investigate the influence of operational parameters such as pH, Calcium (Ca)/P ratio and temperature on P and cations removal from PN/A effluent. pH was raised through NaOH (5M) dosage and Ca^{2+} level was increased by $CaCl_2$ addition. Temperature influence was studied increasing from ambient temperature to 35°C which is the operational temperature of the bioreactor. Recovered products were characterised to identify the main mineral phases.

2.2 Materials and methods

2.2.1 Partial Nitritation/Anammox reactor and experimental operation

The PN/A process was operated according to a single-stage configuration in a glass 3L SBR (Figure S2.1). The bioreactor was inoculated by ANAMMOX© granulated biocatalyst purchased from Paques Europe B.V. coming from the sewage treatment plant in Olburgen (Netherlands), treating wastewater deriving from potatoes production industry. The reactor was operated in fed-batch mode and run with 6-hour working cycles (300 min aerobic phase, 40 min anoxic phase, 15 min sedimentation phase and 5 min withdrawal phase) resulting in 4 cycles per day. The feeding phase was included in the aerobic phase and presented a variable length depending on the targeted operative parameters; influent flow rate was set at 2.0 mL min^{-1}. Oxygen was provided in the bulk liquid through a porous stone using an air compressor. The airflow rate was controlled within the range of

0.05-0.1L/min by an airflow meter, according to nitrite and ammonium accumulation. To assure anaerobic conditions during the anoxic phase inert N_2 gas was sparged in the SBR. Process temperature was controlled at 35 ± 1 ºC by a water jacket and a thermostatic bath (HAAKE, mod. F3-K), and the dissolved oxygen concentration was maintained below 0.2 mgO_2 L^{-1} to preserve anammox bacteria from oxygen inhibition. Mechanical mixing was provided by a double helix marine impeller (70±5 rpm). The pH was maintained within the selected range (7.0-8.0) using 0.5M HCl and 0.5M NaOH. To avoid any external light penetration hindering anammox bacteria activity (12), the vessel was completely shielded with aluminium foil. Temperature, pH, ORP, and DO monitoring were performed using Improv 4280i and 6850i probes (Mettler-Toledo), respectively, connected to a digital transmitter (Mettler Toledo, mod. M400). Process timing and control were performed via a programmable logic module (Siemens, LOGO!, mod. 230rce) connected to the configured electrical panel.

The single-stage PN/A process was run for approximately 118 days. The nitrogen loading rate (NLR) was increased from 0.21 to 0.30 kgN $(m^3 \cdot d)^{-1}$ by lengthening the feeding phase, corresponding to HRT of 3.6 and 2.5 d in phases I and II, respectively. NLR increase was applied when nitrogen removal efficiency showed stable values for at least 3 HRT.

2.2.2 Wastewater characteristics

The wastewater fed to the bioreactor was a supernatant collected at the Aguilera S.r.l. anaerobic digestion plant (Ecopoets, Sardinia, Italy), treating agro-industrial wastes (e.g., crop residues) to produce biogas. After arriving in the lab, the anaerobic digestion supernatant was centrifuged, filtered to remove solids, and collected in plastic tanks. Before feeding, the pre-treated wastewater was flushed with N_2 gas for 25 minutes to avoid any presence of oxygen and placed in a plastic bag, ready to be pumped into the bioreactor. To evaluate P removal potential, this wastewater was employed also for the batch chemical precipitation tests. Since the PN/A process consumed alkalinity and ammonium nitrogen, converting a portion of it into nitrate (theoretically 11% of the influent ammonium nitrogen), the bioreactor effluent presented limited alkalinity and ammonium nitrogen and was enriched in nitrate. The PN/A effluent was collected by the end of phase I and phase II and was used for chemical precipitation batch tests. This strategy allowed to avoid the interference of alkalinity and NH_4^+-N on P chemical removal. Average influent and effluent characterisation are provided in Table 2.1.

Table 2.1 - Average composition of the influent wastewater fed to the bioreactor and the corresponding effluent; AV: average, SD: standard deviation.

Characterisation		**Influent**		**Effluent**	
parameter	unit	AV	SD	AV	SD
pH	-	8.3	0.1	7.3	0.1
EC	mS cm^{-1}	15	3	13	2
NH_4^+-N	mg L^{-1}	744	16	10	3
NO_2^- -N	mg L^{-1}	0	0	0	0
NO_3^--N	mg L^{-1}	0	0	79	5
PO_4^{3-}-P	mg L^{-1}	29	1	29	2
SO_4^{2-}	mg L^{-1}	24	3	26	6
Cl^-	mg L^{-1}	3060	210	3471	235
Mg^{2+}	mg L^{-1}	119	5	117	8
Ca^{2+}	mg L^{-1}	64	3	63	7
K^+	mg L^{-1}	2130	14	2006	30
Na^+	mg L^{-1}	1057	10	1010	13
Alkalinity	mM HCO_3^-	63	5	2	1
COD	mg L^{-1}	218	3	190	10
BOD_5	mg L^{-1}	34	5	34	5
TSS	g L^{-1}	0.21	0.10	0.19	0.11
VSS	g L^{-1}	0.20	0.08	0.17	0.10
Ca/P	mol mol^{-1}	1.64	0.07	1.64	0.09
Mg/P	mol mol^{-1}	5.28	0.04	5.24	0.09

Abbreviations: BOD_5, 5 days biochemical oxygen demand; COD, chemical oxygen demand; EC, electrical conductivity; TSS, total suspended solids; VS, volatile solids; VSS, volatile suspended solids

For comparing upstream and downstream precipitation, the alkali agent demand was estimated experimentally based on a titration test using NaOH (24) on PN/A influent and effluent. Moreover, supersaturation conditions for the different operating parameters tested during batch precipitation tests were evaluated through Visual MINTEQ (13) simulation.

PN/A effluent was collected in plastic tanks and stored at room temperature prior to precipitation tests. To assess Ca/P ratio influence on P removal, a portion of the influent and effluent from the SBR

was doped through concentrated calcium solution ($CaCl_2 \cdot 2H_2O$, 1M) dosage increasing the Ca^{2+} concentration from 63 to 70 mgCa^{2+} L^{-1}. Consequently, the increase in Ca^{2+} concentration led to the corresponding Ca/P ratio increase, which raised from the initial 1.64 mol/mol (Table 2.1) to 2 mol/mol.

2.2.3 Chemical precipitation batch tests

Different influencing parameters such as pH, initial Ca/P ratio and temperature were evaluated in duplicate through batch experiments (Table 2.2). To examine the required reaction time, 0.5 L of PN/A effluent was placed in a beaker, and it was continuously stirred with a magnetic hotplate stirrer. The pH was increased to pH 10 with NaOH (5M) and samples were taken at regular intervals. The test was performed at ambient temperature (25±1ºC). The same 0.5 L-batch equipment was used to study pH influence on precipitation: the pH was increased with NaOH (1M) to 8.0 or 8.5 and after 15 min of continuous stirring, samples were taken for analysis. Afterwards, the pH was further increased in steps of half a pH unit up to a final pH of 10.5 and every time, after 15 min of reaction, a liquid sample was taken for analysis. This assay was repeated to study the Ca/P (i.e., 1.64 and 2.00) and the temperature influence (i.e., 25ºC and 35ºC). In the first case study, Ca/P was increased from the original value (1.64) to 2.00 by the addition of Ca^{2+} ions as concentrated $CaCl_2 \cdot 2H_2O$ solution (1M) to the wastewater before increasing the pH. In the second case study the temperature influence was studied by increasing the solution temperature from ambient temperature to 35ºC through the magnetic hotplate stirrer prior to pH increase. Precipitate samples were collected by the end of precipitation tests. Solids were allowed to settle for 30 min then the supernatant was discarded, and the precipitated product was collected for further analysis.

Table 2.2 – Summary of the different influencing operative parameters tested during the batch precipitation experiments.

TEST	T (ºC)	Ca/P (mol/mol)	pH (-)
1	25	1.64	8 – 10.5
2	25	2.00	8 – 10.5
3	35	1.64	8 – 10.5
4	35	2.00	8 – 10.5

2.2.4 Analytical methods

Samples were periodically collected from influent (once every two weeks), and effluent (three times per week), to evaluate process performances. NH_4^+-N concentration was measured according to

Standard Methods (14) by spectrophotometric analysis (DR2800, Hach Lange, Germany) at a wavelength of 420 nm. Liquid samples were also analysed for quantification of anions, namely chloride (Cl^-), nitrite (NO_2^--N), nitrate (NO_3^--N), phosphate (PO_4^{3-}-P), and sulphate (SO_4^{2-}), using an ion chromatograph (ICS-90, Dionex-Thermofisher, USA) equipped with an AS14A Ion-PAC 5 μm column. Before analysis, samples were filtered (acetate membrane filter, 0.45 μm porosity) and properly diluted with grade II water. The concentrations of the main cations, namely calcium (Ca^{2+}), and magnesium (Mg^{2+}), were determined using an ICP/OES (Varian 710-ES, Agilent Technologies, USA): samples were filtered (acetate membrane filter, 0.45 μm porosity), acidified (nitric acid, 1% v:v) and diluted with grade I water. Alkalinity was measured by potentiometric titration to preselected end-point pH, using an automatic titrator (AT-510, KEM electronics). Free Ammonia (FA) and Free Nitrous Acid (FNA) levels were calculated according to Anthonisen et al. (15). Total COD and soluble COD (i.e., after filtration of samples through a 0.45 μm membrane) concentrations were determined according to Standard Methods (14). Mixed liquor samples were periodically collected from the bioreactor once every two weeks to monitor mixed liquor total suspended solids (MLSS) and mixed liquor volatile suspended solids (MLVSS); both concentrations were determined according to Standard Methods (14).

During batch precipitation tests, pH and temperature were measured using a benchtop meter (mod. HI5522, Hanna Instruments, Italy). Total solids (TS) and volatile solids (VS) were measured according to Standard Methods (14). The mineralogical composition of precipitated solids was carried out by X-ray powder diffraction (XRD) technique, on samples dried at 40 °C. Analysis was performed using a Rigaku Geiger Flex diffractometer equipped with a Cu X-Ray tube, operating at 30kV and 30mA. All XRD analyses were performed in the range from 4 to 70° of 2θ. The Fourier Transform Infrared (FT-IR) spectra of powdered samples were recorded on a Jasco 6300 FT-IR spectrometer having an optical resolution of 0.09 cm^{-1}, in the range from 400 cm^{-1} to 4000 cm^{-1} in a KBr disc medium.

2.2.5 Calculations

Considering the PN/A bioreactor, nitrogen loading rate (NLR [kg N $(m^3\ d)^{-1}$]) is the influent nitrogen total mass that is fed in one day (4 operational cycles per day) over the reactor's working volume. It was calculated using the following expression:

$$NLR = \frac{(NH_4\text{-}N + NO_2\text{-}N + NO_3\text{-}N)_{infl} \times n \times V_{feed}}{V_{TOT}} \qquad (Eq.\ 1),$$

where NH_4–N, NO_2–N and NO_3–N are the main nitrogen species concentrations [g L^{-1}], n is the number of cycles (i.e., 4), V_{feed} is the volume fed during each cycle [L $cycle^{-1}$] and V_{TOT} is the reactor's working volume [L].

Nitrogen removal rate (NRR [kgN $(m^3 \cdot d)^{-1}$] is expressed by considering the nitrogen mass balance in the reactor, as follows:

$$NRR = \frac{((NH_4\text{-}N + NO_2\text{-}N + NO_3\text{-}N)_{infl} - (NH_4\text{-}N + NO_2\text{-}N + NO_3\text{-}N)_{effl})}{HRT} \quad (Eq.2),$$

where HRT is the hydraulic retention time [d].

Removal efficiency of nitrogen, ammonium-nitrogen, and phosphorus (NRE [%], NH_4-RE [%], PRE [%], respectively) was determined through the following equation:

$$NRE = \frac{((NH_4\text{-}N + NO_2\text{-}N + NO_3\text{-}N)_{infl} - (NH_4\text{-}N + NO_2\text{-}N + NO_3\text{-}N)_{effl})}{(NH_4\text{-}N + NO_2\text{-}N + NO_3\text{-}N)_{infl}} \times 100 \quad (Eq.3),$$

$$NH_4\text{-}RE = \frac{((NH_4\text{-}N)_{infl} - (NH_4\text{-}N)_{effl})}{(NH_4\text{-}N)_{infl}} \times 100 \quad (Eq.4),$$

$$PRE = \frac{((P)_{infl} - (P)_{effl})}{(P)_{infl}} \times 100 \quad (Eq.5).$$

The Specific Anammox Activity (SAA) was determined using the chemical tracking method outlined by Van Loosdrecht et al. (16). Kinetic tests were conducted *in situ* (i.e., in the bioreactor) by introducing a solution with both NO_2^- and NH_4^+ (2 gN L^{-1} each, as $NaNO_2$ and NH_4Cl) to establish initial concentrations of 40 mgN/L for both ammonium and nitrite at the end of the feeding phase. Samples were periodically collected and analysed to monitor nitrite, nitrate, and ammonium levels. Linear regression of the data provided volumetric ammonium and nitrite removal rates (r_{NH4} and r_{NO2}, respectively), and nitrate production rate (r_{NO3}), expressed as gN $(L \cdot d)^{-1}$. Finally, SAA (gN_2 $(gMLVSS \cdot d)^{-1}$) was calculated as follows:

$$SAA = \frac{(r_{NH4} + r_{NO2} - r_{NO3})}{MLVSS} \quad (Eq.6).$$

For comparison purposes between upstream and downstream P removal process, the alkali demand of the PN/A influent and effluent was estimated experimentally based on a titration test using NaOH (24).

Considering the composition of the influent and effluent wastewater, the supersaturation conditions and possible mineral phases formed were assessed using the freeware Visual MINTEQ software (13).

The saturation index (SI, $\log_{10}(IAP/K_{sp})$) was calculated as a function of the corresponding ion activity product (IAP) and the mineral phase solubility product constant (K_{sp}). If the SI for a particular mineral is positive, the system is supersaturated with respect to that mineral, and precipitation may occur. Values for the K_{sp} of the mineral phases bobierrite (10-25.2), cattiite (10-23.1), K-struvite (10-12.2), and Na-struvite (10-11.6) were added to the MINTEQ original database according to other sources (32,33).

Regarding batch precipitation tests, P, Ca, and Mg removal efficiencies were calculated as follows:

$$PRE = \frac{((P)_{t0} - (P)_t)}{(P)_{t0}} \times 100 \qquad (Eq.7),$$

$$CaRE = \frac{((Ca)_{t0} - (Ca)_t)}{(Ca)_{t0}} \times 100 \qquad (Eq.8),$$

$$MgRE = \frac{((Mg)_{t0} - (Mg)_t)}{(Mg)_{t0}} \times 100 \qquad (Eq.9),$$

where P, Ca and Mg is phosphorus, calcium, and magnesium concentration [mg L^{-1}] at t_0 which is the start of the test and t which is the generic time of operation.

2.3 Results and discussion

2.3.1 PN/A operation results

The PN/A bioreactor was run at 35±1 ºC for 118 days and fed with anaerobically digested agro-industrial wastewater (Table 2.1). Main results and operating conditions are shown in Table 2.3. By the end of phase I and phase II, N decrease over 80% was achieved with effluent NH_4^+-N concentrations of 13 ± 2 and 15 ± 3 mgN L^{-1}, respectively. Moreover, influent alkalinity was reduced due to bicarbonate consumption by PN/A process, resulting in 125 ± 11 and 120 ± 7 mg$CaCO_3$ L^{-1} in phase I and II respectively. As NH_4^+-N was removed, nitrate levels in the effluent increased due to anammox process and probably due to the presence of nitrite-oxidizing bacteria (Figure S2.2). The nitrate build-up was solved by more accurate flow-rate regulation and the introduction (day 54) of alternated aerating sequences in the aerobic phase following Magrí et al. (17) strategy. In each cycle, 6 repetitive aeration sequences lasting 30 min each were set; every sequence was alternated by 15 min of no aeration. SAA was monitored during the bioreactor operation to ensure the absence of possible biomass inhibition due to the real wastewater feeding. SAA increased consistently with the NLR increase, from 0.21 ± 0.04 up to 0.40 ± 0.07 gN_2 $(gMLVSS \cdot d)^{-1}$. The real wastewater treatment

showed no inhibiting effect as NLR was increased, showing high nitrogen removal and SAA enhancement along the bioreactor operation. Ca^{2+} and Mg^{2+} were not removed in significant amounts by PN/A process (Table 2.1) while some occasional and slight P removal was detected but not during stable N removal conditions. Thus, the concentrations of these ions remained virtually unchanged after the biological treatment. The effluent to be tested in batch chemical precipitation experiments was collected during stable nitrogen removal conditions in phase I and II (i.e., NRE > 80%) and stored in plastic tanks at ambient temperature.

Table 2.3 – Operational parameters and main results of PN/A process operation treating agro-industrial wastes anaerobic digestion supernatant; AV: average, SD: standard deviation.

Phase			**I**	**II**
Time	(d)		0-26	27-120
HRT	(d)		3.6	2.5
NLR	(kgN $(m^3 \cdot d)^{-1}$)	AV	0.21	0.30
		SD	0.001	0.003
NRE	(%)	AV	80%	88%
		SD	2%	5%
NRR	(kgN $(m^3 \cdot d)^{-1}$)	AV	0.20	0.29
		SD	0.005	0.008
MLVSS	(g L^{-1})	AV	4.64	6.40
		SD	0.06	0.31
SAA	gN_2 $(gMLVSS \cdot d)^{-1}$)	AV	0.24	0.37
		SD	0.035	0.051

2.3.2 Influent and effluent characterisation

The agro-industrial wastewater presented a typical brownish colour and a limited TSS content (ca. 0.21 gTSS L^{-1}) (Table 2.1). The pH of PN/A influent and effluent (8.3 and 7.3, respectively) was notably below the suitable pH-range for most of P minerals precipitation (i.e., 9.0–12.0). Hence, the addition of an alkali agent was needed to achieve P removal. In the pH-range from 8.5 to 12.0, the addition of NaOH (5M) to the PN/A influent resulted in a linear increase of the pH-value (Figure 2.1), while for the effluent the pH rise slowed down over pH 11. The lower buffer capacity of the effluent is related to the alkalinity consumption of the biological treatment resulting in a reduced concentration (ca. from 3.8 to 0.12 g HCO_3^- L^{-1}). This limited buffer capacity implied a moderate demand compared to the PN/A influent; a NaOH volume of 10.2 mL was needed to achieve pH 10 in 1L-influent, while only 2.9 mL was needed for the same amount of effluent. As market price for the alkali reagent, 0.50

€ kg^{-1} NaOH (18) was assumed, resulting in 0.71 € m^{-3} vs 0.03 € m^{-3}. Thus, PN/A treatment allowed to decrease of ca. 90% in NaOH dosing costs to achieve the same pH. The combination of the PN/A process for NH_4^+-N and alkalinity removal with following chemical precipitation for P recovery seems promising in terms of limiting environmental pollution and reducing operative costs connected to chemicals. Particularly, some authors reported the interference with NH_4^+-N and alkalinity resulting in lower removal efficiency and higher chemical consumption (9,19). To complement the economic evaluation of PN/A process combined with downstream P precipitation a cost-analysis of the biological process would be needed. Nevertheless, these preliminary results are critical factors within the economic and technological assessment for P downstream removal.

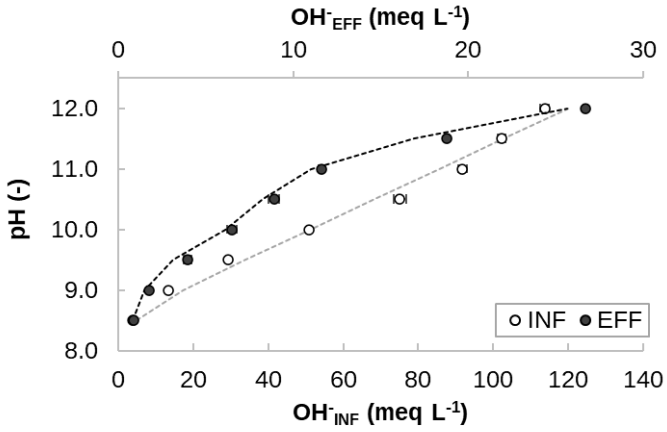

Figure 2.1 - Requirements of alkali as NaOH to raise the pH of the PN/A influent and effluent (primary and secondary x-axis, respectively), including measured (dots) and simulated values through Visual MINTEQ (dashed line) (13).

In an alkaline environment, P can precipitate forming different minerals depending on the availability of complementary ions. Particularly, molar ratios such as Ca/P and Mg/P (Table 2.1) can provide a first indication of whether the wastewater is suitable for phosphate precipitation as magnesium phosphate or as calcium phosphate. Struvite-type material recovery is commonly adopted to simultaneously remove N-NH_4 (magnesium ammonium phosphate, $MgNH_4PO_4 \cdot 6H_2O$, stoichiometric ratio 1.0:1.0:1.0 Mg:NH_4:PO_4) or potassium (magnesium potassium phosphate, $MgKPO_4 \cdot 6H_2O$, stoichiometric ratio 1.0:1.0:1.0 Mg:K:PO_4). The target wastewater in our study presents high levels of N-NH_4, but the P low concentration (Table 2.1) does not favour struvite precipitation over other P minerals. Mg^{2+} and P can precipitate also in the form of Cattiite ($Mg_3(PO_4)_2 \cdot 22H_2O$) or Bobierrite ($Mg_3(PO_4)_2 \cdot 8H_2O$) when Mg/P ratio is close to 1.5. However, also in this case the precipitation could be hindered by the low P level of the agro-industrial wastewater. On the other hand, calcium phosphate minerals such as amorphous calcium phosphate (ACP,

$Ca_xH_y(PO_4)_z \cdot nH_2O$, stoichiometric ratio of 1.3-1.5 Ca/P) and hydroxyapatite (HAP, $Ca_{10}(PO_4)_6 \cdot (OH)_2$, stoichiometric ratio of 1.67 Ca/P) are expected to precipitate since the target wastewater presents a Ca/P ratio of 1.64. Besides, a decisive prediction is not possible since other parameters such as initial P concentration, pH, temperature, and ionic strength concur in the precipitation of the P products. Thus, the SI was calculated as function of pH through Visual MINTEQ (13) for the PN/A influent and effluent. Values reported in Table 2.1 were used as input data for the simulation. When the calculated SI is positive, supersaturation conditions are established for the specific mineral phase. This condition led to spontaneous nucleation and consequently, crystallisation is expected to take place. Indeed, positive SI is not sufficient for precipitation, as the activation energy barrier hinders the ions' aggregation into crystalline structures. However, high SI can help overcome this barrier and a pH increase can promote supersaturation. Considering PN/A influent and effluent, the highest calculated SI corresponded to HAP always showing a positive value in the simulated pH-range (Table 2.4). Thus, HAP precipitation was identified as the most probable mineral phase to be obtained from both PN/A influent and effluent. Yet, HAP precipitation is a relatively gradual process. Consequently, the transient creation of intermediate phases, which are metastable states but display a quicker formation rate, such as ACP, is also plausible (8). Then, these precursor phases may undergo a gradual transformation into HAP. Considering these aspects and the resulting SI for PN/A influent and effluent, ACP may be also considered as a probable precipitate product. From simulation results, magnesium phosphate minerals presented lower SI than calcium phosphate species. These findings suggest that this kind of wastewater is more suited for calcium phosphate precipitation. However, other compounds such as calcium and magnesium carbonates can precipitate due to bicarbonate presence. These salts are not interesting for P removal and can compete in the hydroxyls (OH^-) consumption. PN/A effluent showed lower SI of carbonate species compared to the influent, due to the lower bicarbonate levels resulting from the biological process. Thus, the PN/A effluent looks more promising for obtaining a higher-quality P recovery, due to the lower bicarbonate interference and possibly limited co-precipitation of carbonate compounds.

Table 2.4 - Saturation indexes (SIs) for possible mineral phases (SI>0) in the PN/A influent and effluent as a function of the pH value. Calculations were made using MINTEQ and based on average ionic concentrations resulting from the wastewater characterisation (Table 2.1).

	pH (u.pH)									
	8		9		10		11		12	
	SI (-)									
Mineral phase	INF	EFF	INF	EFF	INF	EFF	INF	EFF	INF	EFF
Hydroxyapatite ($Ca_{10}(PO_4)_6\cdot(OH)_2$)	10.8	11.5	13.9	15.2	16.0	17.8	16.9	19.0	18.1	19.9
Amorphous calcium phosphate $Ca_3(PO_4)_2$	1.6	1.9	3.0	3.8	3.8	4.9	3.9	5.0	4.1	5.1
Newberyte $Mg_3(PO_4)_2$	-1.7	-1.4	0.0	0.5	1.2	1.9	1.7	2.4	1.9	1.8
Cattiite ($Mg_3(PO_4)_2\cdot22H_2O$)	-1.9	-1.6	-0.2	0.3	1.0	1.7	1.5	2.2	1.6	1.5
K-Struvite ($MgKPO4\cdot6H_2O$)	-0.2	-0.2	0.7	0.8	1.4	1.5	1.8	1.8	1.9	1.6
Na-Struvite ($NaMgPO_4\cdot7H_2O$)	-0.9	-0.8	0.0	0.1	0.7	0.9	1.0	1.2	1.1	1.0
Calcite ($CaCO_3$)	1.4	-0.3	2.1	0.5	2.3	0.4	2.3	1.4	2.2	1.4
Dolomite ($CaMg(CO_3)_2$)	3.4	0.1	4.9	1.7	5.4	1.6	5.5	3.7	5.3	3.4
Magnesite ($MgCO_3$)	0.9	-0.8	1.6	0.0	2.0	0.0	2.1	1.1	2.0	0.9
Brucite ($Mg(OH)_2$)	-5.7	-5.6	-3.8	-3.6	-2.0	-1.6	-0.3	0.3	1.6	2.0

Finally, the same simulation was performed considering a Ca/P ratio of 2 and considering 35ºC for PN/A effluent. SI profiles in the tested pH-range are shown in Table S2.1, for the main calcium phosphate and magnesium phosphate species. The supersaturation of calcium phosphate mineral was slightly enhanced by the increasing Ca/P ratio. Conversely, SIs of magnesium phosphate salts decreased with the boost of Ca^{2+} level. Finally, all the species supersaturation was limited by higher temperatures as it increases the salts' solubility. Particularly, magnesium phosphate mineral supersaturation was the most affected by Ca/P ratio and temperature rise.

2.3.3 Main influencing parameters in P precipitation

The influence of pH, Ca/P ratio and temperature on P removal was studied by batch precipitation experiments using PN/A influent and effluent. Each test was performed in duplicate. Literature suggests that a slightly alkaline environment (pH 9.5-10) can promote calcium phosphate precipitation, while higher values are typically associated with the formation of calcium carbonate ($CaCO_3$) which can decrease crystallinity or inhibit CaP precipitation (20). Thus, precipitation tests were performed between 7.5 and 10.5 as the optimal pH range. To evaluate the reaction time, the pH was increased to a target value (i.e., 10.0) at constant temperature (i.e., 25 °C) and liquid samples were collected at regular intervals to calculate ions removal. At such conditions, P, Ca^{2+}, and Mg^{2+} concentrations decreased promptly and reached a stable value (Figure S2.3). The rise in the pH

resulted in an instant precipitation, and the equilibrium was achieved within 15 min. Moreover, this behaviour was not affected by the Ca/P ratio.

PRE, CaRE and MgRE were calculated in the tested pH range for the original PN/A effluent and after increasing the Ca/P ratio (Figure 2.2). As pH increased, ions removal efficiency was promoted. Complete P removal was achieved at 10 pH (for Ca/P = 2) and 10.5 pH. According to Fernandes et al. (21), PRE higher than 98% could be obtained at pH 10 depending on the Ca/P ratio. Even though P was completely removed at high pH, dissolved Ca^{2+} and Mg^{2+} were still present. Since P is the limiting element in the target wastewater, a complete cations removal was not feasible. Particularly, Ca^{2+} was the main cation removed with efficiency reaching up to 75%. The increased Ca/P ratio promoted P and Ca^{2+} removal, as expected. Suzin et al. (9) previously worked with chemical P removal downstream to PN/A process treating anaerobically digested swine manure. When Ca/P was increased to 2 through hydrate lime dosing, 54% PRE was achieved at pH 9. Considering equal values of Ca/P and pH, this work showed a similar resulting PRE (60%). Mg^{2+} removal was also enhanced by pH rising, though its efficiency remained below 20% and, consistently, it was more effective when the Ca/P ratio was lower. Higher Ca/P increased the SI of calcium phosphate minerals, whose precipitation was favoured over magnesium phosphate salts.

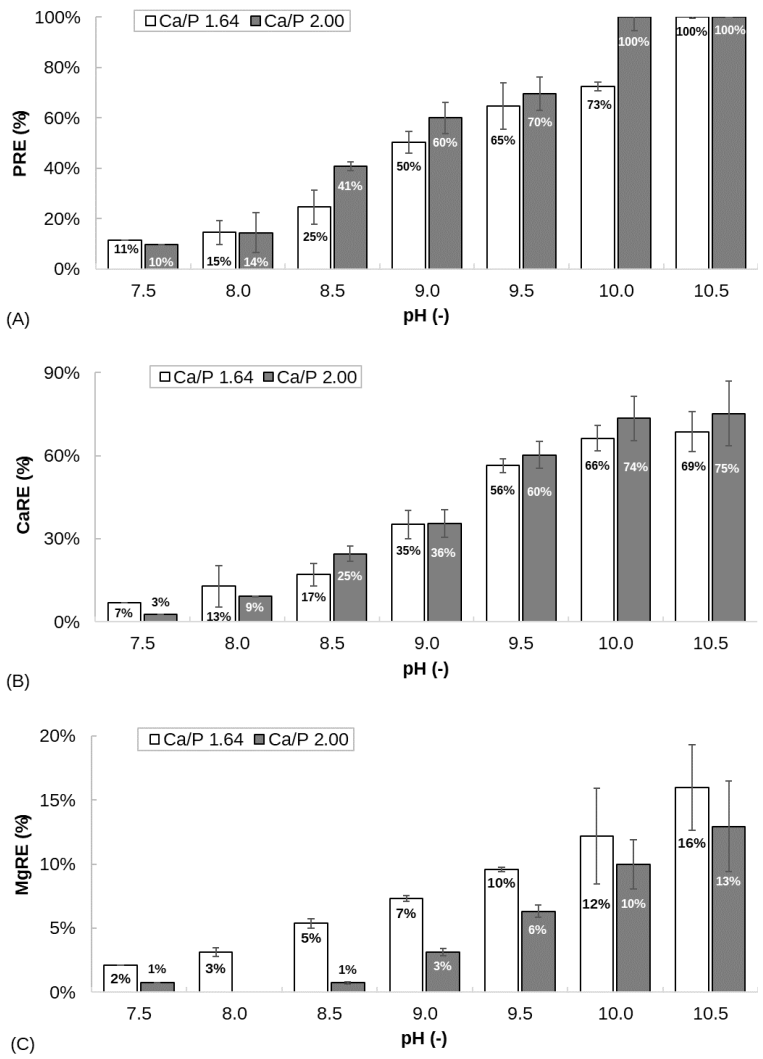

Figure 2.2 – Removal efficiency of P, Mg, Ca^{2+} (PRE (A), MgRE (B) and CaRE (C), respectively), at 25 ºC, as a function of pH in the original PN/A effluent (Ca/P = 1.64) and after increasing the Ca/P ratio to 2.00.

Considering a fixed pH (e.g., 10 pH), the impact of raising effluent temperature was explored. Since the operational temperature of PN/A process was 35ºC, it was selected for comparison to ambient temperature. Mineral phases solubility and, consequently, supersaturation are affected by temperature. Calcium phosphate salts solubility decreases with lower temperature, leading to a higher supersaturation. Thus, precipitation should be improved by decreasing temperature.

HAP synthesis is a relatively slow process that could benefit from increased crystallisation time. Previous studies reported that lowering relative supersaturation to reduce the rates of crystallisation can lead to improved HAP precipitation (22). Considering a fixed pH and Ca/P ratio, no evident impact in terms of P, Ca^{2+} and Mg^{2+} removal was detected by raising temperature from 25°C to 35°C. Johanson et al. (11) reported a reduced removal efficiency when temperature was increased from 20 to 40 ºC treating urban wastewater centrate for struvite recovery. In this work, a higher Ca/P ratio led

to a complete P removal at pH 10 for both tested temperatures (Figure 2.3). Thus, an adequate Ca/P ratio could allow to completely recover P even at the actual bioreactor effluent temperature (i.e., 35ºC). Furthermore, this finding is promising for the implementation of biological P removal in the PN/A bioreactor. Consequently, increasing Ca/P ratio emerges as a promising strategy for promoting P removal while preserving the biomass growth benefit by operation at 35ºC. However, it's worth noting that, since P is the limiting nutrient, the Ca^{2+} dosing strategy to enhance P removal resulted in increased calcium levels in the treated wastewater, thereby increasing its polluting potential. This drawback was previously mentioned in the literature as something to be mindful of when adopting chemical precipitation processes (23).

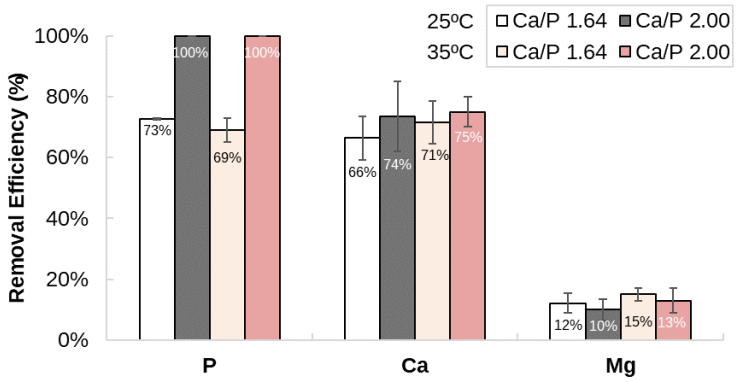

Figure 2.3 – Removal efficiency of P, Mg, Ca^{2+} at pH 10 in the PN/A effluent with natural and enhanced Ca/P ratio (i.e., 1.64 and 2.00, respectively), at 25 ºC and 35 ºC.

2.3.4 Precipitated product characterisation

The precipitated product was collected at the end of each precipitation test. An average production of 1.57 ± 0.05 gTS L^{-1} and 0.14 ± 0.02 gVS L^{-1} was obtained. FT-IR analysis revealed a profile comparable to typical HAP samples, with a similar profile for all the tested conditions (Figure 2.4). The synthesized HAP FT-IR standard spectra present some characteristic chemical groups, including PO_4^{3-}, OH^-, CO_3^{2-} and HPO_4^{2-} (Table 2.5). The resulting profiles from FT-IR analysis showed comparable IR peaks corresponding to the absorption bands of these chemical constituents. Two intense peaks were detected at 550 cm^{-1} and ca. 1000 cm^{-1}. These were identified as related to PO_4^{3-} group which presents absorption bands appearing at 560 and 600 cm^{-1} and at 1000 – 1100 cm^{-1}. Then, CO_3^{2-} group was recognised in the acquired spectra presenting distinct peaks between 1400 and 1580 cm^{-1}. Peaks presence between 2300 and 2400 cm^{-1} could reveal the presence of adsorbed CO_3^{2-}. The OH^- group can appear around 3500 cm^{-1} and some peaks with limited intensity are present from 3500 to 3800 cm^{-1} in the experimental profiles. Finally, a relatively wide peak was detected being relatable to adsorbed water band, appearing from 2600 to 3600 cm^{-1}. Both adsorbed CO_3^{2-} and water are usually

removed in industrial HAP production by thermal treatments (T>1200 ºC). An interesting peak identifying HPO_4^{2-} group could be detected in all the HAP samples at 875 or 880 cm^{-1}. Notably, its presence could suggest the non-stoichiometric nature of the HAP structure.

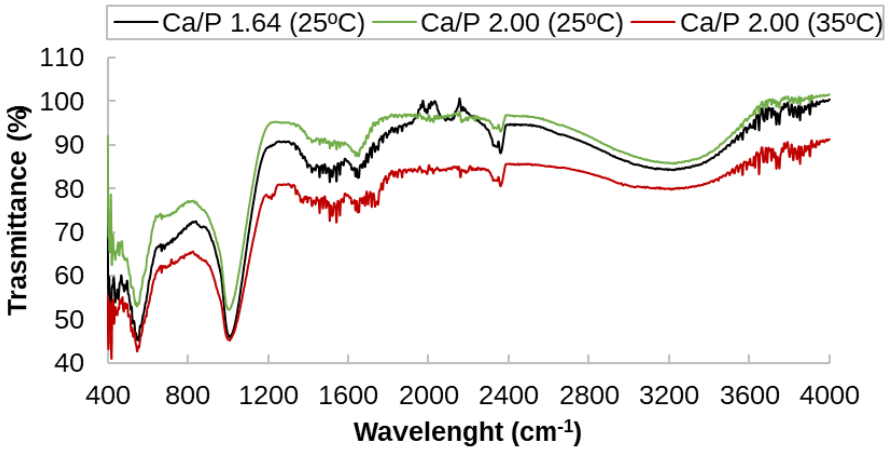

Figure 2.4 – FT-IR spectra of precipitated product at pH 10.

Table 2.5 – Chemical groups characterising the standard synthesised HAP FT-IR spectra (24).

Chemical group	**PO_4^{3-}**	**CO_3^{2-}**	**OH^-**	**HPO_4^{2-}**
Absorption bands (cm^{-1})	560 – 600, 1000 – 1100	1460 – 1530	3500 – 3570	870, 880

XRD analyses were performed on the same samples from batch precipitation tests to confirm the composition (Figure 2.5). No evident difference was revealed by the resulting XRD patterns for the different tested conditions. All samples presented a low crystalline structure evidenced by the lack of sharp peaks at 2θ values of 26°, 32°, and 50° of the standard HAP spectra. Other authors suggest that the calcium phosphate crystallinity decreases with the targeted precipitation pH (25–27). Lei et al. (27) observed a significant loss of typical HAP patterns when precipitation was performed with pH ≥ 9.0. Consistently with the above-mentioned work results, the acquired spectra for all tested conditions presented a wide peak around a 2θ of 30°, which can be related to ACP presence. Particularly, ACP represents the HAP precursor phase, but its evolution to crystalline structure could be hindered by Mg^{2+} which competes with Ca^{2+} for structural sites (22,28,29). Depending on the tested conditions, Mg^{2+} removal was in the range of 13 – 17 %, but the presence of magnesium phosphate compounds was not detected by FTIR and XRD analysis. Thus, this removal might be related to surface adsorption on calcium phosphate that inhibited HAP crystallisation (28).

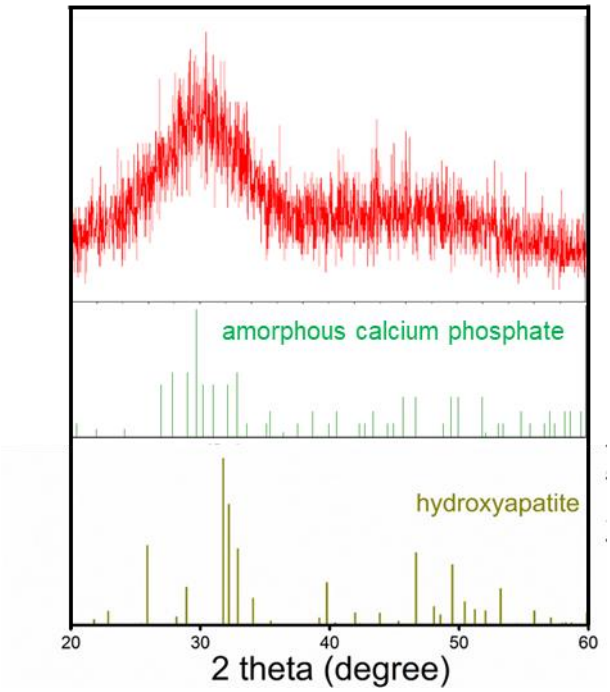

Figure 2.5 – X-ray diffraction (XRD) pattern of recovered product from batch precipitation tests (Ca/P 1.64, 25ºC) and reference pattern of calcium pyrophosphate and hydroxyapatite.

Considering the FT-IR and XRD results, it is likely that the precipitated product was formed by a mixture of ACP and HAP. HAP is the predominant and highly important mineral phase found in the solid tissues of vertebrates, sharing its composition with the mineral components of teeth and bones (24). For this reason, it can be used in the biomedical sector such as bone tissue engineering, metallic implant coating, and drug delivery. Moreover, presenting a similar composition to mined PR, recovered HAP could be used as P secondary raw material for the phosphorus industry (e.g., fertiliser production), or finding application in the environmental pollution remediation field (30). Thus, optimising ACP transfer to HAP is crucial for broadening the industrial applications of the recovered product. More work is needed to investigate the influence of Mg^{2+} when treating the anaerobic supernatant and to find strategies (e.g., dosing of chelating agents) to reduce its possible interference with HAP formation.

2.4 Conclusions

The feasibility of treating the agro-industrial waste anaerobic digestion supernatant through PN/A process combined with a downstream chemical precipitation was proved. NH_4^+-N and P were efficiently removed from the wastewater with a limited use of alkali agents (i.e., NaOH) while promoting biomass growth. The main findings of this study can be summarised as follows:

- PN/A biomass did not face any inhibition related to the treated wastewater during 118 days of operation. By the end of phase I and phase II, N, and alkalinity removal over 80% were achieved with effluent concentrations of 13 ± 2 and 15 ± 3 mgNH_4^+-N L^{-1}, and 125 ± 11 and 120 ± 7 mg$CaCO_3$ L^{-1}, respectively. As the NLR increased, SAA was promoted from 0.21 ± 0.04 up to 0.40 ± 0.07 gN_2 $(gVSS \cdot d)^{-1}$. P, Mg^{2+} and Ca^{2+} concentrations remained basically unchanged after the biological treatment.
- Titration test results suggested that downstream P chemical precipitation is more cost-effective than upstream treatment. Due to the low buffer capacity of the PN/A effluent, a moderate dosage of NaOH was required to achieve the target pH for complete P precipitation, thus reducing of ca. 90% NaOH dosing costs (i.e., 0.71 € m^{-3} vs 0.03 € m^{-3} for upstream and downstream precipitation). Moreover, Visual MINTEQ (13) simulations suggested that PN/A effluent presented lower carbonate compounds SIs, offering a more favourable perspective for achieving higher-quality P recovery due to the lower bicarbonate interference and possibly limited co-precipitation with P minerals.
- Higher pH favoured P and Ca^{2+} precipitation and, particularly, a complete removal of P was achieved for pH≥10 at 2.00 Ca/P ratio. The increased Ca^{2+} levels promoted P and Ca^{2+} removal, the latter reaching up to 75% CaRE. Since P is the limiting ion, higher Ca^{2+} removal was not feasible. Mg^{2+} removal was also enhanced by pH rising, though MgRE remained below 20% and, consistently, it was more effective when the Ca/P ratio was lower. The rise in temperature from 25°C to 35°C did not negatively affect P, Ca^{2+}, and Mg^{2+} removal. This finding is promising from the perspective of implementing biological P removal in the PN/A bioreactor, as biomass growth benefits from temperatures around 35 °C.
- Calcium phosphate minerals are the main products resulting from batch precipitation tests. HAP presence was detected through FT-IR analysis as the main characterising chemical groups were identified (i.e., PO_4^{3-} at ca. 550 cm^{-1} and 1000 cm^{-1}; CO_3^{2-} at 1400-1580 cm^{-1}; OH^- at 3500-3800 cm^{-1}). XRD patterns evidenced the low crystallinity of the samples suggesting that the product might be formed by a mixture of ACP and HAP.

The application of the PN/A process combined with downstream P removal can effectively increase the sustainability of nutrient-rich wastewater treatment by limiting the demand for alkali agents, but

further studies are needed. Future work should continue by exploring operational parameters to achieve high selectivity in downstream precipitation process to improve the economic benefit from the recovered product. In this perspective, a detailed characterisation of precipitated salts (e.g., sodium, heavy metal content) is needed to confirm the possibility of introducing the recovered HAP in the market or using it directly as crop fertiliser. Finally, the integration of calcium phosphate precipitation with PN/A process as a promising alternative to reduce the use of chemicals and to increase the economic and environmental sustainability of the process is worth of being investigated.

References

1. Cieślik B, Konieczka P. *A review of phosphorus recovery methods at various steps of wastewater treatment and sewage sludge management. The concept of "no solid waste generation" and analytical methods.* J. Clean Prod. 2017; 142: 1728–40. https://doi.org/10.1016/j.jclepro.2016.11.116.

2. Chrispim MC, Scholz M, Nolasco MA. *Phosphorus recovery from municipal wastewater treatment: Critical review of challenges and opportunities for developing countries*. J Environ Manage. 2019; 248: 109268. https://doi.org/10.1016/j.jenvman.2019.109268.

3. Van Dijk KC, Lesschen JP, Oenema O. *Phosphorus flows and balances of the European Union Member States.* Science of Total Environonment 2016; 542: 1078–93. http://dx.doi.org/10.1016/j.scitotenv.2015.08.048.

4. Kinnaird JA, Nex PAM. *Critical raw materials.* Routledge Handb Extr Ind Sustain Dev. 2022; 13–33. https://doi.org/10.4324/9781003001317.

5. Jupp AR, Beijer S, Narain GC, Schipper W, Slootweg JC. *Phosphorus recovery and recycling-closing the loop.* Chem Soc Rev. 2021; 50 [1]: 87–101. http://dx.doi.org/10.1039/D0CS01150A.

6. Chen G, Zhang Y, Wang X, Chen F, Lin L, Ruan Q. *Optimizing operation strategies of the single-stage partial nitrification-anammox process.* J Clean Prod. 2020; 256: 120667. https://doi.org/10.1016/j.jclepro.2020.120667.

7. Cao Y, van Loosdrecht MCM, Daigger GT. *Mainstream partial nitritation–anammox in municipal wastewater treatment: status, bottlenecks, and further studies.* Appl Microbiol Biotechnol. 2017; 101 (4): 1365–83. http://dx.doi.org/10.1007/s00253-016-8058-7.

8. Magrí A, Carreras-Sempere M, Biel C, Colprim J. *Recovery of phosphorus from wastewater profiting from biological nitrogen treatment: Upstream, concomitant or downstream precipitation alternatives.* Vol. 10, Agronomy. 2020. 1–37 p. https://doi.org/10.3390/agronomy10071039.

9. Suzin L, Antes FG, Bedendo GC, Bortoli M, Kunz A. *Chemical Removal of Phosphorus from Swine Effluent: the Impact of Previous Effluent Treatment Technologies on Process Efficiency.* Water Air Soil Pollut. 2018; 229 (11). https://doi.org/10.1007/s11270-018-4018-4

10. E. Tarragó, M. Ruscalleda, J. Colprim, M. D. *Balaguer SP. Towards a methodology for recovering K-struvite from manure.* Chem Technol Biotechnol. 2018; 28 [3]: 303–25. https://doi.org/10.1002/jctb.5518.

11. Johansson S, Ruscalleda M, Saerens B, Colprim J. *Potassium recovery from centrate: taking advantage of autotrophic nitrogen removal for multi-nutrient recovery.* J Chem Technol Biotechnol. 2019; 94 [3]: 819–28. https://doi.org/10.1002/jctb.5828.

12. Milia S, Perra M, Tocco G, Carucci A. *The start-up of an anammox reactor as the second step for the treatment of ammonium rich refinery (IGCC) wastewater with high Corg/N ratio.* Ecol Eng. 2017; 106 [2]: 358–68. http://dx.doi.org/10.1016/j.ecoleng.2017.04.068.

13. Gustafsson JP. Visual MINTEQ, ver. 3.1. 2020. https://vminteq.lwr.kth.se/.

14. APHA. *Standard Methods for the Examination of Water and Wastewater, American Public Health Association, Washington, DC (2017).* Am Public Heal Assoc (APHA), Am Water Work Assoc Water Environ Fed Washington, DC, USA. 2017.

15. Anthonisen AC, Loehr RC, Prakasam TBS, Srinath EG. *Inhibition of nitrification by ammonia and nitrous acid.* J Water Pollut Control Fed. 1976; 48 (5): 835–52. https://www.jstor.org/stable/25038971.

16. M.C.M. van Loosdrecht, P.H. Nielsen, C.M. Lopez-Vazquez DB. *Experimental Methods in Wastewater Treatment.* 2016. http://library.oapen.org/handle/20.500.12657/30974.

17. Magrí A, Company E, Gich F, Colprim J. *Hydroxyapatite Formation in a Single-Stage Anammox-Based Batch Treatment System: Reactor Performance, Phosphorus Recovery, and Microbial Community.* ACS Sustain Chem Eng. 2021; 9 (7): 2745–61. https://dx.doi.org/10.1021/acssuschemeng.0c08036.

18. Lei Y, Zhan Z, Saakes M, van der Weijden RD, Buisman CJN. *Electrochemical Recovery of Phosphorus from Acidic Cheese Wastewater: Feasibility, Quality of Products, and Comparison*

with Chemical Precipitation. ACS ES T Water. 2022; 1 (4): 1002–13. https://doi.org/10.1021/acsestwater.0c00263.

19. Monballiu A, Ghyselbrecht K, Crabeels X, Meesschaert B. *Calcium phosphate precipitation in nitrified wastewater from the potato-processing industry.* Environ Technol (United Kingdom). 2019; 40 (17): 2250–66. https://doi.org/10.1080/09593330.2018.1439112.

20. Peng L, Dai H, Wu Y, Peng Y, Lu X. *A comprehensive review of phosphorus recovery from wastewater by crystallization processes.* Chemosphere. 2018; 197: 768–81. https://doi.org/10.1016/j.chemosphere.2018.01.098.

21. Fernandes GW, Kunz A, Steinmetz RLR, Szogi A, Vanotti M, De Moraes Flores ÉM. *Chemical phosphorus removal: A clean strategy for piggery wastewater management in Brazil.* Environ Technol (United Kingdom). 2012; 33 (14): 1677–83. https://dx.doi.org/10.1080/09593330.2011.642896.

22. Yang X, Xie B, Wang L, Qin Y, Henneman ZJ, Nancollas GH. *Influence of magnesium ions and amino acids on the nucleation and growth of hydroxyapatite.* Cryst Eng Comm. 2011; 13 (4): 1153–8. https://doi.org/10.1039/C0CE00470G.

23. Cao L, Yang Y, Xue Y, Ma H, Li YY, Hu Y. *A review of efficient nitrogen removal and phosphorus recovery by anammox-hydroxyapatite based processes: Challenges and opportunities.* J. Environ Chem Eng. 2023; 11 (5): 111103. https://doi.org/10.1016/j.jece.2023.111103.

24. Berzina-Cimdina L, Borodajenko N. *Research of Calcium Phosphates Using Fourier Transform Infrared Spectroscopy.* Infrared Spectroscopy - Materials Science, Engineering and Technology. InTech; 2012. http://dx.doi.org/10.5772/36942.

25. Hermassi M, Valderrama C, Dosta J, Cortina JL, Batis NH. *Evaluation of hydroxyapatite crystallization in a batch reactor for the valorization of alkaline phosphate concentrates from wastewater treatment plants using calcium chloride.* Chemical Engineering J. 2015; 267: 142–52. http://dx.doi.org/10.1016/j.cej.2014.12.079.

26. Cao X, Harris W. *Carbonate and magnesium interactive effect on calcium phosphate precipitation.* Environ Sci Technol. 2008; 42 [2]: 436–42. https://doi.org/10.1021/es071670.

27. Lei Y, Zhan Z, Saakes M, van der Weijden RD, Buisman CJN. *Electrochemical recovery of phosphorus from wastewater using tubular stainless-steel cathode for a scalable long-term operation*. Water Res. 2021; 199: 117199. https://doi.org/10.1016/j.watres.2021.117199.

28. Ding H, Pan H, Xu X, Tang R. *Toward a detailed understanding of magnesium ions on hydroxyapatite crystallization inhibition.* Cryst Growth Des. 2014; 14 [2]: 763–9. https://doi.org/10.1021/cg401619s.

29. Talebi Atouei M, Rahnemaie R, Goli Kalanpa E, Davoodi MH. *Competitive adsorption of magnesium and calcium with phosphate at the goethite water interface: Kinetics, equilibrium and CD-MUSIC modeling.* Chem Geol. 2016; 437: 19–29. http://dx.doi.org/10.1016/j.chemgeo.2016.05.004.

30. Ibrahim M, Labaki M, Giraudon JM, Lamonier JF. *Hydroxyapatite, a multifunctional material for air, water and soil pollution control: A review.* J Hazard Mater. 2020; 383 :121139. https://doi.org/10.1016/j.jhazmat.2019.121139.

Supporting Information – Chapter 2

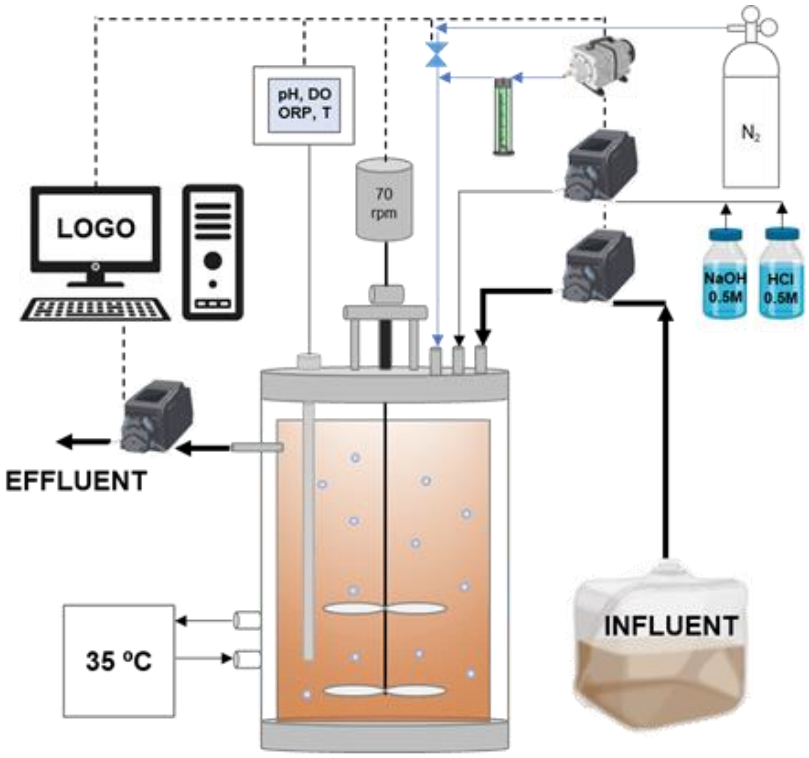

Figure S2.1 – PN/A apparatus set-up.

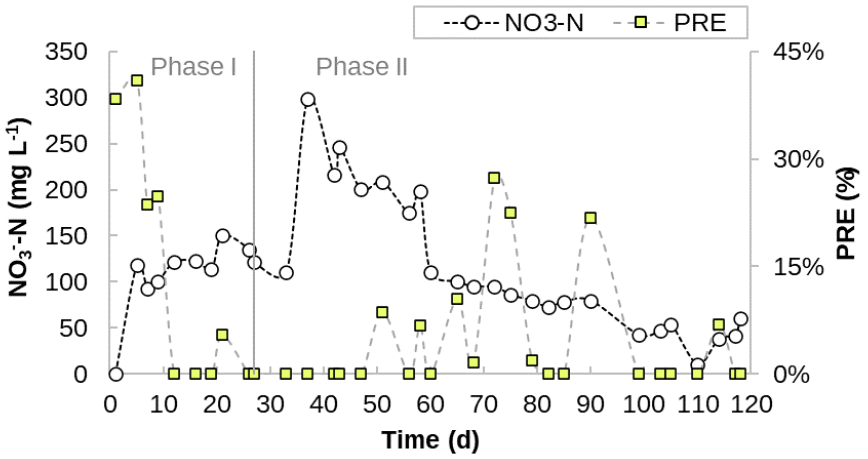

Figure S2.2 – Effluent nitrate (NO_3^--N) concentration and Phosphorus Removal Efficiency (PRE) during Partial Nitritation/Anammox (PN/A) process operation.

Table S2.1 - Saturation indexes (SIs) for calcium and magnesium phosphate mineral phases in the PN/A effluent as a function of the pH and temperature values. Calculations were made using Virtual MINTEQ (13) and based on average ionic concentrations resulting from wastewater characterisation (Table 1).

			pH (u.pH)				
			8	9	10	11	12
Mineral phase	**T (ºC)**	**Ca/P (mol/mol)**	**SI (-)**				
Hydroxyapatite ($Ca_{10}(PO_4)_6\cdot(OH)_2$)	25	1.64	11.5	15.2	17.8	19.0	19.9
	25	2.00	12.3	15.9	18.1	19.5	19.9
	35	1.64	12.2	15.6	17.7	18.5	19.3
	35	2.00	12.0	15.5	17.5	18.7	19.5
Amorphous calcium phosphate $Ca_xH_y(PO_4)_z\cdot nH_2O$	25	1.64	1.9	3.8	4.9	5.0	5.1
	25	2.00	2.5	4.2	5.1	5.3	5.1
	35	1.64	2.4	4.1	4.8	4.8	4.7
	35	2.00	2.3	4.0	4.7	4.9	4.8
Bobierrite ($Mg_3(PO_4)_2\cdot 8H_2O$)	25	1.64	0.5	2.4	3.8	4.4	3.7
	25	2.00	0.5	2.3	3.6	4.0	3.4
	35	1.64	0.6	2.4	3.7	3.9	2.8
	35	2.00	0.3	2.2	3.4	3.7	2.6
Cattiite ($Mg_3(PO_4)_2\cdot 22H_2O$)	25	1.64	-1.6	0.3	1.7	2.2	1.5
	25	2.00	-1.6	0.2	1.5	1.9	1.2
	35	1.64	-1.5	0.3	1.5	1.8	0.7
	35	2.00	-1.8	0.0	1.3	1.6	0.4

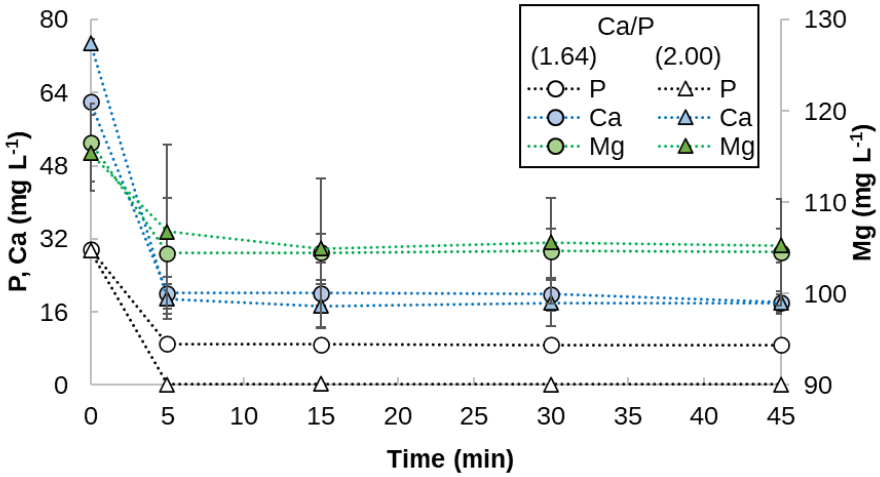

Figure S2.3 – Phosphate, calcium and magnesium concentrations at pH 10 vs the reaction time for different amounts of calcium ions at 25ºC.

CHAPTER 3: Concomitant phosphorus and nitrogen removal from agro-industrial wastewater through Partial Nitritation/Anammox process[1]

Abstract

Sustainable phosphorus management is crucial for safeguarding global food security and preventing soil and water bodies' quality deterioration. Recently, the Anammox process was proven feasible for phosphorus recovery as hydroxyapatite from urban wastewater. This work firstly assessed the feasibility of phosphorus recovery by treating supernatant from agro-industrial waste anaerobic digestion (743±17 mgNH_4^+-N L^{-1} and 29±1 mgPO_4^{3-}-P L^{-1}, and Ca/P 1.64±0.09). The Partial Nitritation/Anammox (PN/A) process was operated according to a single-stage configuration in a 3L sequencing batch reactor. The bioreactor was inoculated by ANAMMOX© granulated biocatalyst and run with 6-hour working cycles (i.e., 4 cycles per day). The nitrogen loading rate was increased throughout the experimental period from 0.11 to 0.33 kgN $(m^3 \cdot d)^{-1}$ by lengthening the feeding phase, taking into account the nitrite and ammonium accumulation. Moreover, a set of experiments was performed to pave the way for a novel non-damaging separation protocol to recover active biomass and mineral P from the sludge. Granules sampled from the bioreactor were exposed to 37 kHz sonication frequency for different periods (i.e., 60, 30, 15 min) and the effect of ultrasonication on biomass was investigated by measuring the specific anammox activity (SAA) through the manometric method. As a result of the increasing nitrogen loading rate strategy, biomass showed significant growth and SAA improvement during the seven months of the bioreactor start-up with an increasing concentration from 4.80 up to 6.77 g L^{-1} and an activity up 0.39 gN_2 $(gMLVSS \cdot d)^{-1}$. In the absence of an external calcium source, simultaneous nutrient removal consisting of ammonium conversion rate up to 0.28 kgNH_4^+-N m^{-3} ·d and P removal efficiency of ca. 34% were achieved. As P concentration started lowering in the bulk liquid, the mixed liquor ratio of volatile suspended solids over the suspended solids decreased over time from 95% reaching a final value of 75%, suggesting precipitation of inorganic compounds inside the granules. The effluent Ca/P ratio was close to 1.50 which is the typical constituent ratio for amorphous calcium phosphate precipitation. Regarding the ultrasonication tests, anammox activity was negatively affected when extending the exposition time. Nevertheless, after 15 min of granules sonication, the SAA showed a limited reduction, up to 15%, compared with untreated granules collected from the bioreactor. Ultrasonic treatment is a promising

method for non-damaging separation limiting the loss of biomass activity while disassembling the granule structure. However, further studies are needed to evaluate the effective mineral-from-biomass separation allowing phosphorus recovery and biomass re-inoculation to the bioreactor.

[1] Part of the work included in this chapter was presented at the conference: 18th International Conference on Environmental Science and Technology (CEST2023), 30/08/23-02/09/23, Athens, Greece.

3.1 Introduction

Wastes volume generated by agro-industry is constantly increasing worldwide due to the rise in the demand for food, fuels, and sustentation products (1). In 2018, about 87 million tons were produced in Europe (2) while focusing on Italy, it was estimated that the agro-waste production was over 320 kt (3). Due to their high eutrophic and polluting potential, these residues must be chemically or biologically treated before disposal, to prevent soil and water quality deterioration. Besides, according to the circular economy strategy, European Union (EU) policies are driving up interest in recovering valuable byproducts and bioenergy from waste streams. Particularly, solutions such as implementing the decentralised anaerobic digestion of agro-industrial residues would allow for achieving nutrient recovery simultaneously with energy production (4). Moreover, the handling of digestate can help to close the nutrient loop in the agricultural sector, being itself a source of essential nutrients for crops, such as nitrogen (N) and phosphorus (P). Struvite precipitation is the main adopted technique for ammonium nitrogen recovery. However, N is more frequently removed from wastewater by conversion to dinitrogen (N_2) rather than recovered due to its readily availability from the atmosphere via the Haber-Bosch process. Conversely, as P is mainly obtained from natural phosphate reserves (i.e., Phosphate Rocks (PR)), which will become depleted soon, the current aim is to recover P rather than remove it. Many physical/chemical (i.e., precipitation, crystallisation, ion exchange membrane, and electrochemical processes) and biological (e.g., Enhanced Biological Phosphorus Removal (5,6) and microalgae-based technologies (7)) approaches have been developed to recover P from wastewater. In conventional wastewater treatment plants, the soluble P is recovered mainly through chemical crystallisation, with abundant use of reagents and high production of sludge. Recently, Partial Nitritation coupled with Anaerobic Ammonium Oxidation process (PN/A) have gained attention for combining N removal with P precipitation as calcium phosphate, namely hydroxyapatite (HAP), treating synthetic (8,9) and real wastewaters (10,11). This biological process allows achieving a completely autotrophic removal of ammonium nitrogen (NH_4^+-N) coupled with the simultaneous removal of orthophosphate−phosphorus (PO_4^{3-}−P), via bio-mineralisation within a double or a one-stage process. When the treated solution presents calcium (Ca)/P ratio ≥1.67 (i.e., the stoichiometric

value for HAP precipitation), appropriate P and inorganic carbon concentrations (12), P can precipitate inside the granules forming a HAP core covered with biofilm. Thus, P is concentrated in the mineral granular sludge which can be harvested. Known the PN/A process benefits compared with Nitrification/Denitrification process (13,14), HAP precipitation within the sludge gives a new perspective in wastewater treatment. In fact, PN/A-HAP process can combine the need for water decontamination with the potential valorisation of a strategic product from waste, according to a circular economy-based approach. HAP, presenting a similar composition to mined PR, offers to broaden industrial applications. Potentially, the biowaste-derived HAP can be exploited as P secondary raw material for the phosphorus industry, or it can be used in the biomedical sector (bone tissue engineering, metallic implant coating, drug delivery), in the environmental pollution remediation field (15), or even applying it directly to the soil as fertiliser (10). Magrí et al. (11) tested the PNA – HAP process to treat N-rich urban sidestream centrate from wastewater treatment plant in a single-stage granular sludge sequencing batch reactor (SBR) achieving NH_4^+−N and PO_4^{3-}−P removal efficiencies of 80% and 74%, respectively (11). A high mineralised sludge was produced with a P content of about 10.7% on a dry weight (DW) basis and the granule's mineral core was mostly composed of HAP (11). Other synthetic and real wastewaters treated with the same process showed comparable P content in the dry sludge remaining in the range of 10–15% (10,11,16,17) which is a promising result considering typical values of activated sludge (1−2%) and EBPR (5−7%) (11). Achieving an efficient P removal combined with high nitrogen removal rates (i.e., maximum value 1.3 kgN/m^3/d (12)) is feasible, but further evaluations concerning process stability for different varieties of real wastewaters are still needed (18). Previous studies conveyed that calcium addition strategy is essential to achieve high phosphorus removal efficiency (HAP stochiometric Ca/P ratio is 1.67), but it can also cause blockage of the equipment and new pollution (12) and increase the cost of the treatment. Thus, the possibility of skipping calcium dosage by a proper wastewater selection was explored in the present work. Besides, Magrí et al. (11) experience pointed out the need of finding an operational compromise between microbial activity long-term optimization and the interest in extracting P-rich granules from the system. To date, the research has not been focused on testing an efficient separation that will allow effective P-recovery from sludge without damaging the biomass. Since PN/A is characterised by low excess sludge production, the excessive withdrawal of sludge from the reactor -from which P-recovery objective benefits- can hinder the NH_4^+-N removal performance. Therefore, the present work is willing to throw the bases for identifying a non-damaging separation protocol that allows to recover active biomass and mineral P.

To the best of the authors knowledge, no previous study was performed concerning the application of the one-stage PN/A – HAP process to real supernatant from anaerobic digestion of agro-industrial

wastes. Thus, the primary investigation objective was to prove the process feasibility and compare the treatment performance with the literature data referring to tested real wastewaters (e.g., urban sidestream). The Partial Nitritation/Anammox (PN/A) process was operated according to a single-stage configuration in a 3L sequencing batch reactor (SBR). The bioreactor was inoculated by ANAMMOX© granulated biocatalyst and fed with a locally produced agro-waste anaerobic digestion supernatant. The process start-up was realised using a nitrogen loading rate (NLR) step-by-step increase strategy (i.e., from 0.11 to 0.33 kgN $(m^3 \cdot d)^{-1}$. Removal performance and biomass growth was monitored during about seven months of operation. The application of the PN/A – HAP process would allow increasing the sustainability of nutrient-rich agro-industrial wastewaters treatment helping to recover fertiliser for crops. Mineral-from-biomass separation tests were performed to evaluate the selected method (i.e., sonication) influence on anammox bacteria (AnAOB) activity. In this first attempt, granules from the reactor were collected and exposed to sonication for different exposition times and the sonication effect on biomass was investigated by measuring the Specific Anammox Activity (SAA) through the manometric method (19). Efficient and non-damaging mineral-from-biomass separation would allow re-inoculating the microorganisms to the reactor, being a key factor for evaluating the effective recovery potential of the PN/A – HAP technology, and eventually for future scaling up of the technique.

3.2 Materials and methods

3.2.1 Partial Nitritation/Anammox reactor and experimental operation

The PN/A process was operated according to a single-stage configuration in a glass-made 3L SBR, with a variable working volume depending on the operating conditions tested. The bioreactor was inoculated by ANAMMOX© granulated biocatalyst purchased from Paques Europe B.V. coming from the sewage treatment plant in Olburgen (Netherlands), treating wastewater deriving from potatoes production industry. The reactor was operated in fed-batch mode and run with 6-hour working cycles (300 min aerobic phase, 40 min anoxic phase, 15 min sedimentation phase and 5 min withdrawal phase) resulting in 4 cycles per day. Alternated aeration sequences were set during the aerobic phase (6 repetitive aeration sequences lasting 30 min each alternated by 15 min of no aeration). The feeding phase was included in the aerobic phase and presented a variable length depending on the targeted operating parameters; influent flowrate was set at 2.0 mL min^{-1}. Oxygen was provided in the bulk liquid through a porous stone using an air compressor with a manually selected airflow rate controlled by an airflow meter (0.05 – 0.5 L min^{-1}). To assure absence of oxygen

during the anoxic phase inert N_2 gas was sparged in the SBR with a flow controlled through a solenoid valve connected to the nitrogen cylinder. Process temperature was controlled at 35 ± 1 ºC, and the dissolved oxygen concentration was maintained below 0.2 mgO_2 L^{-1} to preserve AnAOB from oxygen inhibition during aerobic phase. Mechanical mixing was provided by a double helix marine impeller (70±5 rpm). Temperature was controlled by a water jacket and a thermostatic bath (HAAKE, mod. F3-K), while pH was maintained within the selected range (7.0-8.0) using 0.5M HCl and 0.5M NaOH dosage. To avoid any external light penetration hindering AnAOB activity (20), the vessel was completely shielded with aluminium foil. Temperature, pH, ORP, and DO monitoring was performed using InPro 4280i and 6850i probes (Mettler-Toledo), respectively, connected to a digital transmitter (Mettler Toledo, mod. M400). Process timing and control were performed via programmable logic module (Siemens, LOGO!, mod. 230rce) connected to the configured electrical panel. PN/A apparatus set-up is presented in Figure 3.1.

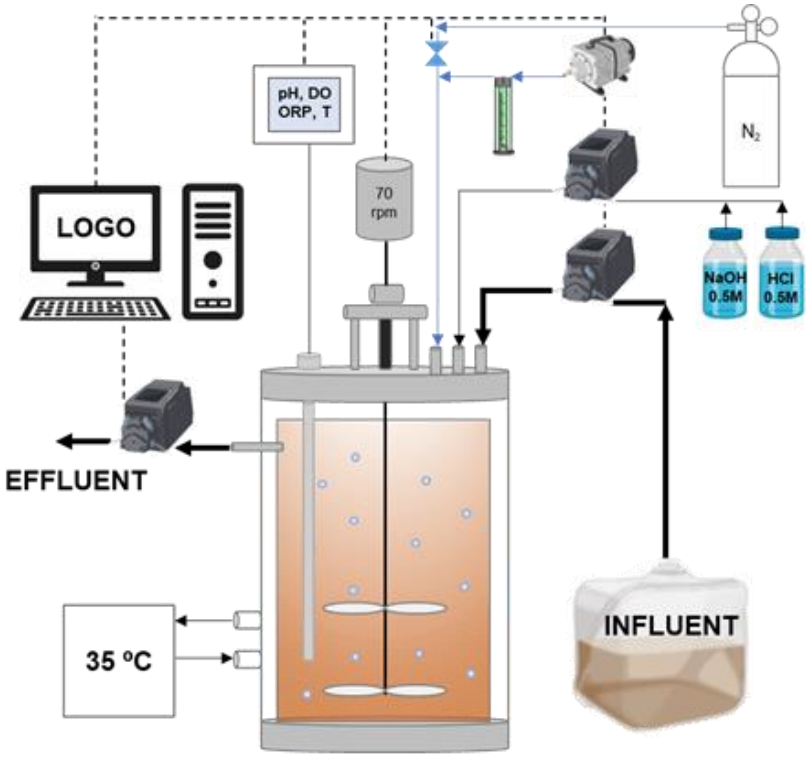

Figure 3.1 – PN/A apparatus set-up.

The single-stage PN/A process was run for approximately 7 months. A stepwise increasing NLR strategy was adopted to cultivate granular sludge in the bioreactor, corresponding to 4 operational phases. The NLR was increased throughout the experimental period from 0.11 to 0.33 kg N $(m^3 \cdot d)^{-1}$ by lengthening the feeding phase; when stable nitrogen removal efficiency showed stable values for at least 3 HRT, the NLR was increased. The air flow rate was manually regulated from 0.05 to 0.1 L min^{-1} according to nitrite and ammonium accumulation.

3.2.2 Treated wastewater characteristics

The wastewater fed to the bioreactor was a supernatant collected at the Agrifera S.r.l. anaerobic digestion plant (Decimoputzu, Sardinia, Italy), treating agro-industrial wastes (e.g., crops residues) to produce biogas. After arriving in the lab, the anaerobic digestion supernatant was centrifuged, filtered to get rid of solids and collected in plastic tanks. Prior to feeding, the pre-treated wastewater was flushed with N_2 gas for 25 minutes to avoid any presence of oxygen and placed in a plastic bag to be pumped into the bioreactor. Average characterization is provided in Table 3.1.

Table 3.1 - Average composition of the wastewater fed to the bioreactor; AV: average, SD: standard deviation.

parameter	unit	AV	SD
pH	-	8.3	0.1
EC	mS cm^{-1}	15	3
NH_4^+-N	mg L^{-1}	744	16
NO_2^--N+ NO_3^--N	mg L^{-1}	0	0
PO_4^{3-}-P	mg L^{-1}	29	1
SO_4^{2-}	mg L^{-1}	24	3
Cl^-	mg L^{-1}	3060	210
Mg^{2+}	mg L^{-1}	119	5
Ca^{2+}	mg L^{-1}	64	3
K^+	mg L^{-1}	2130	14
Na^+	mg L^{-1}	1057	10
Alkalinity	mM HCO_3^-	63	5
COD	mg L^{-1}	218	3
BOD_5	mg L^{-1}	34	5
TSS	g L^{-1}	0.21	0.10
VSS	mg L^{-1}	0.20	0.08
Ca/P	mol mol^{-1}	1.64	0.07

Abbreviations: BOD_5, 5 days biochemical oxygen demand; COD, chemical oxygen demand; EC, electrical conductivity; TSS, total suspended solids; VS, volatile solids; VSS, volatile suspended solids.

3.2.3 Manometric and mineral-from-biomass separation tests

Specific Anammox Activity (SAA) was measured on SBR granular sludge through manometric batch tests which were carried out following the methodology described by Lotti *et al.* (19). Oxitop-IDS

AN6 © measuring heads were used to monitor the overpressure produced by anammox reaction. Overpressure measurements allowed the gaseous nitrogen (N_2 [M]) determination, as they are proportional to the gas production. Presenting low solubility in water, N_2 tends to accumulate in the headspace of a closed system, resulting in overpressure. Using the ideal gas law, the gas production rate can be calculated (21) based on the measured overpressure. The SAA is expressed as the quantity of nitrogen produced per quantity of microorganisms and per unit of time [gN_2 $(gVSS \cdot d)^{-1}$]. Batch tests were performed in duplicate to ensure the reproducibility of the test, using 250 mL as final volume in glass bottles. Temperature (35 ± 0.5 ºC) and mechanical mixing (200 rpm) were maintained constant during the tests by placing the bottles inside an orbital shaker incubator. Sludge was periodically collected from the bioreactor to monitor the SAA evolution. Granules were washed and suspended (final biomass concentration of 2 g Volatile Suspended Solids (VSS) L^{-1}) in a medium solution containing a 5M phosphate buffer (0.14 g KH_2PO_4 L^{-1} and 0.75 g K_2HPO_4 L^{-1}, resulting in 7.8 pH) and the micronutrients necessary for microbial growth (22). Anaerobic conditions were achieved inside the bottles by sparing liquid phase and headspace with N_2 for 15 minutes. Then, overpressures were then dissipated by releasing excess gas from the headspace into a glass column. Finally, bottles were covered by aluminium coat and were placed in the orbital-shaker incubator (35ºC) for 60 minutes to achieve pressure stabilisation. Once the 60 minutes had elapsed, and the pressure values were indeed stabilised, the test started. Medium solution was injected at the start of the tests setting initial NH_4^+-N and NO_2^--N concentrations of 50 mgN L^{-1}. Overpressure evolution typically showed an initial lag phase, followed by a linear increase due to N_2 production, and a final stationary phase. The test ended when nitrite had been completely consumed, and pressure inside the bottles remained constant (corresponding to an overpressure profile plateau) for 30-60 min. At the end of each test, pH was measured, liquid and mixed liquor samples were collected. Liquid samples were filtered (0.45 µm cellulose acetate filter) and stored in a refrigerator at +4ºC for subsequent ammonium and anions analysis, while mixed liquor samples were used for total and volatile suspended solids (TSS and VSS) determination.

Moreover, a set of experiments was performed to pave the way for a novel non-damaging separation protocol to recover active biomass and mineral P from the sludge. An ultrasonic device (mod. D-78224, Elmasonic) was used to test the mineral-from-biomass separation method. Granules sampled from the bioreactor were exposed to 37 kHz sonication frequency for different time lenghts (i.e., 60, 30, 15 min). The effect of ultrasonication on biomass was investigated by measuring the SAA through the manometric method, while the influence on granules integrity (e.g., change in diameter) was assessed with image analysis technique.

3.2.4 Analytical methods

Samples were periodically collected from influent (once every two weeks), effluent (three times per week), to evaluate process performances. NH_4^+-N concentration was measured according to Standard Methods (23) by spectrophotometric analysis (DR2800, Hach Lange, Germany) at a wavelength of 420 nm. Liquid samples were also analysed for quantification of anions, namely chloride (Cl^-), nitrite (NO_2^--N), nitrate (NO_3^--N), phosphate (PO_4^{3-}-P), and sulphate (SO_4^{2-}), using an ion chromatograph (ICS-90, Dionex-Thermofisher, USA) equipped with an AS14A Ion-PAC 5 μm column. Before analysis, samples were filtered (acetate membrane filter, 0.45 μm porosity) and properly diluted with grade II water. The concentrations of the main cations, namely calcium (Ca^{2+}), magnesium (Mg^{2+}), were determined using an ICP/OES (Varian 710-ES, Agilent Technologies, USA): samples were filtered (acetate membrane filter, 0.45 μm porosity), acidified (nitric acid, 1% v:v) and diluted with grade I water. Alkalinity was measured by potentiometric titration to preselected end-point pH, using an automatic titrator (AT-510, KEM electronics). Free Ammonia (FA) and Free Nitrous Acid (FNA) levels were calculated according to Anthonisen et al. (24). Total COD and soluble COD (i.e., after filtration of samples through a 0.45 μm membrane) concentrations were determined according to Standard Methods (23). Mixed liquor samples were periodically collected from the bioreactor once every two weeks to monitor mixed liquor total suspended solids (MLSS) and mixed liquor volatile suspended solids (MLVSS); both concentrations were determined according to Standard Methods (23).

Granular aggregates were morphologically characterized in terms of size and aspect (roundness, aspect ratio) through image analysis (IA) technique. Biomass samples were collected from the reactor and from manometric test vessels, sieve-drained, washed and resuspended in deoxygenated grade I water, and put in 10 cm diameter Petri dishes. High resolution digital images of dark granules contrasted to a white background were acquired via a HP ScanJet 5590 scanner. Measured parameters were mean diameter, aspect (i.e., the ratio between the minor and the major axis of the ellipse equivalent to the object) and roundness (i.e., an index ranging from 0 to 1 based on the ratio between area and perimeter of the object and of its equivalent circle – perfect circular shape giving a value of 1).

3.2.5 Calculations

The nitrogen removed (ΔTN [mg N L^{-1}]) was calculated as follows:

$$\Delta TN = (NH_4\text{-}N + NO_2\text{-}N + NO_3\text{-}N)_{infl} - (NH_4\text{-}N + NO_2\text{-}N + NO_3\text{-}N)_{effl} \quad (Eq.1),$$

where NH_4–N, NO_2–N and NO_3–N are the main nitrogen species concentrations [mg L^{-1}].

Total nitrogen removed through the anammox reaction (ΔNr [mg N L^{-1}]) is defined as shown below:

$$\Delta N_r = (NO_2\text{-}N)_{effl} - (NO_2\text{-}N)_{infl} - (NH_4\text{-}N)_{infl} + (NH_4\text{-}N)_{effl} \quad (Eq.2).$$

Nitrogen loading rate (NLR [kg N $(m^3 \cdot d)^{-1}$]) is the influent nitrogen total mass that is fed in one day (4 operational cycles per day) to the reactor's working volume. It was calculated using the following expression:

$$NLR = \frac{(NH_4\text{-}N + NO_2\text{-}N + NO_3\text{-}N)_{infl} \times n \times V_{feed}}{V_{TOT}} \quad (Eq.3),$$

where NH_4–N, NO_2–N and NO_3–N are the main nitrogen species concentrations [g L^{-1}], n is the number of cycles (i.e., 4), V_{feed} is the volume fed during each cycle [L $cycle^{-1}$] and V_{TOT} is the reactor's working volume [L].

Nitrogen and phosphorus removal rates (NRR [kgN $(m^3 \cdot d)^{-1}$], PRR [mgP $(m^3 \cdot d)^{-1}$]) are expressed by considering the nitrogen and phosphorus mass balance in the reactor, as follows:

$$NRR = \frac{((NH_4\text{-}N + NO_2\text{-}N + NO_3\text{-}N)_{infl} - (NH_4\text{-}N + NO_2\text{-}N + NO_3\text{-}N)_{effl})}{HRT} \quad (Eq.4),$$

$$PRR = \frac{(P_{inf} - P_{effl})}{HRT} \quad (Eq.5),$$

where NH_4–N, NO_2–N and NO_3–N are the main nitrogen species concentrations [g L^{-1}], P is the phosphorus concentration [mgP L^{-1}] and HRT is the hydraulic retention time [d].

Removal efficiencies of nitrogen, ammonium-nitrogen, phosphorus and calcium (NRE [%], NH_4-NRE [%], PRE [%], CaRE [%] respectively) were determined through the following equation:

$$NRE = \frac{\Delta TN}{(NH_4\text{-}N + NO_2\text{-}N + NO_3\text{-}N)_{infl}} \times 100 \quad (Eq.6),$$

$$NH_4N\text{-}RE = \frac{((NH_4\text{-}N)_{infl} - (NH_4\text{-}N)_{effl})}{(NH_4\text{-}N)_{infl}} \times 100 \quad (Eq.7),$$

$$PRE = \frac{\left((P)_{infl} - (P)_{effl}\right)}{(P)_{infl}} \times 100 \qquad (Eq.8),$$

$$CaRE = \frac{\left((Ca)_{infl} - (Ca)_{effl}\right)}{(Ca)_{infl}} \times 100 \qquad (Eq.9),$$

where Ca is calcium concentration [g L^{-1}].

To further evaluate and monitor nitrogen removal performance in the PN/A bioreactor, other important indicators were considered. In real operation, these indicators also allow to detect the potential existence of other concomitant biological reactions. Thus, the nitritation reaction rate (N_iRR) by ammonium-oxidizing bacteria (AOB), nitratation reaction rate (N_aRR) by nitrite oxidizing bacteria (NOB), and nitrogen removal rate through anammox reaction pathway (N_ARR) are calculated as follows (8):

$$N_iRR = \frac{((NO_2\text{-}N)_{effl} - (NO_2\text{-}N)_{infl} + \Delta N_r \times \frac{1.32}{2.32})}{HRT} \qquad (Eq.10),$$

$$N_aRR = \frac{\left((NO_3\text{-}N)_{infl} - (NH_3\text{-}N)_{effl}\right)}{HRT} \qquad (Eq.11),$$

$$N_ARR = \frac{\Delta N_r \times \frac{2.04}{2.32}}{HRT} \qquad (Eq.12).$$

In an ideal operation of one-stage PN/A process, the indicators show proportional relations as the ones indicated below:

N_iRR/N_ARR ratio = 0.65

NRR/N_ARR ratio = 1.00

NO_3^--N/ΔN_r ratio = 0.11

Nitrogen production rate ($(dN_2)\cdot dt^{-1}$ [$(molN_2\cdot min^{-1}$]) due to anammox process, was calculated using the ideal gas law by considering the maximum slope (determined through linear regression) of the overpressure linear increase profile over time (α [$mmHg\cdot min^{-1}$]) measured during the manometric batch tests:

$$\frac{(dN_2)}{dt} = \alpha \times \frac{dV_G}{RT} \qquad (Eq.13),$$

where V_G is the gas volume inside bottles used in the manometric test [L], R is the universal gas constant (8.31 J (mol·K)$^{-1}$) and T is the measured temperature [K]. Then, the related SAA [gN_2-N (gVSS·d)$^{-1}$] is calculated by normalisation to the biomass concentration in the bottle, as follows:

$$SAA = \frac{\left(\frac{dN_2}{dt}\right)}{VSS} \qquad (Eq.\,14),$$

The loss on anammox activity (SAA_{LOSS} [%]) after the sonication treatment was calculated as follows:

$$SAA_{LOSS} = \frac{SAA_{untreated} - SAA_{treated}}{SAA_{untreated}} \times 100 \qquad (Eq.\,15),$$

where $SAA_{untreated}$ and $SAA_{treated}$ [gN_2-N (gVSS·d)$^{-1}$] are the measured activity of untreated and treated granules, respectively.

3.3 Results and discussion

3.3.1 Nitrogen and phosphorus removal

Rapid start-up is the most critical step in anammox application, but the long AnAOB doubling time (10–30 d) poses a significant challenge (25). Guo et al. (8) achieved a fast PN/A-HAP start-up (ca. three months) treating a synthetic wastewater through a step-by-step increase of NLR. Following this strategy, the present work main variable in operation was NLR, being increased from 0.11 to 0.33 kgN (m^3·d)$^{-1}$ throughout the experimentation (Figure 3.2). Consequently, HRT decreased from 6.9 days in phase I to 2.3 days in phase IV. In fact, the NLR increase was obtained by lengthening the feeding phase in each working cycle, while maintaining a constant influent flow rate (2 mL min^{-1}). All along the operation, the bioreactor was fed by the anaerobic digestion supernatant presenting an average concentration of 743 mgNH_4^+-N L^{-1}. Due to the target high-strength wastewater, a limited initial NLR (0.11 kgN (m^3·d)$^{-1}$) was selected to prevent possible biomass inhibition by FA and FNA. Treating urban side stream centrate, Magrí et al. (11) worked in a comparable range of NLR (i.e., 0.09 – 0.13 kgN (m^3·d)$^{-1}$) during the very first phase of PN/A-HAP process start-up. An undesired alkaline shock occurred at day 91 due to a failure in the pH control system. After 79 days of operation the previous biomass activity was recovered (this recovery phase results are not shown).

As a result of the increasing NLR strategy, biomass showed significant growth and SAA improvement during the 7 months operation, reaching a SAA's final value of 0.39 gN_2 (gMLVSS·d)$^{-1}$ (Figure 3.2). Moreover, the main nitrogen removal ratios were monitored during the manometric batch tests. These

indicators were aligned to the stoichiometric values reported in the literature, confirming AnAOB activity (Figure S3.1). Consistently to the SAA increase, the NRR/MLVSS ratio raised from 0.021 to 0.037 gN_2 (gMLVSS d)$^{-1}$ suggesting a progressive improvement in biomass metabolic activity throughout the operation.

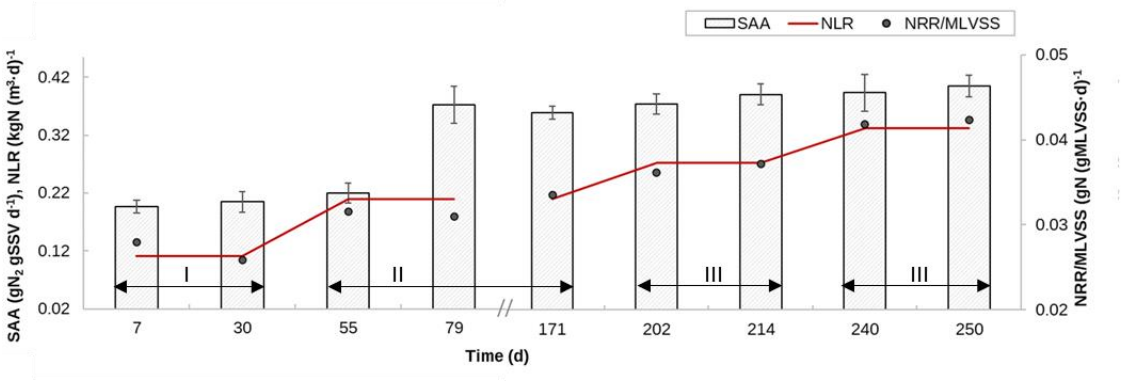

Figure 3.2 – Nitrogen removal performance evolution: Specific Anammox Activity (SAA) measured by manometric batch test, Nitrogen Loading Rate (NLR) and Nitrogen Removal Rate (NRR) over Mixed Liquor Volatile Suspended Solids (MLVSS) ratio; operational phases are represented with black double-headed arrows.

The main parameters representing the bioreactor performance are shown in Table 3.2 and Figure 3.3. NRR increased progressively as the HRT was decreased from phase I to phase III, eventually stabilising at 0.25 kgN (m^3·d)$^{-1}$ in phase IV. Previous studies already shown that HRT shortening is an effective way to improve NRR and can contribute to the inhibition of NOB being easily washed out with flocs (26,27). PN/A process indicators, such as N_iRR/N_ARR and NRR/N_ARR were consistent with the ideal one-stage PN/A process throughout the experimentation, although $\triangle NO_3$-N/$\triangle$N showed a transition from the potential occurrence of nitratation to the presence of denitrification. According to the $\triangle NO_3$-N/$\triangle$N evolution, the presence of potential nitratation pathway raised in phase II. However, after the recovery from the alkaline shock, the $\triangle NO_3$-N/$\triangle$N measured value turned negative in phase III and IV suggesting that partial denitrification was present. Cao et al. (28) already observed a similar behaviour when treating fish processing wastewater. Denitrifying bacteria presence is likely due to the co-existence of organic carbon in the target wastewater and NO_3 produced by anammox process, but no significant COD removal was detected at the effluent. FA monitoring during the reactor operation did not highlight the possibility of biomass inhibition (highest value was 10.2 $mgNH_3$ L^{-1}, measured at day 54), while FNA level was negligible. These results suggest that pH control was efficient during the bioreactor operation.

Despite the rough air-flow control, excellent efficiency in N removal performance was reached during the experimentation. At the beginning of each phase, NRE decreased due to the NLR increase but as

the biomass adapted to the higher initial N concentrations, the NRE reached stability (86% - 88%). It is noteworthy that the achieved NRE approached 89%, namely the maximum theoretical value for one-stage PN/A processes, as indicated by the literature (29). However, other nitrogen removal pathways are not excluded to contribute to this result. From phase I to phase III, P removal was limited (≤15%) and very unstable. In phase III after the recovery from alkaline shock a peak of ca. 40% PRE was achieved but it was likely not connected to inorganic P precipitation. Eventually in phase IV, P removal increased reaching a stable value by the end of the experimentation. In absence of an external calcium source, simultaneous nutrient removal consisting of NRR up to 0.27 kgNH_4^+-N $(m^3 \cdot d)^{-1}$ and P removal efficiency of ca. 34% were achieved in phase IV. Considering this, the PN/A rector operation can be divided into two main stages: the biomass cultivation from phase I to phase III (stage 1) and the possible mineral formation in phase IV (stage 2). Thus, the NLR increase strategy promoted the biomass growth in stage 1, while in stage 2 the growth stabilised, and the inorganic precipitation started.

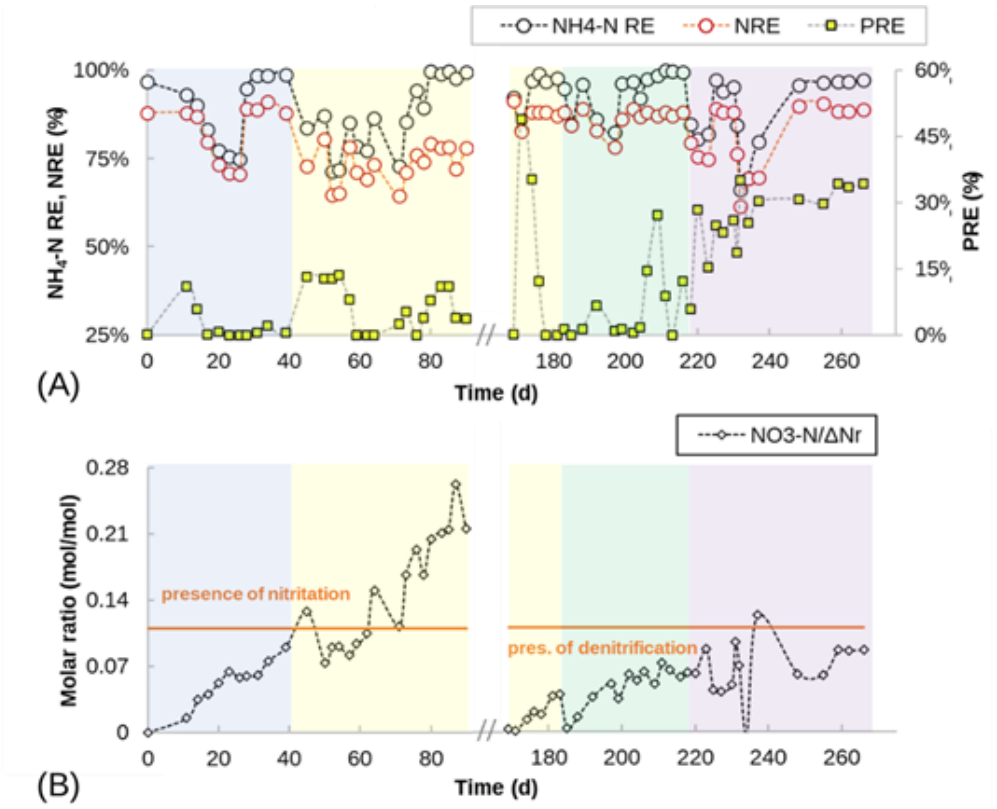

Phase	I	II	III	IV
NLR (kgN$(m^3 \cdot d)^{-1}$)	0.11	0.20	0.27	0.33
HRT (d)	7	4	3	2

Figure 3.3 – Nitrogen and phosphorus removal performance: (A) removal efficiency and (B) indicator of nitrogen removal pathway evolution in the bioreactor; operation was stopped from day 90 to day 169.

Table 3.2 – Process performance and anammox indicators in the bioreactor throughout the experimental period.

Phase		**I**	**II**	**III**	**IV**
Time	(d)	0-39	40-181	182-213	214-266
HRT	(d)	6.9	3.6	2.8	2.3
NLR	(kgN $(m^3 \cdot d)^{-1}$)	0.11 ± 0.001	0.21 ± 0.005	0.27 ± 0.002	0.33 ± 0.008
NRE	(%)	86 ± 8	88 ± 3	87 ± 1	88 ± 1
NRR	(kgN $(m^3 \cdot d)^{-1}$)	0.10 ± 0.002	0.19 ± 0.012	0.24 ± 0.007	0.25 ± 0.002
PRE	(%)	0	13 ± 17	8 ± 10	34 ± 1
N_iRR/N_ARR	(-)	0.65 ± 0.001	0.65 ± 0.001	0.65	0.65
NRR/N_ARR	(-)	1.08 ± 0.03	1.01 ± 0.09	1.01 ± 0.01	0.92 ± 0.03
NO_3-N/ΔNr	(-)	0.05 ± 0.03	0.12 ± 0.08	0.05 ± 0.02	0.07 ± 0.03
MLVSS	(g L^{-1})	4.71 ± 0.17	6.44 ± 0.21	6.90 ± 0.85	6.75 ± 0.04
MLVSS/MLSS	(%)	98 ± 1	93 ± 1	97 ± 3	76 ± 1
$(Ca/P)_{EFF}$	(mol/mol)	0	0	0	1.57 ± 0.07

Consistently to the anammox reaction equation (30), the MLVSS growth increased with the increase of NRR, rising from 4.80 up to 6.77 gMLVSS L^{-1} (Figure 3.4). Probably due to the solids contained in the target wastewater, the granules inorganic matter increase rate was comparable to the MLVSS rate until day 199, resulting in a stable MLVSS/MLSS ratio. After that, MLVSS remained stable while MLSS continued increasing above 8 gMLSS L^{-1}. This condition was likely related to precipitation of inorganic compounds such as calcium phosphate in the bioreactor. Theoretical MLVSS/MLSS was calculated based on PRR/NRR according to Chen et al. (31). As PRR/NRR increased both theoretical and real MLVSS/MLSS decreased (Figure S3.2). Particularly, as P and Ca^{2+} concentration started lowering in the bulk liquid (i.e., PRE and CaRE increase, Figure 3.4), the MLVSS/MLSS ratio decreased over time reaching a final value of 75%. Guo et al. (8) detected a similar behaviour connected to HAP precipitation when Ca/P ratio was increased through calcium external dosage. In this study, since calcium addition was avoided, a clear justification for P precipitation is not provided. Further study would be needed to explore the biomineralisation process since different parameters such as extracellular polymer substances (EPS) production by biomass, might play an important role (32). However, a significant PRR (up to 4.6 mgP $(L \cdot d)^{-1}$) was achieved treating the real anaerobic digestion effluent through the PN/A process. These promising results showed that, depending on the influent Ca/P, it is feasible to obtain P removal avoiding chemical dosages which lead to extra cost and increasing pollution potential.

Regarding precipitate characterisation, no visible precipitation was observed in the granules surface, and it was not feasible to analyse the inorganic solids possibly contained in the granules. Although,

the resulting Ca/P ratio in the effluent varied from 1.47 to 1.61 in phase IV. Thus, Amorphous Calcium Phosphate (ACP) and/or Tricalcium Phosphate have been identified as possible deriving precipitates since their constituent molar ratio (i.e., Ca/P 1.5) is included in the Ca/P range. Notably, ACP is the precursor phase during HAP formation. Previous studies reported HAP crystallisation inhibition due to the presence of magnesium. Particularly, magnesium inhibits HAP formation by stabilising ACP, blocking the conversion from ACP to HAP and extending HAP formation cycle (33–35). Ding et al. (33) found out that the Mg^{2+} inhibition effect is dependent from the initial concentration and that both surface adsorbed Mg^{2+} ions and bulk Mg^{2+} can stabilise the ACP precursor phase. In this study, the target wastewater presented a relevant magnesium content, but no stable Mg^{2+} removal was detected during the PN/A operation. Long-term PN/A operation would be needed to determine whether it is possible to obtain biomineralised HAP treating the anaerobic digestion supernatant. Moreover, long-term operation would be useful to determine how an unstable Ca/P (due to the variations typical of real wastewater) might affect the stability of the coupled process.

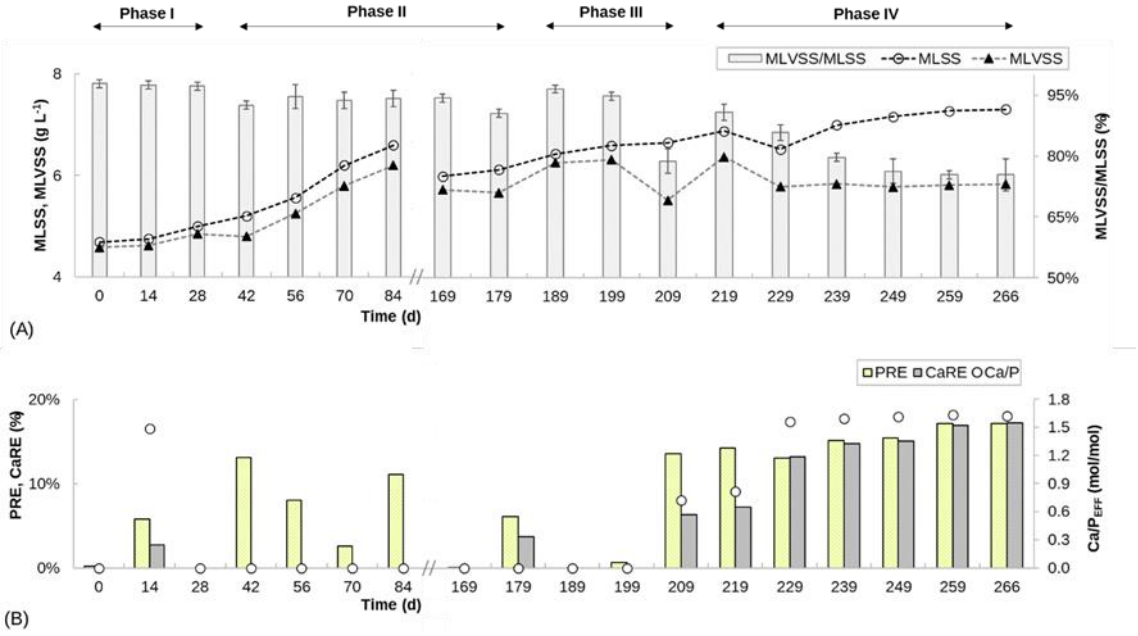

Figure 3.4 – Phosphorus (P) removal performance evolution: (A) total and volatile solids content in the mixed liquor (MLSS, MLVSS) and (B) P, and calcium (Ca) removal efficiency (PRE, CaRE) and Ca/P_{EFF} ratio measured in the effluent.

Several studies have been carried out on PN/A-HAP process using synthetic wastewaters, but very few dealt with real wastewaters (Table 3.3). In the study by Magrí et al. (11), comparable conditions of initial P concentrations and NLR were investigated. A significant 74% PRE was achieved by dosing external calcium ion at a rate of 38 mgP $(L \cdot d)^{-1}$, while simultaneously removing nitrogen by PN/A process. Notably, the presence of HAP precipitates in the sludge was observed in both Magrí's work and in the previous study conducted by Johanson et al. (10) treating urban sidestream centrate.

Chen et al. (28,36) employed an air lift reactor (ALR) inoculated with PN/A granules containing HAP cores to treat wastewater from municipal and fish processing sources. Even when the Ca/P was 4.0, they did not attain effective P removal, primarily due to the low initial phosphorus concentration in the influent. In this work, a significant PRR (4.6 mgP $(L \cdot d)^{-1}$) was achieved treating the raw anaerobic digestion effluent through the PN/A process. Indeed, the promising result obtained in this study highlights the feasibility of achieving P removal without the compelling need for chemical dosages, taking into account both the influent Ca/P ratio and the initial P concentration. Considering this, the proper selection of the wastewater to treat appears critical to reach a simultaneous N and P removal. Potentially, treating anaerobic digestion effluent can provide a tailored wastewater for the PN/A-HAP process. Particularly, by mixing different wastes proper concentrations of N, P, Ca^{2+} and alkalinity can be obtained. For instance, wastes containing high Ca^{2+} levels such as cheese whey can be used to increase the Ca/P of the treated wastewater avoiding the required external calcium dosage to obtain high PRE in the PN/A-HAP process. This approach would allow avoiding additional costs associated with chemical dosage, and it also mitigates the potential for increased water pollution by excessive calcium levels. Besides, as suggested by Chen et al. (37), combining anaerobic digestion with PN/A-HAP process can provide a sustainable and cost-effective method for addressing N and P removal in wastewater treatment processes, boosting circular economy application and contributing to pollution control.

Table 3.3 – Comparison of one-stage PN/A-HAP process treating real wastewater.

Reactor	Sludge	Wastewater	P_{inf} (mg P L^{-1})	NLR (kg N/ $(m^3 \cdot d)^{-1}$)	HRT (d)	Performances N	Performances P	MLVSS/ MLSS	Ca/P	Ref.
SBR	Granule	Anaerobic digestion supernatant	29	0.32	2.3	88.3% 0.25 kgN $(m^3 \cdot d)^{-1}$	34.2% 4.6 mg $(L \cdot d)^{-1}$	0.75	1.6	This work
SBR	Granule	Urban sidestream centrate	57	0.21	4.0	74% 0.18 gN $(gVSS \cdot d)^{-1}$	n.m.	0.65	1.1	(10)
SBR	Granule	Urban sidestream centrate	28	0.40	4.9	75% 0.27 gN $(gVSS \cdot d)^{-1}$	70% 12 mg $(L \cdot d)^{-1}$	0.5 - 0.6	2.3*	(11)
ALR	Granule with HAP	Pretreated urban wastewater	4.7	0.42	0.1	81.6% 0.36 kgN $(m^3 \cdot d)^{-1}$	n.m.	0.48	4.0	(36)
ALR	Granule with HAP	Fish processing wastewater	11	1.82	0.6	88.2% 1.51 kgN $(m^3 \cdot d)^{-1}$	no detected removal	0.6 - 0.7	0.7	(28)

ALR: Air Lift Reactor; *increased by Ca^{2+} external dosage (38 mg $(L \cdot d)^{-1}$)

3.3.2 Mineral-from biomass activity tests

HAP-granules are demonstrated to improve the sludge characteristics (i.e., sludge settleability) in PN/A process (38), but to date an actual mineral recovery strategy was not tested. To study effective P recovery potential of the PN/A-HAP process, a feasible and automatised separation procedure

should be selected. In this work, a separation methodology based on sonication was tested and its effect on AnAOB activity was investigated. Sonication was selected since it is identified by the literature (22,39,40) as an effective technique for removing biofilms from supports such as activated carbon and sediments. Different techniques have been studied to implement sonication treatment such as ultrasonic bath treatment and direct ultrasonic disruption through ultrasound probes. Close et al. (39) used direct sonicator to detach groundwater microorganisms from gravel-containing biobags achieving a 56-74% biomass removal. Besides, Padberg et al. (41) reported an improved bacterial recovery from vascular prostheses when ultrasonic bath treatment was applied rather than using ultrasonic probes. Since detachment results from external forces exceeding internal cohesion, the treatment operative conditions and the appropriate technique might be dependent on the specifical biofilm and adhesion surface. However, the same technique is used in microbiology to cause bacterial cell lysis to release intracellular material for analysis (42) and it has also been studied as an alternative method for disinfection (43). Nevertheless, it was demonstrated that the harmfulness to bacterial cells can be controlled depending on power, time, and frequency of sonication (44,45). Particularly, Joyce et al. (44) observed a limited biomass kill rate when low frequency sonication (20-38 kHz) was applied. Kobayashi et al. (46) findings suggested that exposition time lower than 30 min did not influence bacterial viability, while longer sonication durations (≥180 min) can damage the biomass. Considering these aspects, a preliminary study on granules was carried on focusing on the influence on AnAOB activity. Such results are critical to conclude whether this technique could be a viable candidate to allow effective recovery of HAP from the sludge.

Granules were harvested from the bioreactor (phase I) and treated with 37 Hz sonication. SAA was measured before and after the treatment to determine the loss of anammox activity which was influenced by the exposition time (Figure 3.5). The SAA resulted being strongly negatively affected when extending the treatment time. Nevertheless, after 15 min of granules sonication, the SAA showed a limited reduction, up to 15%, compared with untreated granules collected from the bioreactor. Moreover, size reduction after treatment was detected suggesting granules disaggregation due to sonication exposure (Table 3.4). The mean diameter decreased of ca. 50% and a slight decrease in granules shape regularity was measured. Considering exposition time, no significant difference was revealed among morphological indicators. Untreated granules appeared brownish, but when sonication was applied, they unveiled the typical AnAOB reddish colour (Figure S3.3). This later observed shade is associated with the presence of the heme-c group within the protein cytochrome-c, which plays a significant role in AnAOB metabolism (47). Within PN/A granules, variations in bacterial metabolism result in distinct patterns of dissolved oxygen (DO), pH, and substrate concentration. Consequently, these differences give rise to a stratified zone, comprising both aerobic

(AOB) and anaerobic (AnAOB) regions. Due to the environmental sensitivity of AnAOB, this specific structure allows it to thrive within the inner layers of the granule, being more resilient to external conditions (14). Thus, the sonication treatment might have revealed this deeper layer detaching the external part of the granules.

These preliminary results showed that sonication is a promising separation method for PN/A-HAP granules. Indeed, the multi-layered structure can be disassembled while mitigating SAA decrease through exposition time control. Preserving SAA is a critical point since AnAOB are slow growing bacteria not allowing a sustainable long-term P recovery when a disruptive separation method (e.g., combustion) is applied. Further work is needed to understand the influence of different operating parameters (e.g., sonication frequency) on biomass activity and to evaluate the effective mineral release treating PN/A-HAP granules. Moreover, biomass re-inoculation in the bioreactor should be tested by monitoring possible influence in long-term PN/A process operation.

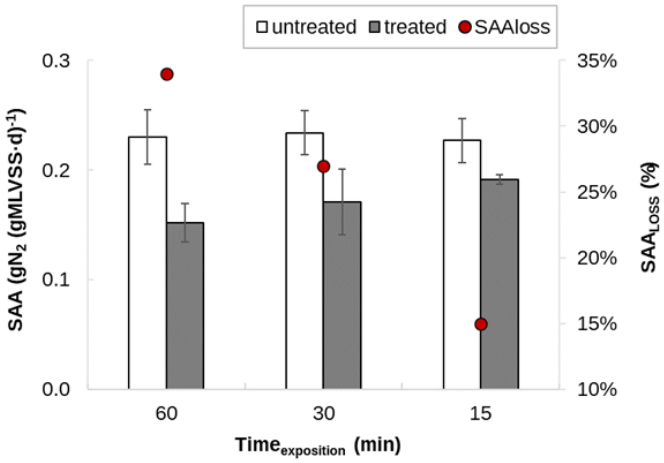

Figure 3.5 – Specific Anammox Activity (SAA) measured through manometric batch tests on the granular sludge before and after ultrasonication pretreatment (bars) and corresponding loss of activity (SAA_{LOSS}) for different exposition time ($Time_{expositiom}$).

Table 3.4 - Main morphological indicators average values of untreated and treated (ultrasonication treatment) granular sludge.

SAMPLE	$Time_{exp}$ [min]	$Diameter_{MEAN}$ [mm]	$Roundness_{MEAN}$ [-]
Untreated	-	1.94 ± 0.81	0.87 ± 0.12
Treated	15	0.52 ± 0.45	0.64 ± 0.25
	30	0.53 ± 0.37	0.72 ± 0.29
	60	0.61 ± 0.54	0.59 ± 0.17

3.4 Conclusions

The PN/A was confirmed to be a promising process to achieve a sustainable and simultaneous NH_4 and P removal from digested agro-industrial wastewater. Moreover, this work represents a first attempt for unveiling an efficient and non-damaging mineral-from-biomass separation through granules sonication. The main conclusions reached are as follows:

- Process start-up was obtained within about seven months of operation in a 3L-SBR with real wastewater. Applying an increasing NLR strategy, MLVSS increased 1.7 times compared to the initial phase, and the MLVSS/MLSS ratio of ca. 75% was achieved.
- Avoiding external calcium addition, PN/A process achieved a stable simultaneous N and P removal from agro-industrial wastewater in phase IV. Particularly, ammonium conversion rate up to 0.28 $kgNH_4^+$-N $(m^3 \cdot d)^{-1}$ and PRE of ca. 34% were reached. Ca/P ratio in the SBR effluent was close to 1.5 suggesting possible ACP mineralisation.
- Ultrasonic treatment is a promising method for mineral-from-biomass separation limiting the loss of AnAOB activity (SAA reduction up to 15% when exposition time was 15 min) while disassembling the multi-layered granule structure.

Future work on PN/A-HAP process treating agro-industrial wastewater should explore higher NLR focusing on a balance optimisation of simultaneous P and N removal; higher P removal may be achieved by increasing the Ca/P ratio with an external calcium source or up-stream to anaerobic digestion by adding Ca-rich compounds/wastes (e.g., cheese whey). Further studies are needed to build a protocol for non-disruptive mineral-from-biomass separation and to evaluate PN/A-HAP process effective P recovery potential. HAP-granules sonication must be tested to determine actual mineral separation and recovery efficiency. Finally, re-inoculating microorganisms to the bioreactor would be a key driver for evaluating the long-term stability of PN/A-HAP process, and eventually for considering the future scaling up of the technique.

Supporting information - Chapter 3

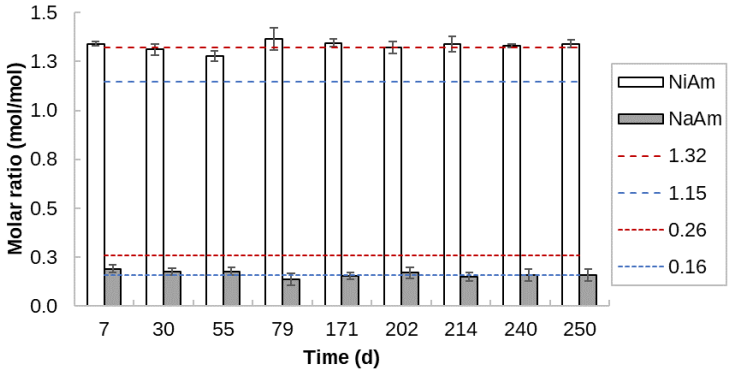

Figure S3.1 – Nitrite- to ammonium-nitrogen molar ratio (NiAm) and nitrate- to ammonium-nitrogen molar ratio (NaAm) measured in manometric batch tests for Specific Anammox Activity (SAA) determination for SBR biomass monitoring (bars); the measured molar ratios are compared to ideal anammox pathway stoichiometric ratios (19,30) (dashed lines).

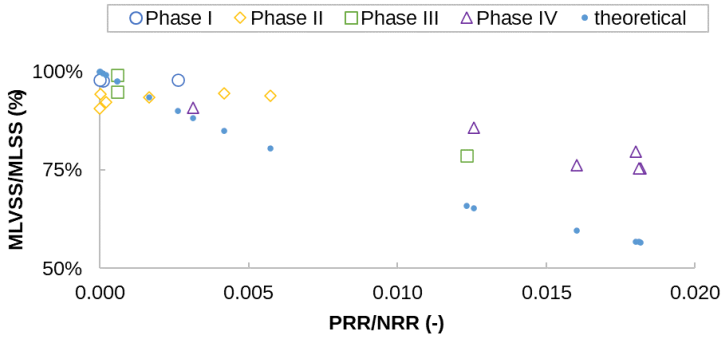

Figure S3.2 – Relationship between mixed liquor volatile suspended solids over mixed liquor suspended solids ratio (MLVSS/MLSS) and phosphorus removal rate over nitrogen removal rate ratio (PRR/NRR) during the experimentation; the theoretical value was calculated according to Chen et al. (31).

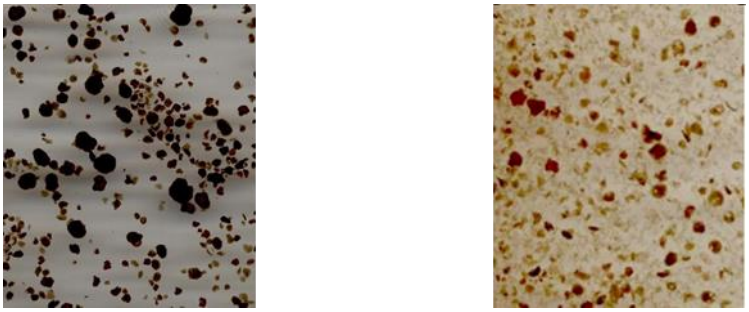

Figure S3.3 – Images of granules before (on the left) and after (on the right) the sonication treatment.

References

1. Cremonez PA, Teleken JG, Weiser Meier TR, Alves HJ. *Two-Stage anaerobic digestion in agroindustrial waste treatment: A review*. J Environ Manage. 2021; 281. https://doi.org/10.1016/j.jenvman.2020.111854.

2. Duquennoi C, Martinez J. *European Union's policymaking on sustainable waste management and circularity in agroecosystems: The potential for innovative interactions between science and decision-making.* Front Sustain Food Syst. 2022; 6. https://doi.org/10.3389/fsufs.2022.937802.

3. Liuzzi S, Rubino C, Stefanizzi P, Martellotta F. *The Agro-Waste Production in Selected EUSAIR Regions and Its Potential Use for Building Applications: A Review.* Sustain. 2022; 14 (2). https://doi.org/10.3390/su14020670.

4. Chojnacka K, Moustakas K, Witek-Krowiak A. *Bio-based fertilisers: A practical approach towards circular economy*. Bioresour Technol. 2020; 295: 122223. https://doi.org/10.1016/j.biortech.2019.122223.

5. Wong PY, Cheng KY, Kaksonen AH, Sutton DC, Ginige MP. *A novel post denitrification configuration for phosphorus recovery using polyphosphate accumulating organisms.* Water Res. 2013; 47 (17): 6488–95. http://dx.doi.org/10.1016/j.watres.2013.08.023.

6. Amann A, Weber N, Krampe J, Rechberger H, Zoboli O, Zessner M. *Operation and performance of austrian wastewater and sewage sludge treatment as a basis for resource optimization.* Water (Switzerland). 2021; 13 (21): 1–15. https://doi.org/10.3390/w13212998.

7. Wang L, Jia X, Xu L, Yu J, Ren S, Yang Y. *Engineering microalgae for water phosphorus recovery to close the phosphorus cycle.* Plant Biotechnol J. 2023; 21 (7): 1373–82. https://doi.org/10.1111/pbi.14040.

8. Guo Y, Qian Y, Shen J, Qin Y, Li YY. *The startup of the partial nitritation/anammox-hydroxyapatite process based on reconciling biomass and mineral to form the novel granule sludge.* Bioresour Technol. 2022; 347: 126692. https://doi.org/10.1016/j.biortech.2022.126692.

9. Ma H, Zhang Y, Xue Y, Kubota K, Li YY. *Efficient phosphorus recovery by enhanced hydroxyapatite formation in a high loading anammox expanded bed reactor at 15 °C.* Chem Eng J. 2021; 425: 130636. https://doi.org/10.1016/j.cej.2021.130636.

10. Johansson S, Ruscalleda M, Colprim J. *Phosphorus recovery through biologically induced precipitation by partial nitritation-anammox granular biomass.* Chem Eng J. 2017; 327: 881–8. http://dx.doi.org/10.1016/j.cej.2017.06.129.

11. Magrí A, Company E, Gich F, Colprim J. *Hydroxyapatite Formation in a Single-Stage Anammox-Based Batch Treatment System: Reactor Performance, Phosphorus Recovery, and Microbial Community.* ACS Sustain Chem Eng. 2021; 9 (7): 2745–61. https://doi.org/10.1016/j.jclepro.2018.08.258.

12. Cao L, Yang Y, Xue Y, Ma H, Li YY, Hu Y. *A review of efficient nitrogen removal and phosphorus recovery by anammox-hydroxyapatite based processes: Challenges and opportunities.* J Environ Chem Eng. 2023; 11 (5): 111103. https://doi.org/10.1016/j.jece.2023.111103.

13. Chen G, Zhang Y, Wang X, Chen F, Lin L, Ruan Q. *Optimizing of operation strategies of the single-stage partial nitrification-anammox process.* J Clean Prod. 2020; 256: 120667. https://doi.org/10.1016/j.jclepro.2020.120667.

14. Cao Y, van Loosdrecht MCM, Daigger GT. *Mainstream partial nitritation–anammox in municipal wastewater treatment: status, bottlenecks, and further studies.* Appl Microbiol Biotechnol. 2017; 101 (4): 1365–83. http://dx.doi.org/10.1007/s00253-016-8058-7.

15. Ibrahim M, Labaki M, Giraudon JM, Lamonier JF. *Hydroxyapatite, a multifunctional material for air, water and soil pollution control: A review.* J Hazard Mater. 2020; 383: 121139. https://doi.org/10.1016/j.jhazmat.2019.121139.

16. Ma H, Xue Y, Zhang Y, Kobayashi T, Kubota K, Li YY. *Simultaneous nitrogen removal and phosphorus recovery using an anammox expanded reactor operated at 25 °C.* Water Res. 2020; 172: 115510. https://doi.org/10.1016/j.watres.2020.115510.

17. Guo Y, Li YY. *Hydroxyapatite crystallization-based phosphorus recovery coupling with the nitrogen removal through partial nitritation/anammox in a single reactor.* Water Res. 2020; 187: 116444. https://doi.org/10.1016/j.watres.2020.116444.

18. Xue Y, Ma H, Kong Z, Li YY. *Formation Mechanism of hydroxyapatite encapsulation in Anammox-HAP Coupled Granular Sludge.* Water Res. 2021; 193. https://doi.org/10.1016/j.watres.2021.116861.

19. Lotti T, van der Star WRL, Kleerebezem R, Lubello C, van Loosdrecht MCM. *The effect of nitrite inhibition on the anammox process.* Water Res. 2012; 46 (8): 2559–69. https://dx.doi.org/10.1016/j.watres.2012.02.011.

20. Milia S, Perra M, Tocco G, Carucci A. *The start-up of an anammox reactor as the second step for the treatment of ammonium rich refinery (IGCC) wastewater with high Corg/N ratio.* Ecol Eng. 2017; 106 (2): 358–68. https://dx.doi.org/10.1016/j.ecoleng.2017.04.068.

21. Dapena-Mora A, Fernández I, Campos JL, Mosquera-Corral A, Méndez R, Jetten MSM. *Evaluation of activity and inhibition effects on Anammox process by batch tests based on the nitrogen gas production*. Enzyme Microb Technol. 2007; 40 (4): 859–65. https://doi.org/10.1016/j.enzmictec.2006.06.018.

22. Magic-Knezev A, van der Kooij D. *Optimisation and significance of ATP analysis for measuring active biomass in granular activated carbon filters used in water treatment.* Water Res. 2004; 38 (18): 3971–9. https://doi.org/10.1016/j.watres.2004.06.017.

23. APHA. *Standard Methods for the Examination of Water and Wastewater, American Public Health Association, Washington, DC (2017).* Am Public Heal Assoc (APHA), Am Water Work Assoc Water Environ Fed Washington, DC, USA. 2017.

24. Anthonisen AC, Loehr RC, Prakasam TBS, Srinath EG. *Inhibition of nitrification by ammonia and nitrous acid.* J Water Pollut Control Fed. 1976; 48 (5): 835–52. https://www.jstor.org/stable/25038971.

25. Kartal B, Rattray J, van Niftrik LA, van de Vossenberg J, Schmid MC, Webb RI. *Candidatus "Anammoxoglobus propionicus" a new propionate oxidizing species of anaerobic ammonium oxidizing bacteria.* Syst Appl Microbiol. 2007; 30 (1): 39–49. https://doi.org/10.1016/j.syapm.2006.03.004.

26. Hubaux N, Wells G, Morgenroth E. *Impact of coexistence of flocs and biofilm on performance of combined nitritation-anammox granular sludge reactors.* Water Res. 2015; 68: 127–39. http://dx.doi.org/10.1016/j.watres.2014.09.036.

27. Gao Y, Liu Z, Liu F, Furukawa K. *Mechanical shear contributes to granule formation resulting in quick start-up and stability of a hybrid anammox reactor.* Biodegradation. 2012; 23 (3): 363–72. https://doi.org./10.1007/s10532-011-9515-8.

28. Chen Y, Sanjaya EH, Guo G, Li YY. *High nitrogen removal performance of anaerobically treated fish processing wastewater by one-stage partial nitritation and anammox process with hydroxyapatite (HAP)-based syntrophic granules and granule structure.* Bioresour Technol. 2021; 338: 125526. https://doi.org/10.1016/j.biortech.2021.125526.

29. Guo Y, Sugano T, Song Y, Xie C, Chen Y, Xue Y. *The performance of freshwater one-stage partial nitritation/anammox process with the increase of salinity up to 3.0%.* Bioresour Technol. 2020; 311: 123489. https://doi.org/10.1016/j.biortech.2020.123489.

30. Strous M, Van Gerven E, Zheng P, Kuenen JG, Jetten MSM. *Ammonium removal from concentrated waste streams with the anaerobic ammonium oxidation (anammox) process in different reactor configurations.* Vol. 31, Water Research. 1997. p. 1955–62. https://doi.org/10.1016/S0043-1354(97)00055-9.

31. Chen Y, Guo Y, Feng G, Urasaki K, Guo G, Qin Y. *Key factors improving the stability and the loading capacity of nitrogen removal in a hydroxyapatite (HAP)-enhanced one-stage partial nitritation/anammox process.* Chem Eng J. 2023; 452: 139589. https://doi.org/10.1016/j.cej.2022.139589.

32. Cheng H, Qin H, Liang L, Li YY, Liu J. *Towards advanced simultaneous nitrogen removal and phosphorus recovery from digestion effluent based on anammox-hydroxyapatite (HAP) process: Focusing on a solution perspective.* Bioresour Technol. 2023; 381: 129117. https://doi.org/10.1016/j.biortech.2023.129117.

33. Ding H, Pan H, Xu X, Tang R. *Toward a detailed understanding of magnesium ions on hydroxyapatite crystallization inhibition.* Cryst Growth Des. 2014; 14 (2): 763–9. https://dx.doi.org/10.1021/cg401619s.

34. Talebi Atouei M, Rahnemaie R, Goli Kalanpa E, Davoodi MH. *Competitive adsorption of magnesium and calcium with phosphate at the goethite water interface: Kinetics, equilibrium and CD-MUSIC modeling.* Chem Geol. 2016; 437: 19–29. http://dx.doi.org/10.1016/j.chemgeo.2016.05.004.

35. Yang X, Xie B, Wang L, Qin Y, Henneman ZJ, Nancollas GH. *Influence of magnesium ions and amino acids on the nucleation and growth of hydroxyapatite.* Cryst Eng Comm. 2011; 13 (4): 1153–8. https://doi.org/10.1039/c0ce00470g.

36. Chen Y, Feng G, Guo G, Luo Z, Rong C, Wang T. *Nitrogen removal by a Hydroxyapatite-enhanced Micro-granule type One-stage partial Nitritation/anammox process following anaerobic membrane bioreactor treating municipal wastewater.* Bioresour Technol. 2022; 348, 126740. https://doi.org/10.1016/j.biortech.2022.126740.

37. Guo Y, Chen Y, Webeck E, Li YY. *Towards more efficient nitrogen removal and phosphorus recovery from digestion effluent: Latest developments in the anammox-based process from the application perspective.* Bioresour Technol. 2020; 299. https://doi.org/10.1016/j.biortech.2019.122560

38. Chen Y, Feng G, Guo G, Urasaki K, Kubota K, Li YY. *Improved Properties and Enhancement Strategies of Hydroxyapatite-Based Functional Granular Sludge for a High-Rate Partial Nitritation/Anammox System.* Environ Sci Technol. 2023; 57 (19): 7624–33. https://doi.org/10.1021/acs.est.3c00491.

39. Close M, Abraham P, Webber J, Cowey E, Humphries B, Fenwick G, et al. *Use of Sonication for Enhanced Sampling of Attached Microbes from Groundwater Systems.* Groundwater. 2020; 58 (6): 901–12. https://doi.org/10.1111/gwat.12984.

40. Amalfitano S, Fazi S. *Recovery and quantification of bacterial cells associated with streambed sediments.* J Microbiol Methods. 2008; 75 (2): 237–43. https://doi.org/10.1016/j.mimet.2008.06.004.

41. Padberg FT, Smith SM, Eng RHK. *Optimal method for culturing vascular prosthetic grafts.* J Surg Res. 1992; 53 (4): 384–90. https://doi.org/10.1016/0022-4804(92)90065-8.

42. Fykse EM, Olsen JS, Skogan G. *Application of sonication to release DNA from Bacillus cereus for quantitative detection by real-time PCR.* J Microbiol Methods. 2003; 55 (1): 1–10. https://doi.org/10.1016/S0167-7012(03)00091-5.

43. Joyce E, Mason TJ, Phull SS, Lorimer JP. *The development and evaluation of electrolysis in conjunction with power ultrasound for the disinfection of bacterial suspensions.* Ultrason Sonochem. 2003; 10 (4–5): 231–4. https://doi.org/10.1016/S1350-4177(03)00109-3.

44. Joyce E, Phull SS, Lorimer JP, Mason TJ. *The development and evaluation of ultrasound for the treatment of bacterial suspensions. A study of frequency, power and sonication time on cultured*

Bacillus species. Ultrason Sonochem. 2003;10(6):315–8. https://doi.org/10.1016/S1350-4177(03)00101-9.

45. Kobayashi H, Oethinger M, Tuohy MJ, Procop GW, Bauer TW. *Improved detection of biofilm-formative bacteria by vortexing and sonication: A pilot study.* Clin Orthop Relat Res. 2009; 467(5): 1360–4. https://doi.org/10.1007/s11999-008-0609-5.

46. Kobayashi N, Bauer TW, Tuohy MJ, Fujishiro T, Procop GW. *Brief ultrasonication improves detection of biofilm-formative bacteria around a metal implant.* Clin Orthop Relat Res. 2007; 457 (457): 210–3. https://doi.org/10.1097/BLO.0b013e3180312042.

47. Ni SQ, Zhang J. *Anaerobic ammonium oxidation: From laboratory to full-scale application.* Biomed Res Int. 2013; 2013. http://dx.doi.org/10.1155/2013/469360.

CHAPTER 4: Reagent-free phosphorus recovery from a swine denitrified effluent in a batch electrochemical system[2]

Abstract

Recently, wastewater treatment has witnessed a growing interest in electrochemical technologies over traditional physicochemical techniques for phosphorus (P) recovery as limited or zero-chemical input is needed. Electrochemical mediated precipitation was explored in the present work to achieve reagent-free phosphorus precipitation from swine denitrified effluent (46 ± 6 mgPO_4-P L^{-1}). Onsite production of hydroxyl ions (OH^-) was carried out in a double-chambered electrochemical system equipped with a cation exchange membrane and running in batch mode. The influence of applied current density (≤1.2 A m^{-2}) and effluent strength (dilution 4x and 1x) on the pH profile and P precipitation was studied considering two final pH values (10.5 and 11.5). Maximum P removal rate (4.5 mM d^{-1}) was achieved at pH 11.5 for the highest CD tested (1.2 A m^{-2}) and it was not affected by the effluent strength. The specific energy consumption behaved inversely to the effluent strength, accounting for 69.07 ± 1.84 (1x) and 118.71 ± 8.22 kWh kg^{-1} P (4x), suggesting that higher influent P levels can favour energy savings. X-ray diffraction analysis revealed that cattiite ($Mg_3(PO_4)_2 \cdot 22H_2O$) was the main mineral formed in the bulk liquid. Moreover, chlorine production was detected in the anode and was favoured by a higher initial pH and a smaller anode surface. The electrochemical impedance spectroscopy tests confirmed that solids deposition into the system along the experimental period was limited, only contributing to a slight increase of the ohmic resistance (quantified as 0.79 Ω m^2 in the two-electrode configuration test). Membrane X-ray analysis revealed that significant precipitation of carbonate compounds occurred, but no phosphate compounds were detected. The electrochemical system operated at low current density (≤1.2 A m^{-2}) was proved as a promising alternative to NaOH dosage for pH adjustment when targeting P recovery and the feasibility of the catholyte neutralisation (final pH of 6.43 ± 0.05) in the anodic compartment was demonstrated. Moreover, the electrochemical treatment of swine denitrified effluent allowed for economic savings as the cost for raising the pH at 11.5 was 0.31 € m^{-3} (13.81 € kg^{-1} P) vs. 0.57 € m^{-3} (14.77 € kg^{-1} P) when dosing NaOH (5M), while the economic benefit from avoiding H_2SO_4 for catholyte neutralisation was 0.26 € m^{-3}.

[2]Part of the work included in this chapter was presented at the: 6th European Meeting of the International Society for Microbial Electrochemistry and Technology (EU-ISMET), 06-08/09/23, Wagenigen, the Netherlands.

4.1 Introduction

Phosphorus (P) is an essential element for all living organisms as a constituent of nucleic acids (DNA and RNA), energy-transfer molecules in metabolism (ATP), cell membranes and body-building blocks (1). The shortage of this irreplaceable nutrient limits the food production, but when discharged in excess to the environment it acts as a pollutant, causing eutrophication and nutrient imbalances (2). Phosphorus is typically extracted by the mining industry from phosphate rock, a non-renewable resource. As reserves of phosphate rock available in geological deposits unevenly distributed around the world are being depleted, uncertainties arise in the supply of this nutrient (3,4). Alternatively, P can be recovered from wastewater streams, which are a renewable source of nutrients available at the local scale, using methods such as the crystallisation of low-soluble phosphate salts, among others (5–7). The pH –as well as other parameters– is a key factor in the crystallisation reactions so the addition of chemicals is traditionally considered to raise its value (e.g., sodium hydroxide (NaOH)) besides increasing the content in metal ions (e.g., calcium hydroxide ($Ca(OH)_2$), magnesium oxide (MgO), etc.).

In recent years, wastewater treatment has witnessed a growing interest in electrochemical technologies (ETs), including P removal and recovery applications (8). Some advantages of using these techniques over traditional physicochemical techniques are the use of compact reactors with small physical footprints, the need for mild operating conditions such as ambient temperature and pressure, the in-situ production of chemicals avoiding transportation and storage, and the lower generation of secondary waste (9). The electrochemical mediated precipitation (EMP) process is advantageous with respect to other ETs like electrochemical coagulation. The latter process applies sacrificial electrodes to release cations (e.g., Al^{3+}, Fe^{2+}, Mg^{2+}) to remove phosphate, which will produce a large amount of sludge, and the electrodes need to be replaced regularly during long-term operation (10,11), leading to an increase in the operational costs. By contrast, the EMP process will produce P minerals and can employ inert electrodes, which are not necessarily consumed during the reaction (8). The EMP process has already been applied in several situations for the recovery of P compounds, such as the case of cheese wastewater and the recovery of calcium phosphate (12), hypophosphite-laden wastewater and the recovery of ferric phosphate (13), and digestate and urine and the recovery of struvite (14,15).

Particularly, water electrolysis has been applied as a clean method for the onsite production of hydroxyl ions (OH^-) (16–18). An electrochemical system typically consists of electrodes (i.e., anode and cathode), an electrolyte solution, and an external power supply. When current is supplied, water molecules at the cathode are reduced to hydrogen (H_2) with the simultaneous production of OH^- (Re. 1), which raises the local pH, while at the anode, water molecules are oxidized to oxygen (O_2) and

protons (H^+) (Re. 2), neutralising the OH^- produced at the cathode. Ion exchange membranes are used in electrolysis cells to prevent the neutralisation of the low-pH anolyte with the high-pH catholyte. In this case, the system typically is split into two compartments and a pH-gradient is formed between the anode and the cathode. Besides, side reactions such as chloride (Cl^-) conversion to chlorine gas (Cl_2) (Re. 3) can take place in the anode.

Cathode: $2H_2O + 2e^- \rightarrow H_2 + 2OH^-$ (Re. 1)

Anode: $2H_2O \rightarrow O_2 + 4H^+ + 4e^-$ (Re. 2)

$2Cl^- \rightarrow Cl_2 + 2e^-$ (Re. 3)

The EMP process has been demonstrated to be effective in the recovery of P, with multiple factors affecting its performance, including the pH, current density (CD), electrode configuration, and water matrix. In the EMP process, the electrode is usually inert, and the removal of P is driven by the production of OH^- and the achievement of high pH-values at the cathode. Cations available in the wastewater are headed toward the cathode due to electro-migration and, as a result, most of the precipitate becomes attached to the cathode's surface, from where it can be collected periodically. Nevertheless, process optimisation, and particularly, sustainable mineral recovery strategies are still necessary to make the electrochemical precipitation economically viable. The electrode's excessive coating leads to an increase in ohmic resistances eventually promoting cathode deactivation (19). The need for arresting the treatment for precipitate collection is limiting for the long-term operational feasibility. To ease the mineral recovery some authors suggested implementing automatic scraping methods (20,21), while Takabe et al. (22) successfully tested polarity inversion to detach the solids from the cathode. Furthermore, the adoption of the electrochemical process is limited by its high energy consumption. A high CD (up to 300 A m^{-2} (22,23)) is commonly applied to improve P removal rates (24) leading to increased operational costs. To contribute to the development of an energy-efficient electrochemical process and limit the precipitation in the electrode surface, the application of a low CD in the electrochemical system could be a viable option. As an example, Lei et al. (25) achieved 70% P removal efficiency from acidic cheese wastewater by applying extremely low CD (0.2 A m^{-2}) reaching a specific energy consumption of 26.4 kWh kg^{-1} P, which was two orders of magnitude lower than their previous system operated with a high CD (27.8 A m^{-2}). Under these conditions, it was also reduced the co-precipitation of calcium carbonate ($CaCO_3$) and brucite ($Mg(OH)_2$).

In the present work, swine denitrified effluent was used to explore the feasibility of reagent-free P recovery through an EMP process. Considering the previous experience reported by Company et al. (26) with this kind of effluent based on the dosage of chemicals (i.e., NaOH) to raise the pH to values

as high as 10.5-11.5 and sulphuric acid (H_2SO_4) to decrease the pH near 7.0), EMP at low CD ($\leq$ 1.2 A m^{-2}) was tested as an alternative approach. This approach also led to a decrease in the supply of Na^+ to the system, which can affect the quality of the recovered product. Particularly, the influence of the targeted pH, wastewater strength and CD on P removal from the liquid phase was investigated using a two-chambered electrochemical system equipped with a cation exchange membrane (CEM) and running in batch mode. Thus, precipitation tests were performed to assess the potential for P removal in the cathodic compartment and the energy consumption efficiency of the system. The recovered products were also characterised. Moreover, catholyte neutralisation before discharge was also explored in the anodic compartment with the outlook of operating the system in continuous-flow mode. Finally, electrochemical impedance spectroscopy (EIS) was used as a fast and non-destructive technique to study the performance of the electrochemical system and, particularly, the resistance increase due to precipitation phenomena.

4.2 Material and methods

4.2.1 Batch electrochemical system set-up

A double-compartment methacrylate square reactor was used in this study as electrochemical system (Figure 4.1). The anode (frame size: 28 x 28 x 2 cm^3, working volume: 830 mL) and the cathode (frame size: 28 x 28 x 3 cm^3, working volume: 1010 mL) compartments were separated by a CEM (CMI-7000, Membranes Int., USA) with a surface of 784 cm^2. A stainless-steel mesh with a total surface of 2418 cm^2 (1.0 mm of light path and 0.4 mm of wire diameter, CISA, Spain) was used as cathode, and a Ti-MMO mesh with a surface of 148 cm^2 (2 mm light path and 1 mm wire diameter, NMT electrodes, South Africa) was used as anode. The reactor was galvanostatically controlled, at a fixed CD value (from 0.4 to 1.2 A m^{-2}), using an external power supply (mod. IMHY3003D, Lendher, Spain). Peristaltic pumps (mod. 323, Watson Marlow, UK) were used to recirculate the denitrified effluent (working flow rate: 192 mL/min) in each compartment, both connected to a 1-L Schott bottle. The pH and electrical conductivity (EC) of both, the catholyte and anolyte, were recorded online using a control panel that included a multimeter (mod. MM44, Crison Instruments SA, Spain) plugged to a memograph (mod. RSG40, Endress+Hauser Inc., Switzerland).

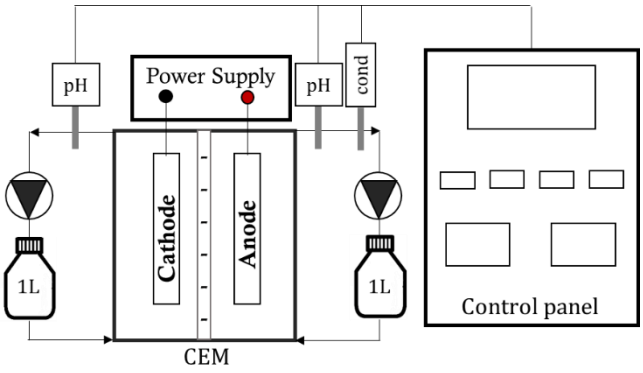

Figure 4.1 – Scheme of the batch electrochemical system set-up.

4.2.2 Swine denitrified effluent characterisation

The swine denitrified effluent used in the electrochemical tests was collected from a pig farm located in Osona (Catalonia, Spain). Following solid-liquid separation, the liquid fraction of the slurry is treated biologically onsite, in a sequencing batch reactor under intermittent aeration, aiming to remove nitrogen (N). The denitrified effluent was sampled after the sludge settling. Samples were transported from the farm to the laboratory in polyethylene containers. Once at the laboratory facilities, these containers were stored at room temperature until performing the experiments. Final compositional characteristics of the denitrified effluent used are given in Table 4.1. Low alkalinity (1056 mg$CaCO_3$ L^{-1}) and no ammonium-N remained in the effluent after biological treatment. The Mg^{2+}:PO_4 molar ratio was 2.8, much higher than the Ca^{2+}:PO_4 molar ratio, which was 0.7.

Table 4.1 - Main physicochemical characteristics of the swine denitrified effluent.

Parameters	Units	Average	SD
pH	-	8.5	0.2
EC	mS cm^{-1}	6.1	0.1
ALK ($CaCO_3$)	mg L^{-1}	1056	26
TIC	mg L^{-1}	248	6
Na^+	mg L^{-1}	456	31
K^+	mg L^{-1}	1068	76
Mg^{2+}	mg L^{-1}	104	8
Ca^{2+}	mg L^{-1}	41	3
Cl^-	mg L^{-1}	864	40
SO_4^{2-}-S	mg L^{-1}	124	7
PO_4^{3-}-P	mg L^{-1}	48	5
NH_4^+-N	mg L^{-1}	0	0
NO_3^--N + NO_2^--N	mg L^{-1}	0	0

ALK, alkalinity; SD, standard deviation; TIC, total inorganic carbon.

4.2.3 Experimental tests performed in the electrochemical system

4.2.3.1 Batch experiments

4.2.3.1.1 Precipitation in the cathodic compartment

Precipitation tests using swine denitrified effluent were performed by operating the electrochemical system in batch (in triplicates) to evaluate the influence of the operational conditions applied including the final pH value (10.5 and 11.5), CD (0.0, 0.4, 0.6, 0.8 and 1.2 A m^{-2}) and effluent strength (dilution factor with deionized water: 1x -undiluted (1:1)- and 4x (1:4)) on the ion removal efficiency. All tests were run at room temperature (20 ± 2°C) using ca. 1.65 L of denitrified effluent in each compartment. Depending on the applied current and the effluent strength, the resulting cell potential ranged from 2.3 to 5.0 V. The experiments ended when the pH value reached 11.5. Once at that point, the power supply was switched off and the cathodic and anodic bottles were emptied. The reactor compartments were then cleaned with an acidic solution and deionized water to ensure that no residual precipitates remained. The final catholyte was filtered through a filtering paper to retain solids, which were dried at room temperature and ground before analysis. Liquid samples from the anodic and cathodic compartments were collected when pH in the catholyte reached values of 10.5 and 11.5. These samples were filtered at 0.2 µm and stored at room temperature before analysis. By the end of the experimental period, the electrochemical cell was opened to characterise the solids deposited on the surface of the membrane.

4.2.3.1.2 Neutralisation in the anodic compartment

To explore the feasibility of modifying the electrochemical system looking for its operation in continuous-flow mode, where the catholyte could be potentially neutralised in the anodic compartment before discharge, neutralisation tests were carried out. The solution to be recirculated in the anodic compartment was obtained from the previous precipitation test (i.e., final catholyte at pH 11.5), while in the cathode the recirculated liquid was fresh denitrified effluent. Additionally, the influence of the anode surface on the chlorine production was assessed by tripling the electrode area (i.e., from 148 cm^2 to 444 cm^2). Acid requirements to neutralise (pH 7.0) the pH of the catholyte were assessed titrimetrically using an H_2SO_4 solution (26).

4.2.3.2 Electrochemical impedance spectroscopy (EIS) tests

A BioLogic potentiostat (mod. VSP, France) was used to perform the EIS tests on the batch electrochemical system. A volume of ca. 1.65 L of fresh denitrified effluent was recirculated in each compartment. At least two EIS runs were performed to characterise the system's electrochemical performance prior to and after conducting the precipitation tests. The internal resistance was

investigated using two- and three-electrode configurations. In the latest case, an Ag/AgCl sat. KCl reference electrode (+0.197 V vs. SHE, SE 11, Xylem Analytics Germany Sales GmbH & Co. KG Sensortechnik Meinsberg, Germany) was placed in the cathodic compartment, as much closer as possible to the electrode. Firstly, before any EIS measurement, steady-state conditions were reached considering voltage stabilisation for a minimum of 1.5 h in open circuit voltage (OCV). To ensure that the relevant physical phenomena were captured in the EIS spectrum, all EIS measurements occurred over the frequency range from 100 kHz to 10 MHz. A sinusoidal perturbation with an amplitude of 10 mA was used with 10 points per logarithmic decade for the analysis (27). A potential of 0 V vs. three different fixed potential values (-0.8, -1.0 and -1.2 V vs. Ag/AgCl) was applied as input signals to investigate the influence on the components of the overall system internal resistance. To study the impedance results, the so-called Nyquist plot was used. In this plot, every interface can ideally be visualised as a semicircle. The EIS parameters were extracted by fitting an equivalent electrical circuit model (ECM) using Zfit (EC-lab software). The ECM produces pseudo-electrochemical parameters which can be sorted to represent anode and cathode impedances separately, as well as individually to assess the ohmic, kinetic, and mass transfer limitations of the system. Common configurations of ECM have included a resistor representing solution resistance connected in series to parallel combinations of resistors representing charge transfer reactions, but when the mass transfer is expected to be a limiting factor in system performance Warburg elements are also included (28). Thus, these above-mentioned elements were used in the fitting model to represent the obtained results. Particularly, the EIS spectra intersection with the x-axis identifies the ohmic resistance of the system.

4.2.4 Analytical methods

Water samples were analyzed following APHA et al. (29). The pH was measured offline using a bench pH-meter (mod. Sension+ PH3, Hach, Germany), and electrical conductivity (EC) measurements were carried out using a conductivity-meter (mod. EC-Meter Basic 30+, Crison Instruments SA, Spain). Total alkalinity (ALK, reported as $CaCO_3$) was determined by acid titration to an endpoint pH of 4.5 and total inorganic carbon (TIC) was measured through the 5-pH point titration method (30). The concentration of the soluble cations (i.e., ammonium (NH_4^+), sodium (Na^+), potassium (K^+), magnesium (Mg^{2+}), and calcium (Ca^{2+})), as well as the concentration of the soluble anions (i.e., nitrite (NO_2^-), nitrate (NO_3^-), chloride (Cl^-), sulfate (SO_4^{2-}), and phosphate (PO_4^{3-})), was determined by ion chromatography (mod. ICS-5000, Dionex, USA) after filtering samples with 0.2 µm nylon filters. The precipitated salts were analyzed using X-ray diffraction (XRD) (mod. D8

Advance, Bruker, USA). Precipitate and membrane images were taken through scanning electrode microscopy (SEM) (mod. DSM-960A, Zeiss, Germany). The total content of the main constituents (i.e., Na, K, Ca, Mg, and P) in membrane deposits was measured after microwave digestion with a $HNO_3/H2O_2$ mixture using inductively coupled plasma-optical emission spectrometry (ICP-OES) (mod. 5100, Agilent Technologies, USA). Chlorine gas (Cl_2) was determined using a spectrophotometer (mod. DR1900, Hach Lange, Germany) according to the DPD-free chlorine method (Hach Lange).

4.2.5 Calculations

The hydroxyl production (OH^-_{prod}) (mol OH^- L^{-1}), namely the amount of electrons that went from the anode to the cathode, can be calculated considering the electric current that was applied during the test, as it is shown in Eq. 1 (100% faradaic efficiency is assumed),

$$OH^-_{prod} = \frac{I \cdot t_{pH}}{F \cdot V_{CAT}} \quad (\text{Eq. 1}),$$

where: t_{pH} (s) is the time needed to raise the initial pH of the denitrified effluent (Table 4.1) in the cathode compartment up to the targeted pH value (10.5 or 11.5) according to the applied electric current (I (A)), F is the Faraday constant (96485.332 C mol^{-1}) and V_{CAT} (L) is the recirculating catholyte volume. For comparison purposes, the hydroxyl demand of the denitrified effluent was estimated experimentally based on a titration test using NaOH (26).

The specific pH raising rate in the cathodic compartment ($pHRR_{CAT}$) (u.pH $(L \cdot h)^{-1}$) was calculated according to Eq. 2. To ensure a linear profile, the pH-time slope ($s_{pH,CAT}$) (u.pH h^{-1}) was obtained by linear regression considering the pH values measured between 10.5 and 11.5.

$$pHRR_{CAT} = \frac{s_{pH,CAT}}{V_{CAT}} \quad (\text{Eq. 2}).$$

The specific energy consumption (sEC) (kWh m^{-3}) in the electrochemical system was calculated according to Eq. 3,

$$sEC = \frac{I \cdot \int V dt}{V_{CAT}} \quad (\text{Eq. 3}),$$

where: V (V) is the electric potential, and t (h) is the time lasted by the experiment.

The ion removal rate (IRR) (mol $(L \cdot d)^{-1}$), particularly for P, Mg and Ca (i.e., PRR, MgRR and CaRR, respectively), was calculated according to Eq. 4,

$$IRR = \frac{(C_{CAT,t0} - C_{CAT,t})}{t_{pH}} \quad (\text{Eq. 4}),$$

where: C_{CAT} is the ion molar concentration (M) measured in the catholyte at time t_0 (i.e., at the start of the test) and time t (i.e., at the time when pH 10.5 or 11.5 was reached). Otherwise, the ion removal efficiency (IRE) (%), was calculated as shown in Eq. 5.

$$IRE = \frac{(C_{CAT,t0} - C_{CAT,t})}{C_{CAT,t0}} \quad \text{(Eq. 5)}.$$

The specific energy consumption in relation to the P removal from the liquid phase (sEC_P) (kWh kg^{-1} P) is calculated according to Eq. 6, once accounted for the molecular weight of P (MW_P).

$$sEC_P = \frac{\text{sEC}}{(P_{CAT,t0} - P_{CAT,t}) \cdot MW_P} \quad \text{(Eq. 6)}.$$

The cost of dosing NaOH was calculated according to 0.50 € kg^{-1} NaOH (12) and considering the titration test results for the denitrified effluent (22.8 mmol L^{-1} to reach pH 11.5). The cost of dosing H_2SO_4 was calculated according to 0.26 € kg^{-1} (31) and considering the titration test results for the catholyte to move down the pH from 11.5 to 7.0 (20.8 mmol H^+ L^{-1}). On the other hand, the cost of operating the electrochemical system (i.e., external power supply) was calculated considering the cost of energy for an industrial application (0.20 € kWh^{-1}, European electricity price for the second semester of 2022) and the experimental sEC (kWh m^{-3}).

Considering the composition of the swine denitrified effluent, the supersaturation conditions and possible mineral phases formed were assessed using the freeware Visual MINTEQ (32). The saturation index (SI, $\log_{10}(IAP/K_{sp})$) was calculated as a function of the corresponding ion activity product (IAP) and the mineral phase solubility product constant (K_{sp}). If the SI for a particular mineral is positive, the system is supersaturated with respect to that mineral, and precipitation may occur. Values for the K_{sp} of the mineral phases bobierrite ($10^{-25.2}$), cattiite ($10^{-23.1}$), K-struvite ($10^{-12.2}$), and Na-struvite ($10^{-11.6}$) were added to the MINTEQ original database according to other sources (33,34).

4.3 Results and discussion

4.3.1 Precipitation tests in the cathodic compartment

A two-chamber electrochemical system equipped with a CEM was run in batch mode to achieve chemical-free P removal from a swine denitrified effluent (i.e., OH^- ions needed for raising the pH were produced onsite rather than supplied as NaOH). The rate of OH^- production at the cathode of the electrochemical cell is directly influenced by the applied CD. Fixed the operation time, an increase in the current boosts P removal since it accelerates OH^- production (Re. 1), thus triggering a faster rise of the local pH value. Nevertheless, as the applied CD increases, so does the energy consumption, leading to higher operational costs. This study explores the feasibility of electrochemical P removal from real wastewater when applying low CD (≤ 1.2 A m^{-2}). Moreover, the low current values were tested also aiming to prevent the deposition of the mineral phase on the cathode and its scaling on the membrane, thus allowing the precipitate recovery from the bulk solution.

4.3.1.1 Influence of current density and denitrified effluent strength

The electric charge required to reach the targeted pH is dependent on the applied CD and the denitrified effluent strength (Table S4.1). Considering the maximum CD tested (1.2 A m^{-2}) and the fresh denitrified effluent (1x dilution), an electric charge of 1.12 ± 0.02 kC L^{-1} was required to reach pH 10.5, and an additional 1.16 kC L^{-1} were needed to reach pH 11.5 (2.28 ± 0.02 kC L^{-1} in total). The theoretical cell potential can be calculated with the Nernst equation as a function of the initial and final pH reached in the compartments. The pH of the catholyte increased from 8.5 to 10.5 and 11.5, while the pH of the anolyte decreased from 8.5 to 7.3 and 6.1, respectively. According to this criterion, a cell potential of 1.4 and 1.6 V was theoretically needed to drive water reduction (cathode) and oxidation (anode) reactions, to reach a pH of 10.5 and 11.5 at the cathodic compartment, respectively. However, due to the existence of overpotentials, ohmic resistance, and precipitation phenomena, the cell voltage supplied increased during the tests up to 2.6 V (justifying the existence of two calculations for the sEC in Table S4.1). Thus, the real sEC was estimated to be about 50-60% higher than the theoretical value, which was calculated considering the theoretical cell potential.

The pH of the catholyte increased as a function of the OH^- produced and the estimated profiles for the CDs assayed matched well with the titration curve (using NaOH) of the fresh denitrified effluent (Figure 4.2). These results suggest high faradaic efficiency and limited migration and diffusion of OH^- and H^+ from or to the cathodic compartment. Thus, the amount of OH^- produced to reach pH 10.5 and 11.5 was calculated as 11.62 ± 0.20 mmol L^{-1} and 23.59 ± 0.17 mmol L^{-1}, respectively.

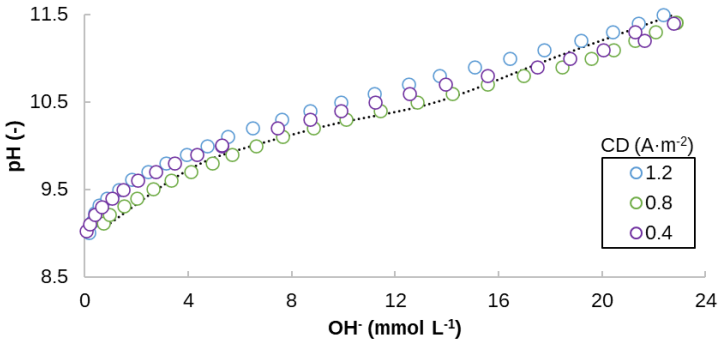

Figure 4.2 – Evolution of the pH of the denitrified effluent (1x diluted) according to the addition of NaOH (dashed black line) and measured pH profiles in the cathodic compartment as a function of the OH^- produced, considering different current densities (CDs).

All the time-dependent pH profiles in the cathodic compartment (regardless of the CD applied) show a characteristic pH increase in two stages due to the buffering capacity characteristics of the denitrified effluent (the pH slope is more sharped in the range 8.5-9.5 than in the range 10.5-11.5). This is why the $pHRR_{CAT}$ was calculated considering only the second slope in the pH profile (Figure S4.1, Figure 4.3). The $pHRR_{CAT}$ increased according to the CD applied (i.e., the higher the CD the shorter the time needed to reach pH 11.5) but decreased according to the denitrified effluent strength (i.e., the lower the strength (less buffer capacity) the shorter the time needed). Thus, the time needed for 1 L of undiluted effluent to reach pH 11.5 was 265 ± 16 minutes ($pHRR_{CAT}$: 0.16 u.pH $(L \cdot h)^{-1}$) at 0.4 A m^{-2} but 126 ± 1 minutes at 1.2 A m^{-2} ($pHRR_{CAT}$: 0.36 u.pH $(L \cdot h)^{-1}$), which corresponded to (real) sEC values of 1.05 ± 0.04 and 1.55 ± 0.13 kWh m^{-3}, respectively. If considering 1 L of 4x diluted effluent the time needed to reach pH 11.5 at 1.2 A m^{-2} was only 26 ± 0.86 minutes ($pHRR_{CAT}$: 0.99 u.pH $(L \cdot h)^{-1}$), which is equivalent to a sEC of 0.63 ± 0.03 kWh m^{-3}. According to Figure 4.3, the sEC remained constant for 1x dilution when the CD was increased from 0.8 to 1.2 A m^{-2}. A similar pattern can be observed in 4x dilution experiments regardless of the CD applied. The optimal selection of the CD to be applied in the electrochemical system must be taken into account according to both factors, short running time and low sEC. Based on the experimental tests conducted, the CD of 1.2 A m^{-2} was the most effective for reaching the targeted pH for both water strengths tested (Figure 4.3). This CD allowed for fast processing while keeping the energy consumption at a reasonable level.

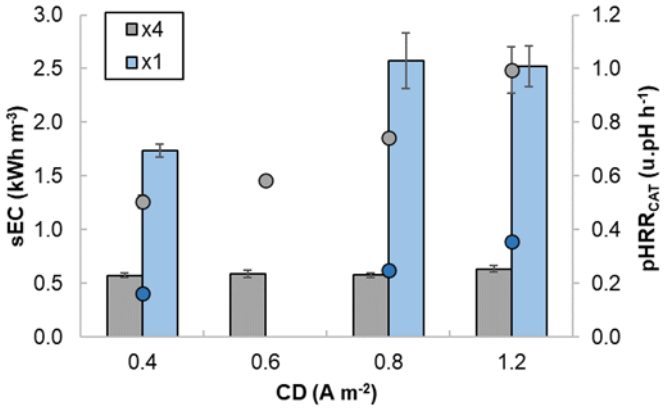

Figure 4.3 – Specific energy consumption (sEC) (bars), and specific pH raising rate in the cathodic compartment ($pHRR_{CAT}$) (dots), against current density (CD) for 1x and 4x dilution.

The OH^- production rate in the cathodic compartment is correlated with the applied CD. As far as the rate increases with the current, P removal is boosted to occur faster. Thus, the maximum PRR (ca. 4.5 mmol $(L \cdot d)^{-1}$) was achieved at the highest CD tested (1.2 A m^{-2}) when targeting pH 11.5 and it

was unaffected by the effluent strength (Figure 4.4). Nevertheless, the effluent strength may affect the PRE due to the initial ion activities, which affect the saturation conditions. In fact, for 1.2 A m^{-2} and targeted pH 11.5, the PRE was higher when using undiluted effluent than when using 4x diluted effluent (91 ± 2% and 72 ± 2%, respectively) (Figure S4.3). In line with Company et al. (26), higher PREs were reached at pH 11.5 than at pH 10.5. Together with P, the concentration of bivalent cations (i.e., Ca^{2+} and Mg^{2+}) in the catholyte decreased as far as the pH increased (Figure 4.4). The cation removal rate was favored by the increase of the CD, especially for Mg^{2+}. Considering 1.2 A m^{-2} as the applied CD and pH 11.5, in the case of working with undiluted effluent, the removed Mg/P molar ratio was higher than 1.5, which is the typical value for the formation of magnesium phosphates such as cattiite ($Mg_3(PO_4)_2$ $22H_2O$). These results might suggest that Mg^{2+} was precipitating also in other forms such as $Mg(OH)_2$ (38) or as a magnesium carbonate.

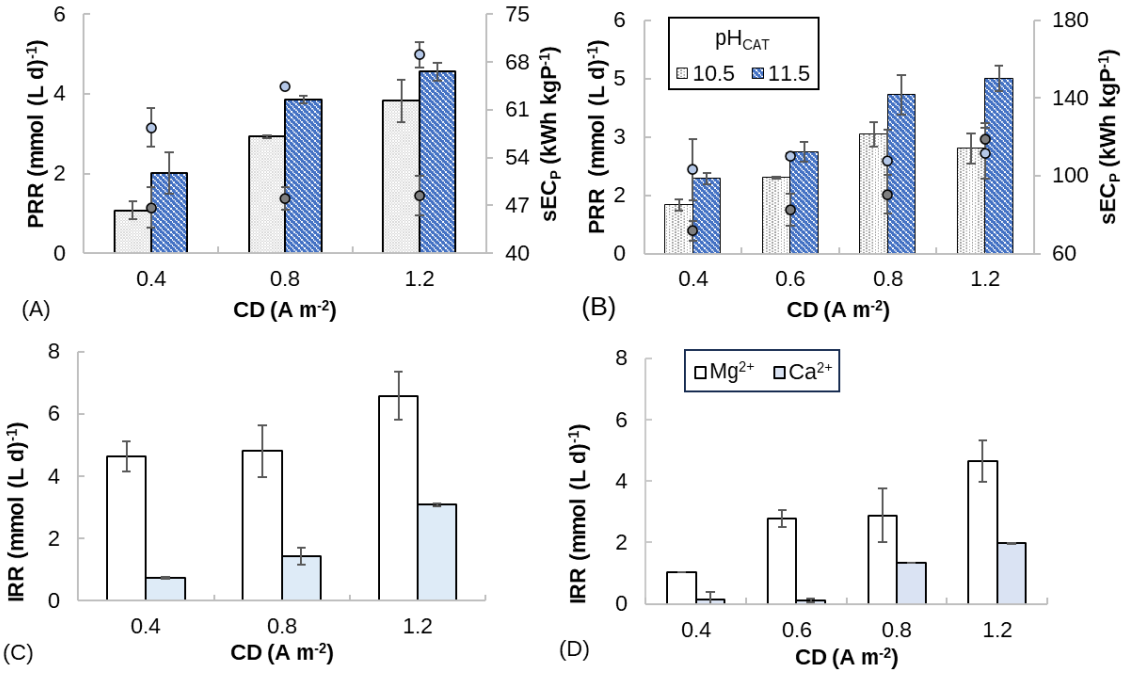

Figure 4.4 – *Top:* phosphorus removal rate (PRR) (bars) and specific energy consumption based on P removal (sEC_P) (dots) against current density (CD) considering 1x (A) and 4x (B) dilution of the denitrified effluent (pH 10.5 and 11.5). *Bottom:* magnesium (Mg) and calcium (Ca) removal rate (IRR) against CD considering 1x (A) and 4x (B) dilution of the denitrified effluent (at pH 11.5).

Promisingly, the present work showed high removal efficiencies compared to the authors operating in a low CD range (Table 4.2). On the other hand, the sEC_P was affected by the effluent strength; 69.07 ± 1.84 and 118.71 ± 8.22 kWh kg^{-1} P were consumed considering 1x and 4x diluted effluent, respectively. Thus, the higher specific energy consumption was associated with the lower P concentration in the treated wastewater, as already reported by Lei et al. (20). Moreover, these results

are consistent with Lei et al. (35) and Perera et al. (36) which treated wastewater with low P concentration (7.5 and 11.7 mgP L^{-1}, respectively) obtaining 110 kWh kg^{-1} P (at 1.4 A m^{-2}) and 112 kWh kg^{-1} P (at 1.31 A m^{-2}), respectively. In a comparable range of applied CD, lower sEC_P values were only obtained by Lei et al. (20) who treated a P-rich cheese wastewater (836 mgP L^{-1}) using an electrochemical system with tubular stainless-steel cathode operated in continuous mode (Figure 4.5, Table 4.2).

Table 4.2 – Phosphorus removal efficiency (PRE) and specific energy consumption in relation to the P removal from the liquid phase (sEC_P) comparison of electrochemical phosphate recovery technologies operated with low current density (CD).

CD (A m^{-2})	Anode	Cathode	Products	Conc. (mg P L^{-1})	$pH_{INITIAL}$ (-)	pH_{FINAL} (-)	PRE (%)	sEC_P (kWh kg^{-1} P)	Ref.
0.4 - 1.2	Ti-MMO mesh	Stainless-steel mesh	Cattiite	48	8.55	10.5	69 - 74%	47 – 49	This work
						11.5	90 - 91%	58 – 69	
				12		10.5	24 - 61%	103 – 111	
						11.5	73 - 90 %	79 – 119	
0.04 - 0.2	Pt-Ti mesh disk	Graphite felt	Calcium phosphate	19	4.5	7	≤70 %	4 – 13	(25)
1.0 - 1.9	Ru-Ir coated titanium sheet	Tubular-shaped stainless-steel	Calcium phosphate	836	4.5	7	40 - 60 %	27 – 34	(20)
1.4	Pt-Ti mesh disk	Titaniun square shaped	Calcium phosphate	8	3.5	7.5	44%	110	(37)
0.4 - 1.3	Isomolded graphite plate	Isomolded graphite plate	Calcium phosphate	12	7	9.7	83 - 90%	105 – 112	(36)

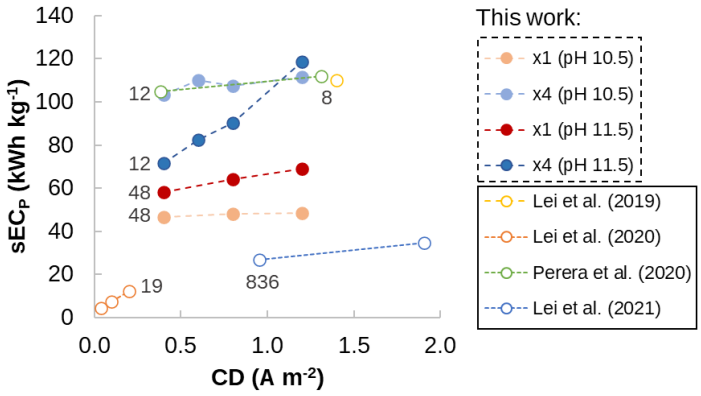

Figure 4.5 – Energy consumption of electrochemical phosphate recovery technologies operated with low current density based on the literature (numbers by the symbols represent the corresponding average P concentration expressed in mgP L^{-1}).

No visible precipitate was found at the bottom of the cathode compartment although the turbidity of the catholyte increased during the experiments due to the formation of small crystallisation nuclei (Figure S4.2). The P removal from the liquid phase attributable to deposition into the electrochemical system was assumed as the difference in concentrations between the unaltered catholyte at the end of the experiment and the catholyte after acidification. Tests with undiluted effluent (Figure S4.3) shown that P deposition was not influenced by the applied CD, but that it was significantly affected by the targeted pH. Thus, assuming CD as 1.2 A m^{-2}, while deposition was absent when final pH was 10.5, it accounted for ca. 20% when final pH was 11.5 (total PRE was ca. 90%). Consequently, it was hypothesized that at pH 11.5 approximately 70% of the precipitation occurred as suspended solids in the catholyte, rather than in the form of deposits (e.g., membrane, electrode, and chamber bottom). Lei et al. (12) suggested that if a high pH value is established in the catholyte, it may result in a homogeneous phosphate mineral formation and suspension in the liquid. Low applied CD, combined with high pH could have promoted this condition despite favoring mineral deposition in the electrochemical system. Even though sediment formation facilitates the recovery of precipitated phosphate salts since there is no need for filtration, solids deposition into the cathodic compartment leads to the necessity of arresting the treatment for recurring cleaning. Thus, P removal at low CD could reduce this drawback commonly related to the EMP process.

4.3.1.2 Mineral phase formed

The supersaturation conditions in the catholyte were assessed through the calculation of the SI in order to identify the precipitation of possible mineral phases (pH range: 10.0-11.5; Table S4.2). When considering the Mg-phosphate minerals, the highest SI was reached by bobierrite ($Mg_3(PO_4)_2 \cdot 8H_2O$) followed by cattiite, which switches from unstable to stable state in air when dried at room temperature (32). Potential formation of Mg- and Ca-carbonates was also envisaged. The XRD analysis of the solids formed in the catholyte revealed that cattiite was the main mineral (Figure 4.6). These results are consistent with Company et al. (26) who already pointed out that when raising the pH of the swine denitrified effluent if ammonium is not available, cattiite is the prevalent crystal formed.

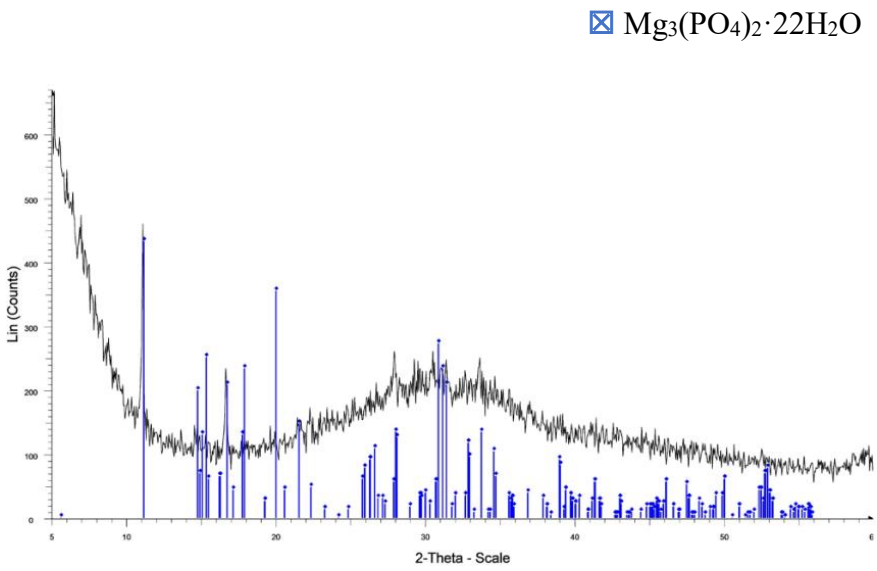

Figure 4.6 – XRD pattern for the solids collected from the catholyte by the end of a batch test (pH 11.5). The liquid was filtered, and the retained solids were dried at room temperature and ground before analysis.

4.3.1.3 Chlorine production

To evaluate chlorine formation as a side-product in the anodic compartment (Re. 3), chlorine concentration was measured in the anolyte by the end of each precipitation test (time when the pH value reached 11.5 in the cathodic compartment). Considering treatment of undiluted effluent, the CD boosted the chlorine production, resulting in 0.62 ± 0.02 and 1.24 ± 0.03 $mgCl_2$ L^{-1} for 0.4 and 0.6 A m^{-2}, respectively, and reaching the maximum value of 2.97 ± 0.30 $mgCl_2$ L^{-1} at 1.2 A m^{-2}. Nonetheless, the chlorine concentration measurement was likely limited since the Schott bottles, in which the anolyte was recirculated, were not sealed. Chlorine could represent a value-added product since it is a disinfecting agent which can be used in water treatment or, possibly, directly in the swine farm. Different authors already explored chlorine production as an interesting side-product in ETs treating different wastewaters (39,40). The preliminary results of this work concerning chlorine production suggest that the accumulation of this value-added product could be feasible when treating swine denitrified effluent, but the electrochemical system must be optimized. The appropriate selection of the CD will allow for a balanced P removal and chlorine production.

4.3.2 Neutralisation tests in the anodic compartment

According to the results reported above, pH 11.5 allows for a better recovery of the P in the cathodic compartment. Considering an eventual operation of the electrochemical system in continuous, beyond

the collection of the precipitates, it will be needed the neutralisation of the catholyte before discharge to make it possible for soil irrigation. High-pH water can negatively affect nutrient availability in soil by reducing micronutrient solubility (41) but, on the contrary, low-pH recycled water can lead to an increased metal mobility, contributing to the contamination of the water bodies (42). Thus, catholyte neutralisation within a specific pH range is critical for preserving the soil quality. As an alternative to acid dosage to correct the pH, catholyte neutralisation through an anode (Re. 2) was studied (in triplicates). To do this, undiluted denitrified effluent was treated in the cathodic compartment (CD as 1.2 A m^{-2} targeting pH 11.5) and cathodic treated effluent (pH 11.5 -the pH decreased to 11.0 after turning off the power supply-) collected by the end of the previous batch experiment was treated in the anodic compartment. The test was repeated but increasing the anode surface from 148 to 444 cm^2 to check the influence on chlorine production.

The PRE was not affected by the different composition of the anolyte (fresh denitrified effluent vs. final catholyte from a previous batch test) nor by the different anode surfaces tested, reaching values of ca. 90%. The increase in the anode surface did not influence the pH profiles either, which typically presented a sharp slope change in the range 9.5-7.0 (Figure 4.7). Thus, the pH of the anolyte (i.e., catholyte from a previous test) reached neutrality (i.e., pH 7.0) when the pH of the catholyte was 11.0 regardless the anode surface, coming down to pH 6.43 ± 0.05 by the end of the experiments -the pH had decreased from 8.45 ± 0.18 to 5.29 ± 0.05 when using fresh denitrified effluent-. This value is acceptable for agricultural applications (i.e., common required pH values in agricultural water reuse regulations are in the range from 6.0 to 9.0 (42)). By H_2SO_4 titration was possible to assess that the acid requirement to neutralise the catholyte pH (pH 7.0) was 20.8 meq $H^+ L^{-1}$. Considering an average H_2SO_4 price of \$275 ton^{-1} (31), the catholyte chemical neutralisation would produce a cost of 0.26 € m^{-3}. These are promising results for the operation of the electrochemical system in continuous, since the final catholyte could be directly neutralised in the anodic compartment, thus avoiding the dosage of chemicals, and reducing the treatment cost. Moreover, the opportunity to recover a valuable side-product was considered for the process comprehensive assessment. On this, the anode surface showed to play a role in chlorine production. The measured concentration in the anolyte (if considering the catholyte from a previous test) was 8.65 ± 0.08 and 1.48 ± 0.37 $mgCl_2 L^{-1}$ when considering 148 and 444 cm^2 as the anode surface, respectively. Thus, the larger the anodic surface the lower the concentration of chlorine in the anolyte by the end of the tests. According to the initial pH of the anolyte (8.4 vs. 11.5), the higher the pH value the higher the measured concentration of chlorine (Figure 4.7). In this regard, if considering undiluted denitrified effluent as the initial anolyte, the measured concentrations were 2.79 ± 0.18 $mgCl_2 L^{-1}$ (148 cm^2) and 1.48 ± 0.05 $mgCl_2 L^{-1}$ (444 cm^2). In conclusion, catholyte neutralisation through the anodic compartment was proven as feasible

reaching an appropriate pH for soil irrigation. Moreover, chlorine production could be boosted -for the recovery aim- by decreasing the anode surface and increasing the initial pH of the solution to be neutralised. These promising results are worthwhile for the optimisation of the system configuration in a future operation in continuous mode.

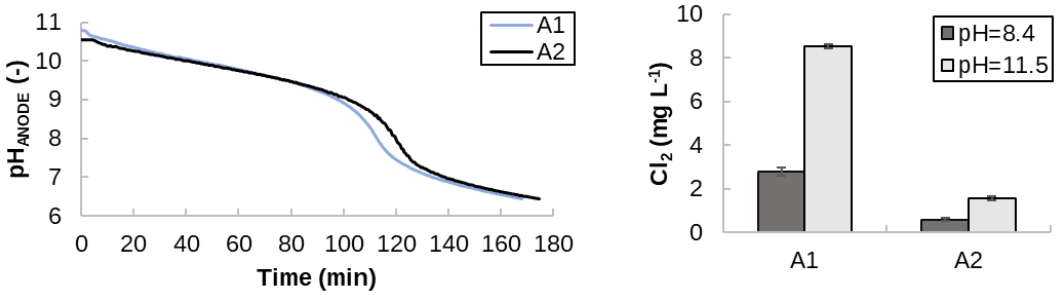

Figure 4.7 – Neutralisation batch test. pH against time profile (A) considering different anode areas (A1: 148 cm^2; A2: 444 cm^2). Final chlorine concentrations (B) considering different anode areas (A1, A2) and different initial pH of the anolyte.

The EC also plays an important role in the feasibility of water reuse in irrigation. Particularly, high salinity is usually associated with a reduction in the plants' growing yields. The FAO's guideline on the water use restriction states that EC > 3 dS m^{-1} can result in a severe negative impact on crops (41). The final EC of the anolyte exceeded this limit (5.89 ± 0.22 dS m^{-1}) although it was 4% below the value for the fresh denitrified effluent. Considering that crops will only be partially irrigated with this water (replacing the denitrified effluent), the main concern should be to preserve the quality of the soil. To decrease further the EC of the anolyte, dilution prior to its use could be considered.

4.3.3 EIS and membrane analyses

4.3.3.1 EIS tests

EIS is a fast and non-destructive technique offering kinetics and mechanistic data that could be used to study the performance of the electrochemical systems and, particularly, the overall resistance components. In this study, the EIS tests aimed to detect an eventual increase in the system's electrical resistance, which could be caused by mineral deposition over the surfaces of its components. The EIS spectra and the considered equivalent circuits are shown elsewhere (Figure S4.4). The two-electrode test (in OCV mode) allows characterising the total internal resistance of the electrochemical system, resulting in 1.20 ± 0.06 Ω m^2. The ohmic resistance (R_Ω) is the value resulting from the EIS spectra intersection with the x-axis which is multiplied by the cathode surface. It was estimated as 0.56 Ω m^2, thus contributing to 47% of the total resistance. Concerning the three-electrode test, three main resistances (R_1, R_2 and R_Ω) were identified (Figure 4.8). The first two resistances ($R_{1\text{-}2}$) showed large

variability depending on the applied voltage -attributable to electron transport processes such as those happening at the electrodes (43)-, while R_Ω did not appreciably change. Thus, $R_{1\text{-}2}$ can be related directly to the cathode, while R_Ω is likely to be caused by ohmic resistances. Particularly the presence of more than one resistance for the cathode could be ascribed to imperfect connection in the electrode which is identified as two distinct interfaces in the EIS spectra. When an increase in the voltage was applied, the cathodic resistance decreased, but the ohmic resistance was stable. The resulting current increased with the applied voltage (-0.8, -1.0 or -1.2 V resulted in -14, -60 or -130 mA) leading to a decrease in the $R_{1\text{-}2}$ values. Thus, the relevance of the R_Ω with respect to the total cathodic compartment resistance increased as far as the voltage was increased (Figure 4.8). The R_Ω could be limited by increasing the cathode electrical conductivity while electrode resistances ($R_{1\text{-}2}$) and by improving the internal connections (i.e., R_2 is attributable to the mesh connection with the wire, which increases the cathodic resistance).

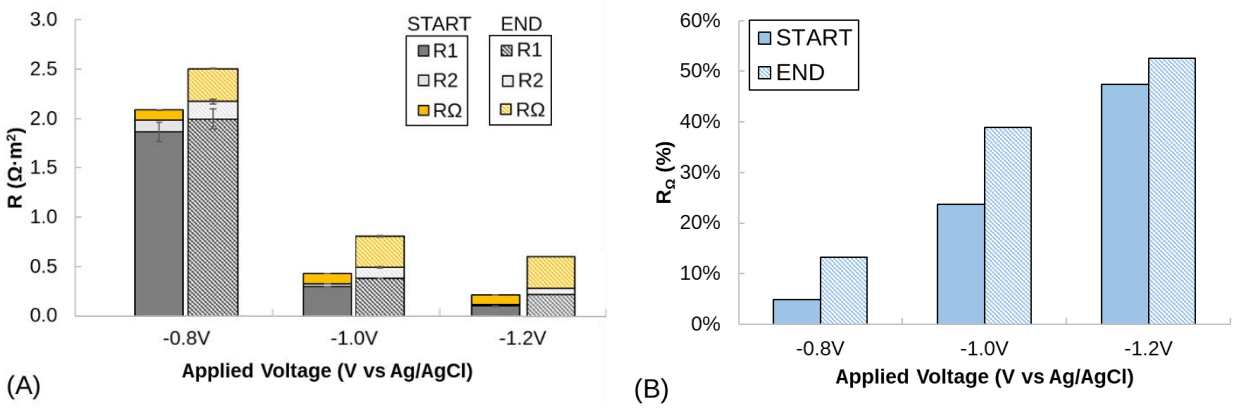

Figure 4.8 – Resistances calculated by fitting the EIS spectra to equivalent electrical circuit models at different voltages through the three-electrode configuration. At the left (A), the cathode-related resistance ($R_{1\text{-}2}$) and the ohmic resistance (R_Ω) are measured in $\Omega \cdot m^2$. At the right (B), the R_Ω is measured as percentage of the total internal resistance ($R_{1\text{-}2}$, R_Ω). Start and End labels identify the initial and final conditions before and after performing the precipitation tests.

The ohmic resistance in the electrochemical system after carrying out all the precipitation tests was 0.79 (two-electrode test) and 0.23 $\Omega\ m^2$ (three-electrode test) higher than the initial. Specifically, when 1.2 A m^{-2} was applied in the precipitation test with undiluted effluent, a 0.08 $\Omega\ m^2$ increase was detected with the two-electrode test. These results suggest a limited mineral deposition on the cathode and on the membrane surface due to the pH increase.

4.3.3.2 Membrane analysis

By the end of the precipitation tests, the electrochemical system was disassembled, which revealed scaling in the membrane surface facing the cathode. The XRD analysis of the precipitate attached to the membrane (Figure 4.9) revealed that carbonate compounds (such as $CaCO_3$ and magnesium calcite ($Ca_xMg_y(CO_3)$) were deposited on the membrane surface. This was likely because of the high pH-values reached in the electrode proximity owing to the OH^- produced, which led to an increased concentration of the carbonate ion (CO_3^{2-}) that promoted its precipitation (44). Such deposition could be the main reason for the increase of the ohmic resistance in the two-electrode EIS test (i.e., while the ohmic resistance detected with the three-electrode test is representative of the cathode compartment, the resistance in the two-electrode test is influenced by the overall system also including the membrane). Notably, the presence of precipitated carbonates was not identified in the solids recovered from the catholyte through XRD analysis. The solids collected from the membrane, and the membrane itself, were analysed by SEM. The resulting images revealed mineral depositions with a shape similar to that of amorphous carbonate, low-Mg calcite and mono-hydrocalcite (45). Phosphate mineral phases were not identified in this case.

The composition of the solids formed in the cathodic compartment when working with undiluted denitrified effluent at 1.2 A m^{-2}, and also of those solids deposited on the membrane by the end of the experimental period, was analysed by ICP-OES (Table 4.3). Concerning the membrane deposits, results were in line with those of XRD and SEM, since Ca^{2+} was the main element detected (23% on a dry weight basis). The elements P and Mg^{2+} were also present but in a more limited percentage (4.7% and 2.3%, respectively). Conversely, catholyte precipitates showed a prevalent content in Mg, followed by Ca^{2+} and P (11.0%, 6.9%, and 5.4%, respectively). Thus, the presence of Ca^{2+} in the denitrified effluent strongly affected the characteristics of the membrane deposits but also induced an interference in the formation of magnesium phosphate in the cathodic compartment. As already tested by Company et al. (26) on the sludge wasted from a nitrification/denitrification reactor, a pretreatment through a chelating agent (e.g., ethylenediaminetetraacetic acid (EDTA)) could increase the purity of the precipitated product by preventing the Ca^{2+} interference and might also help to limit the internal resistance rise during the operation of the electrochemical cell.

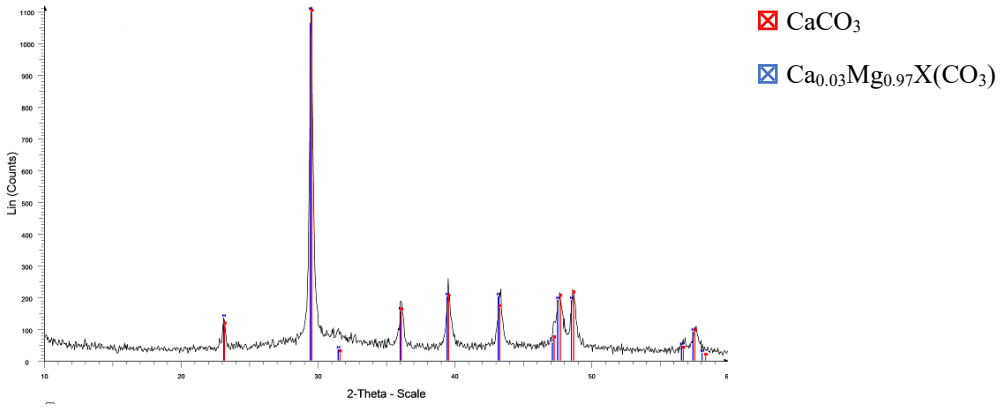

(A)

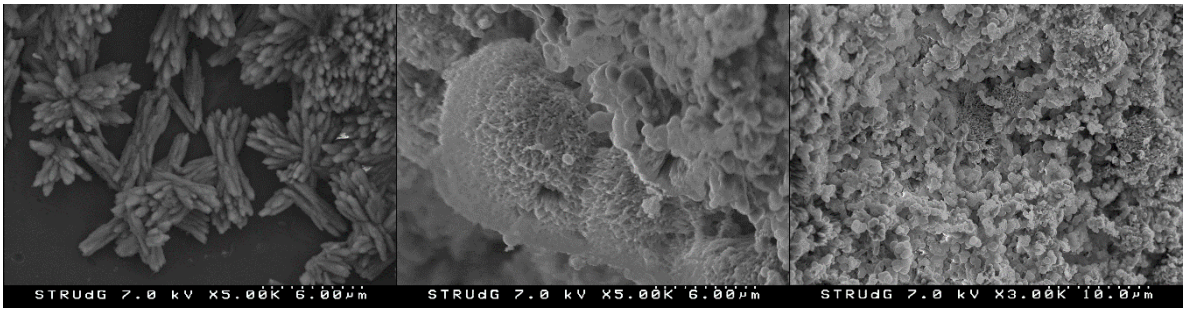

(B)

Figure 4.9 – XRD pattern (A) and SEM images (B) of the solids collected from the CEM by the end of the precipitation tests (once disassembled the electrochemical system).

Table 4.3 – Elemental composition analysed by ICP-OES of the deposits collected on the cationic exchange membrane (CEM) surface by the end of precipitation experiments and of the precipitate collected from the catholyte when working with undiluted effluent at 1.2 A m^{-2}. Results are in expressed in percentage on a dry weight basis (solids dried at room temperature).

Element	Membrane	Catholyte
P	4.7	5.4
Ca	29.6	6.9
Mg	2.3	11.0
K	0.1	1.0
Na	0.1	0.3

4.3.4 Economic assessment

Based on experimental results, a preliminary economic assessment of the electrochemical process is presented in this section. In the batch precipitation experiments, 1.2 A m^{-2} was selected as optimal CD allowing a short time for reaching the target pH, and an increased ions removal while keeping the electricity cost at a reasonable level. In this regard, the cost of dosing NaOH to raise the pH to 11.5 in a conventional crystalliser was calculated as 0.40 € m^{-3} while the energy cost related to the operation of the electrochemical system was 0.31 € m^{-3} (considering undiluted effluent and 1.2 A m^{-2} as CD). Thus, since the electrochemical system can help to reduce the operational costs in the crystallisation process, it appears to be a promising alternative to NaOH dosage in order to raise the pH of the denitrified effluent, even in the case of certain variability in the water strength. Particularly, the operational cost to drive P precipitation in the denitrified influent by NaOH addition, considering a PRE of 81% at pH 11.5, was 14.77 € kg^{-1}P, which is close to the commercial chemical precipitation range cost (i.e., from 18.9 to 61.1 € kg^{-1} P) (22). Promisingly, this cost is higher than the electrochemical system operation cost; when applying a CD ≤1.2 A m^{-2} to reach 11.5 the cost related to energy consumption is in the range of 11.68 – 13.81 € kg^{-1} P. Even though the cost of the electrochemical process should include the electrode and membrane charge (considering the possibility of replacement need), and the pumping system operational costs, these results showed that the EMP at low current density is a viable alternative to chemical precipitation for the denitrified effluent. For an overall process assessment, finally, the mined phosphorus price (1 − 2 € kg^{-1}P (22)) must be considered and taken as a benchmark for improving the energy efficiency of the technology. As an alternative to acid dosage to correct the effluent pH, catholyte neutralisation through the anode was successfully proved with the outlook of continuous system operation. By H_2SO_4 titration was possible to assess that the acid requirement to neutralise the catholyte pH (pH 7.0) was 20.8 meq H^+ L^{-1}. Considering an average H_2SO_4 price of 275 $ ton^{-1} (31), the catholyte chemical neutralisation would produce a cost of 0.26 € m^{-3}. Thus, compared to a complete chemical treatment, EMP process operated with low applied current density (≤1.2 A m-2) can limit the operational cost when treating swine denitrified effluent. In fact, 0.40 and 0.26 € m^{-3} would be needed for NaOH and H_2SO_4 addition to increase the effluent pH to 11.5 and for catholyte neutralisation, respectively, while the electrochemical process cost was just 0.31 € m^{-3} (considering undiluted effluent and 1.2 A m^{-2} application). Further, the opportunity to recover a valuable side-product such as chlorine must be considered for the process comprehensive assessment. Since chlorine production was limited in the batch experiments, the recovery was not considered, but with the outlook of continuous operation, this factor is promising as it can foster the cost-effectiveness of the electrochemical process.

4.4 Conclusions

Chemical-free P recovery from a swine denitrified effluent was successfully demonstrated using a two-chambered electrochemical batch reactor equipped with a CEM and operating at low CD (0.4-1.2 A m^{-2}). The main conclusions reached are as follows:

- Maximum PRR (ca. 4.5 mmol P ($L \cdot d^{-1}$)) with a PRE of 91 ± 2% (1x diluted effluent) and 72 ± 2% (4x diluted effluent) was reached when applying 1.2 A m^{-2} as CD to reach pH 11.5. The sEC_P behaved inversely to the effluent strength, accounting for 69.07 ± 1.84 (1x) and 118.71 ± 8.22 kWh kg^{-1} P (4x). According to this result, higher initial concentrations of P favored savings in energy consumption. Limited deposition of solids occurred during the tests and precipitates mostly remained suspended. Main mineral phase formed was cattiite.
- The electrochemical system was shown as a promising alternative to NaOH dosage for pH adjustment when targeting P recovery from denitrified effluents allowing for economical savings (cost for raising the pH at 11.5 was estimated as 0.57 € m^{-3} or 14.77 € kg^{-1} P when dosing NaOH vs. 0.31 € m^{-3} or 13.81 € kg^{-1} P in the electrochemical treatment).
- Feasibility for neutralising the catholyte in the anodic compartment was demonstrated achieving a final pH of 6.43 ± 0.05 (this is a suitable value for irrigation) with an associated economic benefit (0.26 € m^{-3} when dosing H_2SO_4 for catholyte neutralisation).
- Chlorine production in the anode was favored by a high initial pH of the catholyte and a small anode surface. Although the production reached was limited (the highest measured concentration was 8.45 ± 0.18 $mgCl_2$ L^{-1}) these findings represent a new opportunity for the recovery and onsite use of this side-product.
- The EIS tests confirmed that the deposition of solids into the system along the experimental period was limited, only contributing to a slight increase of the ohmic resistance (quantified as 0.79 Ω m^2 in the two-electrode configuration test). Membrane analysis revealed the significant precipitation of carbonate compounds but not phosphate compounds.
- Future investigations should involve testing the electrochemical system running in continuous, evaluating different configurations to enable solids recovery, and exploring chlorine recovery. Such endeavours could advance the practical application of this method as a sustainable wastewater treatment process to recover valuable products.

References

1. Elser J. *Phosphorus: a limiting nutrient for humanity?* Curr Opin Biotechnol. 2012, 23: 833–838. http://dx.doi.10.1016/j.copbio.2012.03.001
2. Carpenter, SR. *Phosphorus control is critical to mitigating eutrophication.* Proc Natl Acad Sci USA. 2008, 105: 11039–11040. https://doi.org/10.1073/pnas.08061121.
3. Cordell D, Drangert JO, White S. *The story of phosphorus: Global food security and food for thought.* Glob Environ Chang. 2009, 19: 292–305. https://doi.org/10.1016/j.gloenvcha.2008.10.009.
4. Jupp AR, Beijer S, Narain GC, Schipper W, Slootweg JC. *Phosphorus recovery and recycling-closing the loop.* Chem Soc Rev. 2021, 50: 87–101. http://dx.doi.org/10.1039/D0CS01150A.
5. Egle L, Rechberger H, Zessner M. *Overview and description of technologies for recovering phosphorus from municipal wastewater.* Resour Conserv Recycl. 2015, 105: 325–346. http://dx.doi.org/10.1016/j.resconrec.2015.09.016.
6. Rittmann BE, Mayer B, Westerhoff P, Edwards M. *Capturing the lost phosphorus.* Chemosphere. 2011, 84: 846–853. http://dx.doi.org/10.1016/j.chemosphere.2011.02.001.
7. Magrí A, Carreras-Sempere M, Biel C, Colprim J. *Recovery of phosphorus from waste water profiting from biological nitrogen treatment: upstream, concomitant or downstream precipitation alternatives.* Agronomy. 2020, 10: 1039. https://doi.org/10.3390/agronomy10071039.
8. Wang Y, Kuntke P, Saakes M, van der Weijden RD, Buisman CJN, Lei Y. *Electrochemically mediated precipitation of phosphate minerals for phosphorus removal and recovery: Progress and perspective.* Water Res. 2022, 209: 117891. https://doi.org/10.1016/j.watres.2021.117891.
9. Ren Y, Zheng W, Duan X, Goswami N, Liu Y. *Recent advances in electrochemical removal and recovery of phosphorus from water: A review.* Environ Funct Mater. 2022, 1: 10–20. https://doi.org/10.1016/j.efmat.2022.04.003.
10. Devlin TR, Kowalski MS, Pagaduan E, Zhang X, Wei V, Oleszkiewicz JA. *Electrocoagulation of wastewater using aluminum, iron, and magnesium electrodes.* J Hazard Mater. 2019; 368: 862–868. https://doi.org/10.1016/j.jhazmat.2018.10.017.
11. Xie S, Bai Z, Shao W, Wang C, Qin J, Liu Z. *Phosphate removal by ex situ generated Fe (hydr)oxides from scrap iron electrocoagulation: the critical role of coprecipitation.* Environ Sci Adv. 2023, 2: 898–907. https://doi.org/10.1039/D3VA00024A.

12. Lei Y, Zhan Z, Saakes M, van der Weijden RD, Buisman CJN. *Electrochemical recovery of phosphorus from acidic cheese wastewater: feasibility, quality of products, and comparison with chemical precipitation.* ACS ES&T Water. 2022, 1: 1002–1013. https://doi.org/10.1021/acsestwater.0c00263.

13. Zhang J, Zhao X, Wang Y, Djellabi R. *Recovery of phosphorus from hypophosphite-laden wastewater: a single-compartment photoelectrocatalytic cell system integrating oxidation and precipitation.* Environ. Sci. Technol. 2019, 54: 1204–1213. https://doi.org/10.1021/acs.est.9b05125.

14. Lin X, Han Z, Yu H, Ye Z, Zhu S, Zhu J. *Struvite precipitation from biogas digestion slurry using a two-chamber electrolysis cell with a magnesium anode.* J Clean Prod. 2018, 174: 1598–1607. https://doi.org/10.1016/j.jclepro.2017.10.224.

15. Hug A, Udert KM. *Struvite precipitation from urine with electrochemical magnesium dosage.* Water Res. 2013, 47: 289–299. http://dx.doi.org/10.1016/j.watres.2012.09.036.

16. Saha J, Gupta SK. *The production and quantification of hydroxyl radicals at economically feasible tin-chloride modified graphite electrodes.* J Environ Chem Eng. 2018, 6: 3991–3998. https://doi.org/10.1016/j.jece.2018.05.049.

17. Clauwaert P, De Paepe J, Jiang F, Alonso-Fariñas B, Vaiopoulou E, Verliefde A, Rabaey K. *Electrochemical tap water softening: A zero chemical input approach.* Water Res. 2020, 169: 115263. https://doi.org/10.1016/j.watres.2019.115263.

18. De Paepe J, Clauwaert P, Gritti MC, Ganigué R, Sas B, Vlaeminck SE, Rabaey K. *Electrochemical in situ pH control enables chemical-free full urine nitrification with concomitant nitrate extraction.* Environ Sci Technol. 2021, 55: 8287–8298. https://doi.org/10.1021/acs.est.1c00041.

19. Ceballos-Escalera A, Pous N, Balaguer MD, Puig S. *Electrochemical water softening as pretreatment for nitrate electro bioremediation.* Sci Total Environ. 2022, 806: 150433. https://doi.org/10.1016/j.scitotenv.2021.150433.

20. Lei Y, Zhan Z, Saakes M, van der Weijden RD, Buisman CJN. *Electrochemical recovery of phosphorus from wastewater using tubular stainless-steel cathode for a scalable long-term operation.* Water Res. 2021, 199: 117199. https://doi.org/10.1016/j.watres.2021.117199.

21. Cid CA, Jasper JT, Hoffmann MR. *Phosphate recovery from human waste via the formation of hydroxyapatite during electrochemical wastewater treatment.* ACS Sustain Chem Eng. 2018, 6: 3135–3142. https://doi.org/10.1021/acssuschemeng.7b03155.

22. Takabe Y, Ota N, Fujiyama M, Okayasu Y, Yamasaki Y, Minamiyama M. *Utilisation of polarity inversion for phosphorus recovery in electrochemical precipitation with anaerobic digestion effluent.* Sci Total Environ. 2020, 706: 136090. https://doi.org/10.1016/j.scitotenv.2019.136090.

23. Zhang Q, Ba X, Liu S, Li Y, Cai L, Sun H. *Synchronous anodic oxidation-cathodic precipitation strategy for efficient phosphonate wastes mineralization and recovery of phosphorus in the form of hydroxyapatite.* Sep Purif Technol. 2021, 272: 118895. https://doi.org/10.1016/j.seppur.2021.118895.

24. Jin H, Yu Y, Zhang L, Yan R, Chen X. *Polarity reversal electrochemical process for water softening.* Sep Purif Technol. 2019, 210: 943–949. https://doi.org/10.1016/j.seppur.2018.09.009.

25. Lei Y, Geraets E, Saakes M, van der Weijden RD, Buisman CJN. *Electrochemical removal of phosphate in the presence of calcium at low current density: Precipitation or adsorption?* Water Res. 2020, 169: 115207. https://doi.org/10.1016/j.watres.2019.115207.

26. Company E, Farrés M, Colprim J, Magrí A. *Exploring the recovery of potassium-rich struvite after a nitrification-denitrification process in pig slurry treatment.* Sci Total Environ. 2022, 847: 157574. https://doi.org/10.1016/j.scitotenv.2022.157574.

27. Romans-Casas M, Feliu-Paradeda L, Tedesco M, Hamelers HVM, Bañeras L, Balaguer MD, Puig S, Dessì P. *Selective butyric acid production from CO_2 and its upgrade to butanol in microbial electrosynthesis cells.* Environ Sci Ecotechnol. 2024, 17: 100303. https://doi.org/10.1016/j.ese.2023.100303.

28. Timmerman LR, Raghavan S, Borole AP. *Advancing microbial electrolysis technology via impedance spectroscopy and multi-variate analysis.* Front Energy Res. 2022, 10: 756900. https://doi.org/10.3389/fenrg.2022.756900.

29. APHA, AWWA, WEF. *Standard Methods for the Examination of Water and Wastewater. American Public Health Association, American Water Works Association, Water Environment Federation.* Washington, DC, USA. 2017.

30. Vannecke TPW, Lampens DRA, Ekama GA, Volcke EIP. *Evaluation of the 5 and 8 pH point titration methods for monitoring anaerobic digesters treating solid waste.* Environ Technol. 2015, 36: 861-869. https://doi.org/10.1080/09593330.2014.964334.

31. Gerner G, Meyer L, Wanner R, Keller T, Krebs R. *Sewage sludge treatment by hydrothermal carbonization: Feasibility study for sustainable nutrient recovery and fuel production.* Energies. 2021, 14: 2697. https://doi.org/10.3390/en14092697.

32. Gustafsson JP. Visual MINTEQ, ver. 3.1. 2020. https://vminteq.lwr.kth.se/.

33. Taylor AW, Frazier AW, Gurney EL. *Solubility products of magnesium ammonium and magnesium potassium phosphates.* Trans Faraday Soc. 1963, 59: 1580–1584. https://doi.org/10.1039/TF9635901580.

34. Xu K, Li J, Zheng M, Zhang C, Xie T, Wang C. *The precipitation of magnesium potassium phosphate hexahydrate for P and K recovery from synthetic urine.* Water Res. 2015, 80: 71–79. https://doi.org/10.1016/j.watres.2015.05.026.

35. Lei Y, Song B, Saakes M, van der Weijden RD, Buisman CJN. *Interaction of calcium, phosphorus and natural organic matter in electrochemical recovery of phosphate.* Water Res. 2018, 142: 10–17. https://doi.org/10.1016/j.watres.2018.05.035.

36. Perera MK, Englehardt JD, Cohn JL, Dauer EA, Shukla D. *Electrohydromodulation for phosphate recovery from wastewater.* Sep Purif Technol. 2020, 247: 116909. https://doi.org/10.1016/j.seppur.2020.116909.

37. Lei Y, Remmers JC, Saakes M, Van Der Weijden RD, Buisman CJN. *Influence of cell configuration and long-term operation on electrochemical phosphorus recovery from domestic wastewater.* ACS Sustain Chem Eng. 2019, 7: 7362–7368. https://doi.org/10.1021/acssuschemeng.9b00563.

38. Tarragó E, Ruscalleda M, Colprim J, Balaguer MD, Puig S. *Towards a methodology for recovering K-struvite from manure.* J Chem Technol Biotechnol. 2018, 93: 1558-1562. https://doi.org/10.1002/jctb.5518.

39. Varigala S, Krishnaswamy S, Lohia CP, Hegarty-Craver M, Grego S, Luettgen M, Cid CA. *Optimal design of an electrochemical reactor for blackwater treatment.* Water Environ Res. 2021, 93: 148–158. https://doi.org/10.1002/wer.1374.

40. Puggioni G, Milia S, Dessì E, Unali V, Pous N, Balaguer MD, Puig S, Carucci A. *Combining electro-bioremediation of nitrate in saline groundwater with concomitant chlorine production.* Water Res. 2021, 206: 117736. https://doi.org/10.1016/j.watres.2021.117736.

41. Valdez-Aguilar LA, Grieve CM, Poss J. *Salinity and alkaline pH in irrigation water affect marigold plants: I. Growth and shoot dry weight partitioning.* HortScience. 2009, 44 :1719–1725. https://doi.org/10.21273/HORTSCI.44.6.1719.

42. Shoushtarian F, Negahban-Azar M. *World wide regulations and guidelines for agricultural water reuse: A critical review.* Water. 2020, 12: 971. https://doi.org/10.3390/w12040971.

43. Rossi R, Baek G, Logan BE. *Vapor-fed cathode microbial electrolysis cells with closely spaced electrodes enables greatly improved performance.* Environ Sci Technol. 2022, 56: 1211–1220. https://doi.org/10.1021/acs.est.1c06769.

44. Edvardsen L, Gawel K, Wenner S, Gawel B, Torsæter M. *Electrochemical enhancement and inhibition of calcium carbonate deposition.* J Environ Chem Eng. 2020, 8: 104239. https://doi.org/10.1016/j.jece.2020.104239.

45. Blue CR, Giuffre A, Mergelsberg S, Han N, De Yoreo JJ, Dove PM. *Chemical and physical controls on the transformation of amorphous calcium carbonate into crystalline $CaCO_3$ polymorphs.* Geochim Cosmochim Acta. 2017, 196: 179–196. http://dx.doi.org/10.1016/j.gca.2016.09.004.

Supporting Information - Chapter 4

Table S4.1 - Electric charge, estimated OH^- production and specific energy consumption (sEC) required to reach the targeted pH (10.5 and 11.5) considering the applied current density (CD; 0.4-1.2 A m^{-2}) and dilution factor (1x and 4x) for the denitrified effluent. AV: average, SD: standard deviation.

Dilution factor	**1x -undiluted-**					
CD (A m^{-2})	**0.4**		**0.8**		**1.2**	
	AV	SD	AV	SD	AV	SD
Time to reach pH 10.5 (h)	1.05	± 0.03	0.87	± 0.11	0.63	± 0.02
Time to reach pH 11.5 (h)	2.68	± 0.27	1.81	± 0.24	1.96	± 0.05
Electric charge and OH^- production						
pH 10.5						
Electric charge (kC L^{-1})	0.64	± 0.05	1.06	± 0.08	1.12	± 0.02
OH^- production (mmol L^{-1})	5.99	± 0.86	10.75	± 0.94	11.62	± 0.20
pH 11.5						
Electric charge (kC L^{-1})	1.51	± 0.16	2.16	± 0.17	2.28	± 0.02
OH^- production (mmol L^{-1})	15.62	± 1.69	22.34	± 1.78	23.59	± 0.17
Theoretical sEC*						
pH 10.5						
Cell potential (V)	1.42		1.43		1.43	
sEC (kWh m^{-3})	0.25	± 0.04	0.42	± 0.03	0.45	± 0.01
pH 11.5						
Cell potential (V)	1.55		1.59		1.56	
sEC (kWh m^{-3})	0.65	± 0.07	0.95	± 0.08	0.99	± 0.01
Real sEC**						
Cell potential (V)	2.39	± 0.05	2.46	± 0.17	2.60	± 0.24
pH 10.5						
sEC (kWh m^{-3})	0.45	± 0.02	0.78	± 0.07	0.76	± 0.06
pH 11.5						
sEC (kWh m^{-3})	1.05	± 0.04	1.48	± 0.12	1.55	± 0.13

Dilution factor	**4x**							
CD (A m^{-2})	**0.4**		**0.6**		**0.8**		**1.2**	
	AV	SD	AV	SD	AV	SD	AV	SD
Time to reach pH 10.5 (h)	0.62 ±	0.04	0.33 ±	0.04	0.19 ±	0.01	0.33 ±	0.01
Time to reach pH 11.5 (h)	1.36 ±	0.06	0.79 ±	0.00	0.20 ±	0.01	0.26 ±	0.01
Electric charge and OH^- production								
pH 10.5								
Electric charge (kC L^{-1})	0.15 ±	0.02	0.26 ±	0.02	0.19 ±	0.01	0.28 ±	0.12
OH^- production (mmol L^{-1})	3.83 ±	0.16	3.19 ±	0.23	2.33 ±	0.04	1.54 ±	0.15
pH 11.5								
Electric charge (kC L^{-1})	0.81 ±	0.02	0.59 ±	0.04	0.56 ±	0.02	0.63 ±	0.03
OH^- production (mmol L^{-1})	8.35 ±	0.21	7.51 ±	0.37	6.23 ±	0.36	5.10 ±	0.57
Theoretical sEC*								
pH 10.5								
Cell $potential_{th}$ (V)	1.46		1.46		1.44		1.43	
sEC (kWh m^{-3})	3.83 ±	0.16	0.12 ±	0.01	0.09 ±	0.00	0.06 ±	0.01
pH 11.5								
Cell $potential_{th}$ (V)	1.74		1.72		1.61		1.57	
sEC (kWh m^{-3})	0.39 ±	0.01	0.35 ±	0.02	0.27 ±	0.02	0.22 ±	0.03
Real sEC**								
Cell potential (V)	2.83 ±	0.03	3.02 ±	0.03	3.27 ±	0.21	5.03 ±	0.14
pH 10.5								
sEC (kWh m^{-3})	0.25 ±	0.08	0.26 ±	0.02	0.19 ±	0.01	0.28 ±	0.12
pH 11.5								
sEC (kWh m^{-3})	0.57 ±	0.02	0.59 ±	0.04	0.56 ±	0.02	0.63 ±	0.03

*****The theoretical sEC was calculated considering the theoretical cell potential (cell $potential_{th}$) value which was calculated with the Nernst equation as a function of the initial and final pH reached in the compartments.

**The real sEC was calculated considering the average cell potential (cell potential) which was measured in the individual precipitation tests.

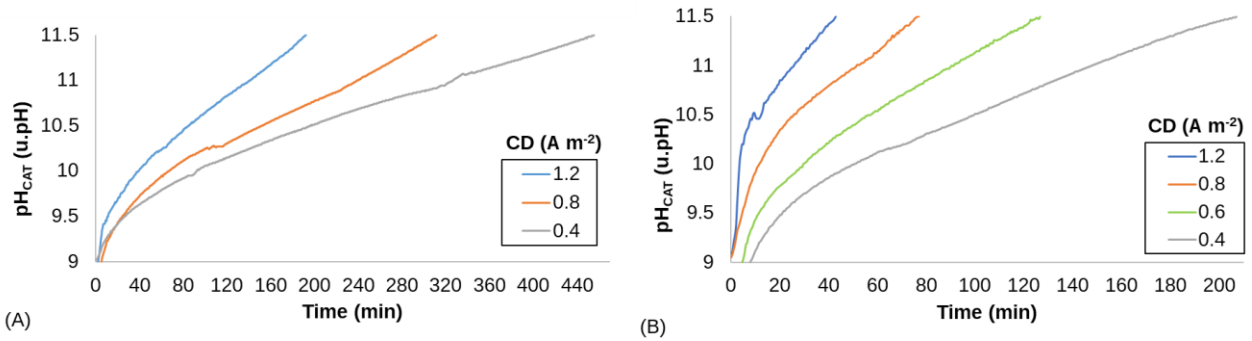

Figure S4.1 – pH against time profiles in the catholyte of the batch electrochemical system for the 1x -undiluted- (A) and 4x diluted (B) denitrified effluent.

Figure S4.2 – From left to right, fresh swine denitrified effluent, anolyte and catholyte by the end of a precipitation test in the batch electrochemical system.

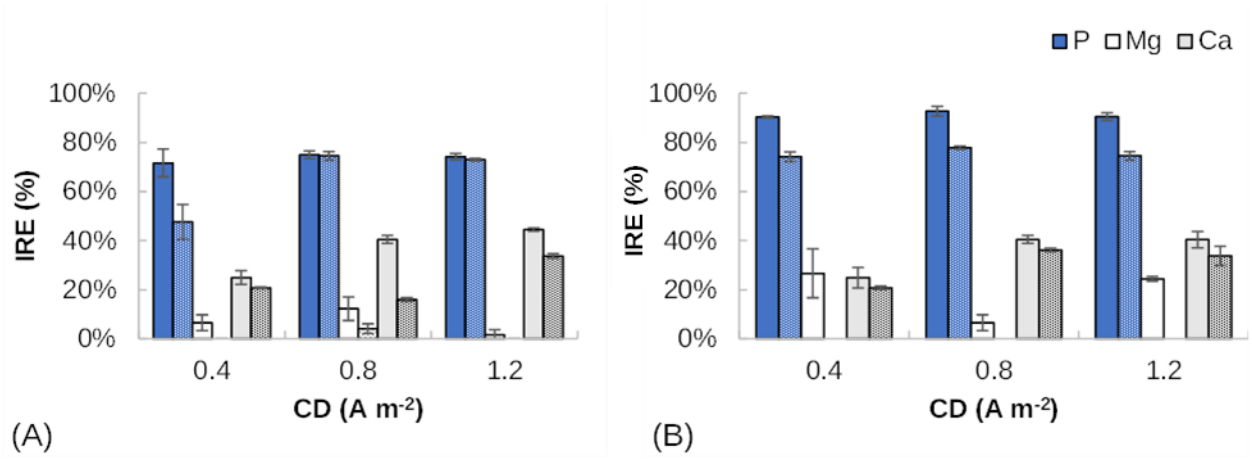

Figure S4.3 – Ions removal efficiency (IRE) against current density (CD) for final pH 10.5 (A) and 11.5 (B) in tests performed with fresh denitrified effluent (1x diluted). Solid bars represent the resulting removal efficiency calculated considering the measured concentrations for unaltered catholyte whereas dotted bars represent the results considering the measured concentrations for acidified catholyte (acidified to pH 2 dosing H_2SO_4 5 M).

Table S4.2 – Saturation indexes (SIs) for possible mineral phases (SI>0) in the catholyte of the electrochemical system as a function of the pH value. Calculations were made using MINTEQ and based on average ionic concentrations in the swine denitrified effluent (Table 4.1).

	pH (u.pH)			
	10.0	10.5	11.0	11.5
Mineral phase	**SI (-)**			
Hydroxyapatite ($Ca_{10}(PO_4)_6 \cdot (OH)_2$)	16.56	17.11	17.48	17.32
Calcium phosphate ($Ca_3(PO_4)_2$)	5.08	5.18	5.16	4.16
Bobierrite ($Mg_3(PO_4)_2 \cdot 8H_2O$)	4.25	4.86	5.33	5.18
Cattiite ($Mg_3(PO_4)_2 \cdot 22H_2O$)	2.14	2.74	3.22	3.06
Magnesite ($MgCO_3$)	1.70	1.75	1.72	1.87
Calcite ($CaCO_3$)	1.76	1.63	1.44	1.53
Dolomite ($CaMg(CO_3)_2$)	4.61	4.53	4.32	4.55
Huntite ($CaMg_3(CO_3)_4$)	5.97	5.99	5.72	6.25
K-Struvite ($MgKPO_4 \cdot 6H_2O$)	1.49	1.79	2.05	2.21
Na-Struvite ($MgNaPO_4 \cdot 7H_2O$)	0.82	1.14	1.40	1.42

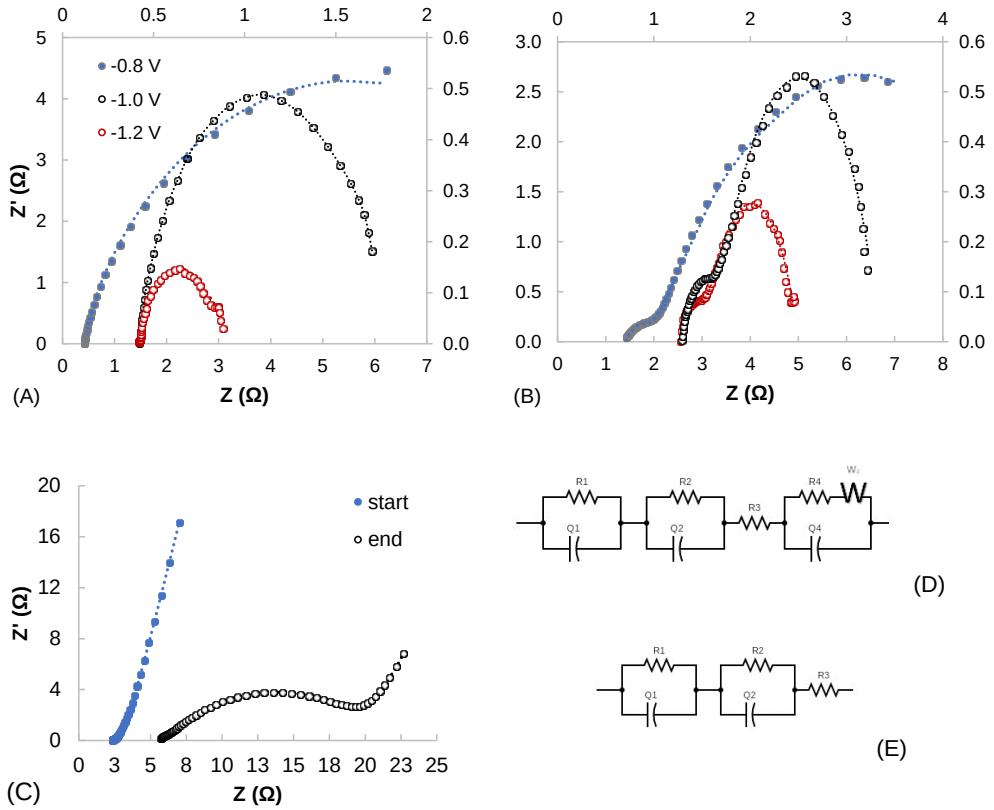

Figure S4.4 – Three-electrode electrochemical impedance spectroscopy (EIS) spectra at different voltages (values for the potential -0.8 V must be read in the principal axes whereas values for the potentials -1.0 V and -1.2 V must be read in the secondary axes) corresponding to the beginning of the precipitation tests -before performing any experiment- (A) and the end of the experimental period (B). Two-electrode EIS spectra corresponding to the initial and final condition as above-described (C). Dots represent experimental values and dashed line fittings achieved. Equivalent electric circuits used for fitting the EIS spectra in two-electrode tests (D) and three-electrode tests (E). The circuit components are resistance (R), constant phase element (Q, CPE) and Warburg element (W). The EIS spectra intersection with the x-axis identifies the ohmic resistance (R_3) which is usually expressed considering the cathode surface ($\Omega \cdot m^2$).

CHAPTER 5: Achieving reagent-free K-struvite recovery from a swine denitrified effluent using an electrochemical cell-crystalliser combined system

Abstract

K-struvite is a slow-release fertiliser simultaneously providing phosphorus, potassium and magnesium that recently gained increasing attention as it can be produced from waste valorisation. Precipitation pH normally ranges between 9.0 and 12.0, requiring large amount of chemicals. In the present work reagent-free K-struvite was successfully achieved from a denitrified swine effluent using a two-chambered electrochemical cell assembled together with a crystalliser. Onsite OH^- and H^+ production ions was promoted in order to modify the pH while saving in chemicals and decreasing the availability of Na^+. The combined system was operated in batch and continuous-flow modes. Precipitation experiments in batch aimed to select the optimal configuration of the electrochemical cell according to the ions removal efficiency, energy consumption and mineral deposition in the cathodic chamber. Three different electrochemical cell designs have been tested by applying 2.65A (corresponding to 8h of electrolysis time). While ions removal efficiency, and the solid productivity, slightly varied among configurations, specific energy consumption and ohmic resistance increase were more affected by the dimensional features. Cell3 was selected as the best configuration since it allowed for ion removal efficiencies of 94 ± 1% for PO_4^{3-}-P (9.3 mmol $(L \cdot d)^{-1}$), 38 ± 1% for Mg^{2+} (6.6 mmol $(L \cdot d)^{-1}$) and 9 ± 4% for K^+ (10.2 mmol $(L \cdot d)^{-1}$) while achieving the lowest specific energy consumption (134 ± 22 kWh kg^{-1} P) and ohmic resistance increase (28 ± 1 Ω m^2). The main mineral phase recovered from the denitrified effluent was K-struvite regardless cell configuration, presenting a richness on dry weight above 10% for phosphorus, potassium, and magnesium. Precipitation experiments in continuous aimed to evaluate the mineral recovery efficiency and to test the neutralisation of the precipitated effluent in the anodic chamber of the electrochemical cell before discharge. Measured ions removal efficiencies were 85 ± 3% for PO_4^{3-}-P (8.4 mmol $(L \cdot d)^{-1}$), 81± 8% for Mg^{2+} (13.9 mmol $(L \cdot d)^{-1}$) and 16 ± 2% for K+ (19.9 mmol $(L \cdot d)^{-1}$). Through the power supply on/off control, the targeted pH (11.5) was successfully maintained in the crystalliser. The specific energy consumption was quantified as 122.9 kWh kg^{-1} P. Process arresting for a few days and starting up again did not affect the overall performances. Catholyte neutralisation in the anodic compartment was proven as feasible, leading to a decline in the pH-value down to 6.05 ± 0.71 when current was applied. Promising levels of chlorine (44 $mgCl_2$ L^{-1}) were measured in the outlet, which opens the

door to combining K-struvite recovery with production of value-added chemicals such as free chlorine.

5.1 Introduction

Phosphorus (P) and potassium (K) are two essential macronutrients for crops, typically extracted from ores by the mining industry as non-renewable resources (1-3). Owing to the growing world population, P and K demand in the fertiliser industry is rising to sustain adequate food production. In recent years, a number of viable technologies such as chemical precipitation, ion exchange, or membrane separation processes including reverse osmosis and electrodialysis, have been tested for nutrient recovery from liquid streams (e.g., wastewater, urine, livestock effluents, brines, seawater) with the aim of limiting fertiliser manufacturing environmental impacts (3,4).

As a waste valorisation product, the precipitated phosphate salt K-struvite ($MgKPO_4 \cdot 6H_2O$; magnesium-potassium-phosphate hexahydrate, MPP) has received great attention as it can be applied to crops as a slow-release fertiliser simultaneously providing P, K and Mg^{2+} (5,6). Under supersaturation conditions, MPP forms according to a Mg^{2+}:K^+:PO_4^{3-} molar ratio of 1:1:1 and the incorporation of six water molecules (7). MPP crystallisation is affected by a combination of factors including the pH, temperature, constituent ion activities, and the coexistence of competing ions. Research findings showed that MPP precipitation normally occurs at pH between 9.0 and 12.0, which is above the optimal values (pH 8.5–9.5) for the precipitation of its analogue NH_4-struvite ($MgNH_4PO_4 \cdot 6H_2O$; magnesium-ammonium-phosphate hexahydrate, MAP) (6,7). Thus, large amounts of an alkali agent such as sodium hydroxide (NaOH) or magnesium hydroxide ($Mg(OH)_2$) are needed as a source of hydroxyl ions (OH^-) when precipitating MPP (8). Although NaOH is the chemical more frequently used to adjust the pH of the precipitation reaction, its addition implies an increased concentration of Na^+ ions in the aqueous matrix, which will compete with K^+ ions for Mg^{2+} and PO_4^{3-}. Such additional availability of Na^+ may result in an increased Na^+ content in the precipitated salt and eventually the formation of Na-struvite (9,10). Additionally, chemical dosage will lead to an increase of the ionic strength in the solution which can hinder the formation of MPP (6). When applying chemical precipitation, the use of reagents can be necessary even as a post-treatment. In fact, strongly alkaline precipitated effluents introduce a subsequent need for protons (H^+) supply (e.g., sulphuric acid (H_2SO_4)) to neutralise them before discharge.

Electrolysis is a clean method for the simultaneous onsite production of OH^- and H^+ ions (11), which recently has gained attention as an alternative to chemical dosage. When current is supplied to an electrochemical cell water molecules at the cathode are reduced to hydrogen (H_2) with the

simultaneous production of OH^- (Re. 1), which raises the local pH, while at the anode, water molecules are oxidized to oxygen (O_2) and H^+ (Re. 2). Selective electrochemically mediated precipitation (EMP) processes have already been described for struvite recovery from wastewater streams such as digestate and landfill leachate (12-14). If compared with conventional precipitation technologies, the EMP is promising since highly efficient PO_4-P removal can be achieved through an easily automatized process permitting a controllable reaction and with limited sludge production (11,15).

Cathode: $2H_2O + 2e^- \rightarrow H_2 + 2OH^-$ (Re. 1)

Anode: $2H_2O \rightarrow O_2 + 4H^+ + 4e^-$ (Re. 2)

Alongside intense natural reserves consumption, the growing world population is also causing a substantial food production expansion with an increased demand for animal protein (16). Pork meat has been reported as the most widely consumed worldwide implying the generation of large amounts of swine manure which requires appropriate management and treatment due to the high pollution potential (17). The high nutrient content in swine manure has raised interest in the valorisation and recovery of valuable by-products and the production of bio-based fertilisers. Particularly, livestock denitrified effluents are poor in ammonium-N but still rich in PO_4^{3-}-P and K^+ thus representing a viable source to obtain MPP (8,18,19). In this regard, Company et al. (8) tested the feasibility of producing K-rich struvite from a swine denitrified effluent through chemical precipitation. When the pH of the denitrified effluent was raised to 11.5 through NaOH dosing, 93% PO_4^{3-}-P and 10% K^+ were recovered from the liquid phase as MPP.

The aim of the present work is to precipitate MPP from a denitrified swine effluent by means of water electrolysis for the onsite production of OH^- and H^+ ions in order to modify the pH while saving in chemicals and decreasing the availability of Na^+. A two-chambered electrochemical cell (i.e., where OH^- and H^+ were produced) was assembled together with a crystalliser (i.e., where precipitation should occur) to achieve a reagent-free recovery of MPP. Similar combined configurations were previously used by other authors to achieve water softening (20,21), urine stabilisation (22) and the removal of Mg^{2+} and Ca^{2+} from lithium-rich brines (23). In this work, three different electrochemical cell designs have been tested. The electrochemical cell-crystalliser combined system was operated in batch and continuous-flow modes. Precipitation experiments in batch aimed to evaluate the optimal configuration of the electrochemical cell according to the ions removal efficiency, energy consumption and mineral deposition in the cathodic chamber. Precipitation experiments in continuous aimed to evaluate the mineral recovery efficiency and to test the neutralisation of the precipitated effluent in the anodic chamber of the electrochemical cell before discharge. Finally, the process was

arrested for a few days and then resumed again to investigate the possible influence on the system performance.

5.2 Material and methods

5.2.1 Experimental set-up

Precipitation experiments were conducted using a 14.6-L crystalliser (8,24) combined with a two-chambered electrochemical cell connected to a power supply. The system was operated in batch and continuous-flow mode (Figure S5.1). Both elements conforming the precipitation unit were made of methacrylate. Three different configurations were tested for the electrochemical cell -Cell1, Cell2, and Cell3- (Table 5.1), in which, the anode and the cathode compartments were separated by a cation exchange membrane (CEM) (CMI-7000, Membranes Int., USA). A stainless-steel mesh (1.0 mm of light path and 0.4 mm of wire diameter, CISA, Spain) was used as the cathode, while a Ti-MMO (MMO, mixed metal oxides) electrode mesh (2 mm light path and 1 mm wire diameter, NMT electrodes, South Africa) was used as the anode. A power supply (mod. IMHY3003D, Lendher, Spain) was used to control the cathode potential, working in chronopotentiometry mode. Peristaltic pumps (mod. 505 and 520, Watson Marlow, UK) were used as needed to feed the denitrified effluent provided as influent into the crystalliser (0-48.2 L d^{-1}), to recirculate the liquid from the crystalliser through the cathodic compartment (657 L d^{-1}), to withdraw the sedimented sludge from the bottom of the crystalliser (0.6 L d^{-1}), and to discharge the liquid from the crystalliser through the anodic compartment (0-47.6 L d^{-1}). The recirculated liquid passed through a 0.8-mm filter (volume of 1.13 L) located before the cathodic compartment to prevent solids from entering. The hydraulic residence time (HRT) of the precipitation unit was 8 hours. Air was supplied into the crystalliser at 0.6 L min^{-1} through a mass flow meter (mod. 2100, Tecfluid, Spain). The pH was monitored in the crystalliser (clarification zone), in the outlet of the cathodic chamber and in the outlet of the anodic chamber (i.e., the effluent of the precipitation unit) while the electrical conductivity (EC) was monitored only in this last point. The power supply was controlled online according to a pH set-point (pH 11.5 (8)) in the crystalliser using a control panel that included a multimeter (mod. MM44, Crison Instruments SA, Spain) plugged to a memograph (mod. RSG40, Endress+Hauser Inc., Switzerland). Data regarding pH and EC were recorded regularly through this control panel.

Table 5.1 − Dimensional characteristics of the three electrochemical cells used in the experiments.

		Electrochemical cell		
Parameter	**Units**	**Cell1**	**Cell2**	**Cell3**
Size	cm	28 x 28 x 6.5	24.5 x 9.5 x 6	18.8 x 9.8 x 4.8
V_{ANODE}	L	0.83	0.18	0.40
$V_{CATHODE}$	L	1.01	0.11	0.13
S_{ANODE}	cm^2	444	148	264
$S_{CATHODE}$	cm^2	2418	331	726
S_{CEM}	cm^2	701	154	184
$(S/V)_{CATHODE}$	$m^2\ m^{-3}$	239	301	558
$d_{ELECTRODE}$	cm	2	3	1.5

V, volume; S, surface; d, distance between electrodes.

5.2.2 Swine denitrified effluent

The swine denitrified effluent used in the precipitation tests was collected from a pig farm located in Osona (Catalonia, Spain). Following solid-liquid separation, the liquid fraction of the slurry is treated biologically onsite, in a sequencing batch reactor under intermittent aeration, aiming to remove nitrogen (N). The denitrified effluent was sampled after the sludge settling as it was done in Company et al. (8) work. Samples were transported from the farm to the laboratory in polyethylene containers. Once at the laboratory facilities, these containers were stored at room temperature until performing the experiments. Final compositional characteristics of the denitrified effluent used in the experiments are given in Table 5.2. The denitrified effluent had a characteristic brownish colour and a low solids content. The pH-value (8.0 ±0.4) was notably below the suitable pH for MPP precipitation. Low alkalinity (1831 ±148 $mgCaCO_3\ L^{-1}$) and NH_4^+-N (21 ±3 $mgN\ L^{-1}$) remained after the biological treatment. The K^+ content was high (1523 ±29 $mgK\ L^{-1}$) compared to PO_4^{3-}-P and Mg^{2+}, resulting in a Mg^{2+}:K^+:PO_4 molar ratio of 1.7:11.7:1.0. The low concentration of Ca^{2+} (40 ±3 $mgCa\ L^{-1}$) was favourable for the formation of MPP.

Table 5.2 - Physicochemical characteristics of the swine denitrified effluent.

Parameter	Units	Average	SD
pH	-	8.0	0.4
EC	mS cm^{-1}	8.1	0.1
ALK ($CaCO_3$)	mg L^{-1}	1831	148
TIC	mg L^{-1}	294	10
Na^+	mg L^{-1}	687	19
K^+	mg L^{-1}	1523	29
Mg^{2+}	mg L^{-1}	141	9
Ca^{2+}	mg L^{-1}	40	3
Cl^-	mg L^{-1}	1082	150
SO_4^{2-}-S	mg L^{-1}	125	13
PO_4^{3-}-P	mg L^{-1}	103	10
NH_4^+-N	mg L^{-1}	21	3
NO_2^--N + NO_3^--N	mg L^{-1}	0	0

ALK, alkalinity; EC, electrical conductivity; TIC, total inorganic carbon; SD, standard deviation.

5.2.3 Experimental tests

5.2.3.1 Alkalinization test

The amount of alkali (i.e., NaOH solution) needed to raise the pH of the denitrified effluent to the desired pH-value was measured by titrimetry, as in Company et al. (8). The OH^- demand (e.g., 50 mmol OH^- L^{-1} to raise the pH-value to 11.5), which is equivalent to the amount of electrons to be transferred from the anode to the cathode (Re. 1), allowed for calculating the electric current to be applied in the electrochemical cell (Eq. 1).

5.2.3.2 Batch precipitation experiments

Batch precipitation tests were performed (in duplicates) by operating the combined electrochemical cell-crystalliser system in order to identify the optimal electrochemical cell configuration (Table 5.1). The cathodic compartment was connected to the crystalliser with a recirculation loop while the anolyte was recirculated from a stirred buffer tank (Figure S5.1). Both, the catholyte and anolyte were recirculated at a flow rate of 657 L d^{-1}. All tests were run at room temperature (20 ± 2°C) using ca. 32 L of denitrified effluent (total volume) equally divided in the two compartments (i.e., 16 L in the cathodic chamber and 16 L in the anodic chamber). Based on the results of the alkalinisation test, and assuming 8 hours of electrolysis time, the applied current was calculated as 2.65 A. Once reached the

targeted pH in the crystalliser, the power supply was switched off. The solids formed in the crystalliser and the cathodic chamber were collected (i.e., separated on a filter paper), and dried at 35ºC before analysis. Next, the system was completely emptied and cleaned with acidic and deionized water to ensure that no residual precipitates remained in the following test. Liquid samples from the anodic and cathodic compartments were collected by the end of the experiment, filtered at 0.2 µm, and stored at room temperature before analysis.

5.2.3.3 Continuous-flow precipitation experiments

For those experiments performed in continuous-flow mode, the start-up of the electrochemical cell-crystalliser combined system was carried out in batch (see paragraph 2.3.2), and when the targeted pH was reached (pH 11.5), the operational mode was switched to continuous-flow following the set-up scheme shown in Figure S5.1. The electrochemical cell used was that selected in the previous batch experiments (Cell3). Based on the results of the alkalinisation test, the applied current was 2.65 A, corresponding to an HRT of 8 hours (inflow rate of 48.2 L d^{-1}). The precipitated effluent (namely the anodic compartment effluent), and the sludge accumulated in the crystalliser, were withdrawn preserving the total working volume. The catholyte was recirculated at a flow rate of 657 L d^{-1} to ensure an extremely low HRT in the cathodic compartment (i.e., 15 sec) to limit precipitation inside. The power supply was then switched on/off according to the pH in the crystalliser (pH set-point of 11.5). The precipitation system was operated for 3 days (time equivalent to 9 HRTs), completely stopped for 4 days, and then resumed again for 2 days to study the influence of arresting the operation on the treatment performance. The solids formed in the crystalliser were collected (i.e., separated on a filter paper), and dried at 35ºC before solids analysis. Liquid samples from the crystalliser, anodic and cathodic compartments were periodically collected, filtered at 0.2 µm, and stored at room temperature before analysis.

5.2.4 Electrochemical impedance spectroscopy (EIS) tests

A BioLogic potentiostat (mod. VSP, France) was used to perform the electrochemical impedance spectroscopy (EIS) tests on the electrochemical cells. A volume of ca. 1 L of denitrified effluent was recirculated in each compartment. At least two EIS runs were performed to characterize the system's electrochemical performance prior to and after the batch precipitation tests. The internal resistance was investigated using two- and three-electrode configurations. In the latest case, an Ag/AgCl sat. KCl reference electrode (+0.197 V vs. SHE, SE 11, Xylem Analytics Germany Sales GmbH & Co. KG Sensortechnik Meinsberg, Germany) was placed in the cathodic compartment, as much closer as possible to the electrode. Firstly, before any EIS measurement, steady-state conditions were reached

considering voltage stabilisation for a minimum of 1.5 h in open circuit voltage (OCV). To ensure that the relevant physical phenomena were captured in the EIS spectrum, all EIS measurements occurred over the frequency range from 100 kHz to 10 MHz. A sinusoidal perturbation with an amplitude of 10 mA was used with 10 points per logarithmic decade for the analysis (25). A potential of 0 V vs. three different fixed potential values (-0.8, -1.0 and -1.2 V vs. Ag/AgCl) were applied as input signals to investigate the influence on the components of the overall cell internal resistance. To study the impedance results, the so-called Nyquist plot was used. In this plot, every interface can ideally be visualised as a semicircle. The EIS parameters were extracted by fitting an equivalent electrical circuit model (ECM) using Zfit (EC-lab software). The ECM produces pseudo-electrochemical parameters which can be sorted to represent anode and cathode impedances separately, as well as individually to assess the ohmic, kinetic, and mass transfer limitations of the system. Common configurations of ECM have included a resistor representing solution resistance connected in series to parallel combinations of resistors representing charge transfer reactions, but when the mass transfer is expected to be a limiting factor in system performance Warburg elements are also included (26). Thus, these above-mentioned elements were used in the fitting model to represent the obtained results. Particularly, the EIS spectra intersection with the x-axis identifies the cell ohmic resistance.

5.2.4 Analytical methods

Water samples were analysed following APHA et al. (27). The pH was measured offline using a bench pH-meter (mod. Sension+ PH3, Hach, Germany), and electrical conductivity (EC) measurements were carried out using a conductivity-meter (mod. EC-Meter Basic 30+, Crison Instruments SA, Spain). Total alkalinity (ALK, reported as $CaCO_3$) was determined by acid titration to an endpoint pH of 4.5 and total inorganic carbon (TIC) was measured through the 5 pH point titration method (28). The concentrations of the soluble cations (i.e., ammonium (NH_4^+), sodium (Na^+), potassium (K^+), magnesium (Mg^{2+}), and calcium (Ca^{2+})), as well as the concentrations of the soluble anions (i.e., nitrite (NO_2^-), nitrate (NO_3^-), chloride (Cl^-), sulfate (SO_4^{2-}), and phosphate (PO_4^{3-})), were determined by ion chromatography (mod. ICS-5000, Dionex, USA) after filtering samples with 0.2 µm nylon filters. The precipitated salts were analyzed using X-ray diffraction (XRD) (mod. D8 Advance, Bruker, USA) and the total content of the main constituents (i.e., Na, K, Ca, Mg, and P) was measured after microwave digestion with a HNO_3/H_2O_2 mixture using inductively coupled plasma-optical emission spectrometry (ICP-OES) (mod. 5100, Agilent Technologies, USA) (Method 3120 B). Chlorine gas (Cl_2) was determined using a spectrophotometer (mod. DR1900, Hach Lange, Germany) according to the DPD-free chlorine method (Hach Lange).

5.2.5 Calculations

The current intensity (I) (A) to be supplied by the power supply to the electrochemical cell was determined as a function of the OH^- demand (mol L^{-1}) of the denitrified effluent to reach the targeted pH-value (i.e., this is equivalent to the amount of electrons that went from the anode to the cathode), as it is shown in Eq. 1 (i.e., this is assuming 100% faradaic efficiency),

$$I = \frac{OH^-_{demand} \cdot V_{CAT} \cdot F}{t_{electrolysis}} \qquad \text{(Eq. 1)},$$

where: V_{CAT} (L) is the total recirculating catholyte volume, F is the Faraday constant (96485.332 C mol^{-1}), and $t_{electrolysis}$ (s) is the selected time for electrolysis in order to reach the targeted pH (when the electrochemical cell-crystalliser system is operated under continuous-flow mode this time corresponds to the HRT). Thus, once defined the targeted value for pH and $t_{electrolysis}$, the corresponding current to be supplied was calculated. Feasible values for the power supply used were $I \leq 3$ A. For the particular case of pH-value 11.5 and $t_{electrolysis}$ 8 hours, I was calculated as 2.65 A.

To compensate for the flow of electrons, an equal amount of charge should migrate between compartments. The relative contribution of a given cation to the total migration (CRC) (%) through the CEM was calculated according to Eq. 2,

$$CRC = \frac{\left(C_{INF,t0} - C_{AN,t}\right) \cdot V_{AN} \cdot cation\ valence}{amount\ of\ electrons} \cdot 100 \qquad \text{(Eq. 2)},$$

where: $C_{INF,t0}$ is the ion concentration (M) measured in the denitrified effluent at time t_0 (i.e., at the beginning of the test), $C_{AN,t}$ is the ion concentration (M) measured in the anolyte at time t, and V_{AN} is the total anolyte volume (L). The amount of electrons corresponds to the total OH^- demand (mol). The relative contribution of H^+ was calculated as the one hundred percent complement to the other cation relative contribution sum.

The specific energy consumption (sEC) (kWh m^{-3}) in the electrochemical cell was calculated according to Eq. 3,

$$sEC = \frac{I \cdot \int V dt}{V_{CAT}} \qquad \text{(Eq. 3)},$$

where: V (V) is the electric potential, and t (h) is the time of experiment.

In those experiments performed in batch, the P removal rate (PRR) (mol P $(L \cdot d)^{-1}$) was calculated according to Eq. 4,

$$PRR = \frac{(P_{CAT,t0} - P_{CAT,t})}{t} \qquad \text{(Eq. 4)},$$

where: $P_{CAT,t0}$ is the concentration of P (M) measured in the catholyte at time t_0 (i.e., at the beginning of the test) and $P_{CAT,t}$ is the concentration of P (M) measured in the catholyte at time t (i.e., every 1

hour from the start to the end of the experiment). Otherwise, the P removal efficiency (PRE) (%) was calculated as shown in Eq. 5.

$$PRE = \frac{(P_{CAT,t0} - P_{CAT,t})}{P_{CAT,t0}} \cdot 100 \quad \text{(Eq. 5)}.$$

Taking into account the cation migration through the CEM, the cations removal rate (CRR) (mol $(L \cdot d)^{-1}$), particularly for Mg^{2+}, K^+ and Na^+ (i.e., MgRR, KRR, and NaRR, respectively), was calculated according to Eq. 6,

$$CRR = \frac{(2 \cdot C_{INF,t0} - (C_{CAT,t} + C_{AN,t}))}{t} \quad \text{(Eq. 6)},$$

where: C_{CAT} and C_{AN} are the ion concentration (M) measured in the catholyte and the anolyte at time t, respectively. Otherwise, the cation removal efficiency (CRE; MgRE and KRE) (%) was calculated as shown in Eq. 7.

$$CRE = \frac{(2 \cdot C_{INF,t0} - (C_{CAT,t} + C_{AN,t}))}{C_{INF,t0}} \quad \text{(Eq. 7)}.$$

Finally, the specific energy consumption in relation to the P removal from the liquid phase (sEC_P) (kWh kg^{-1} P) is calculated according to Eq. 8, once accounted for the molecular weight of P (MW_P).

$$sEC_P = \frac{\text{sEC}}{(P_{CAT,t0} - P_{CAT,t}) \cdot MW_P} \quad \text{(Eq. 8)}.$$

When considering the continuous-flow operation of the electrochemical cell-crystalliser system, the numerator in Eq. 4-7 corresponds to the difference between the concentration of the influent and the effluent, the denominator in Eq. 4 and 6 corresponds to the HRT, and the denominator in Eq. 8 corresponds to the difference between the concentration of the influent and the effluent.

The cost of operating the electrochemical cell (i.e., external power supply) was calculated considering the cost of the energy for an industrial application (0.20 € kWh^{-1}, European electricity price for the second semester of 2022) and the experimental sEC. According to Muys et al. (29), struvite is typically sold at 0–100 € t^{-1} but also at considerable higher prices (350-1000 € t^{-1}). Thus, according to a conservative criterion, the economic benefit for MPP commercialisation was calculated considering a potential market price of 100 € t^{-1}.

5.3 Results and discussion

5.3.5 Alkalinisation test: current intensity selection

The results of the alkalinisation test allowed for calculating the appropriate current intensity to be applied in the precipitation experiments with the electrochemical cell-crystalliser combined system. Based on a previous study (8), the swine denitrified effluent was titrated to pH 10, 10.5, 11, and 11.5

using a NaOH solution (i.e., these are considered as suitable pH-values for MPP precipitation). The above referred pH values demanded for the addition of 22, 33, 44, and 50 mmol OH^- L^{-1}. Thus, once fixed the operation time, the higher the pH to be reached, the higher the current intensity to be applied (Figure 5.1). Such current intensity was limited within the 0–3 A range due to the characteristics of the power supply used. According to such calculations, if assuming a targeted pH of 11.5 and an electrolysis time of 8 hours, the required current to be applied was 2.65 A. This value was then applied in the precipitation tests performed in batch and continuous modes.

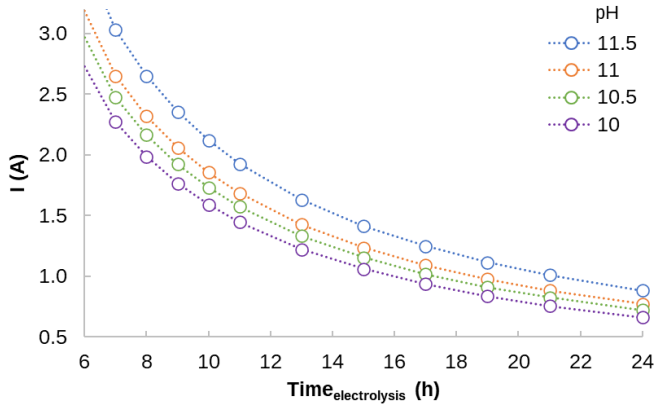

Figure 5.1 – Current intensity (I) required to raise the pH of the denitrified effluent to 10.0-11.5 as a function of the electrolysis time.

5.3.2 Batch precipitation experiments

5.3.2.1 Precipitation in the cathodic compartment

Three different two-chambered electrochemical cells (Table 5.1), each one equipped with a CEM, were alternatively coupled with the crystalliser. The resulting combined systems were run in batch mode to achieve chemical-free P removal from the liquid phase by phosphate salt precipitation. A current intensity of 2.65 A was applied in the electrochemical cell (see section 3.1). The aim was to evaluate the optimal configuration of the cell by considering ion removal, energy consumption and mineral deposition in the cathodic chamber.

In all the configurations tested for the electrochemical cell, the CEM was used to separate anodic and cathodic compartments, and to create a pH gradient between the anode and cathode. By applying current, OH^- were generated at the cathode increasing the pH of the catholyte, while H^+ were generated at the anode acidifying the anolyte. To restore the flow of electrons from the anodic to the cathodic compartments, cations (H^+ included) migrated in the same direction. Thus, while the migration of Na^+, K^+, and Mg^{2+} presented a relevant contribution to the total migration of cations (Figure 5.2), the relative contribution of NH_4^+-N and Ca^{2+} was negligible (i.e., 0-1%). Particularly,

K^+ presented the highest CRC (40-44%) followed by Na^+ (whose contribution varied from 22% (Cell3) to 32% (Cell1) depending on the configuration tested). These results are consistent whith the electromigration theory, since monovalent ions are typically subjected to heightened migration from the anode to the cathode through the CEM. Additionally, Mg^{2+} presented a lower CRC for the configurations tested, with the smallest value for Cell3 (i.e., 5%). This lower value might be attributed to the smaller electrode gap, which could promote H^+ diffusion, particularly over bivalent cations (30), which reached a CRC of 33% in Cell3. Since the aim of the electrochemical treatment is to recover MPP from the denitrified effluent, K^+ and Mg^{2+} migration to the cathodic compartment is desirable because it could promote mineral precipitation. Nevertheless, PO_4^{3-}-P is the limiting element in the denitrified effluent (Table 5.2) for MPP crystallisation, thus K^+ and Mg^{2+} in excess cannot form the targeted mineral unless an external source of P is introduced in the cathodic compartment.

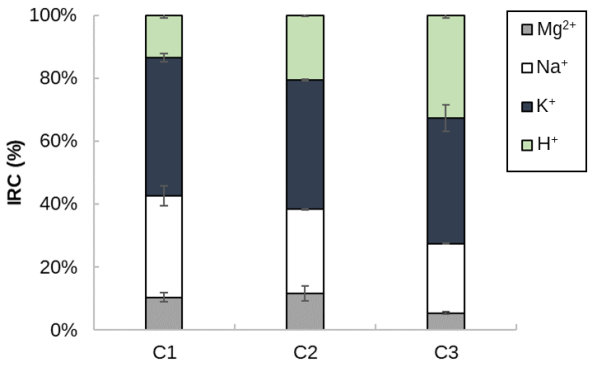

Figure 5.2 – Relative contribution of the cations (CRC) H^+, K^+, Na^+ and Mg^{2+} to the total migration from the anodic to the cathodic compartments in Cell1, Cell2, and Cell3 in the eight hours batch precipitation experiments. The CRC for NH_4^+ and Ca^{2+} was negligible (less than 1%).

The pH-value measured in the crystalliser evolved analogously during the 8 hour batch experiments regardless the electrochemical cell configuration tested (Figure 5.3). As far as the pH increased, the ion removal improved, reaching the highest values in the range 10.0-11.5. The slight increase in ion removal observed in the previously referred pH range suggests that, under the experimental conditions applied (progressive increase in the pH value), the targeted pH-value (11.5) might be decreased in order to reduce also the energy consumption. Particularly, and depending on the configuration of the cell, PRR, KRR and MgRR values of 8.2–9.3, 7.3–10.2 and 6.6–9.3 mmol $(L \cdot d)^{-1}$ were achieved, respectively, once reached pH 11.5, which is equivalent to PRE, KRE and MgRE

values of 90–94%, 6–9%, and 38-43%, respectively. The high PRE achieved indicates that almost all the PO_4^{3-}-P present in the denitrified effluent was removed from the liquid phase, thus limiting KRE and MgRE. Mg^{2+} removal was less pronunced in Cell3 than in the other two configurations. Lei et al. (30) found that the distance between the electrodes can influence cations removal by precipitation. Thus, closer electrodes might had fostered the direct recombination of H^+ with OH^- at the cathode, resulting in a lower local pH, which would lead to a relatively lower CRE for bivalent ions. According to this assumption, precipitation could be highly influenced by the pH in the cathode proximity, even though it is supposed to occur in the crystalliser, and the small volume close to the eletrode could play a foundamental role in the process.

Beyond MPP ion constituents, the precipitation of other cations such as NH_4^+ and Ca^{2+} remained quite constant with the pH increase. Otherwise, the precipitation of Na^+ increased when the pH raised above 10.0-10.5. While the availability of small amounts of NH_4^+ is desired for the precipitation process since it can help to the formation of MPP (8), Ca^{2+} and Na^+ precipitation will result in the formation of untargeted minerals (e.g., calcium phosphate, Na-struvite), affecting the composition of the recovered product, or eventually triggering membrane scaling (e.g., due to the formation of calcium carbonate). In this later case, the pretreatment of the swine denitrified effluent by means of Ca^{2+} sequestring agents (e.g., EDTA, oxalic acid) could be planned to reduce its availability.

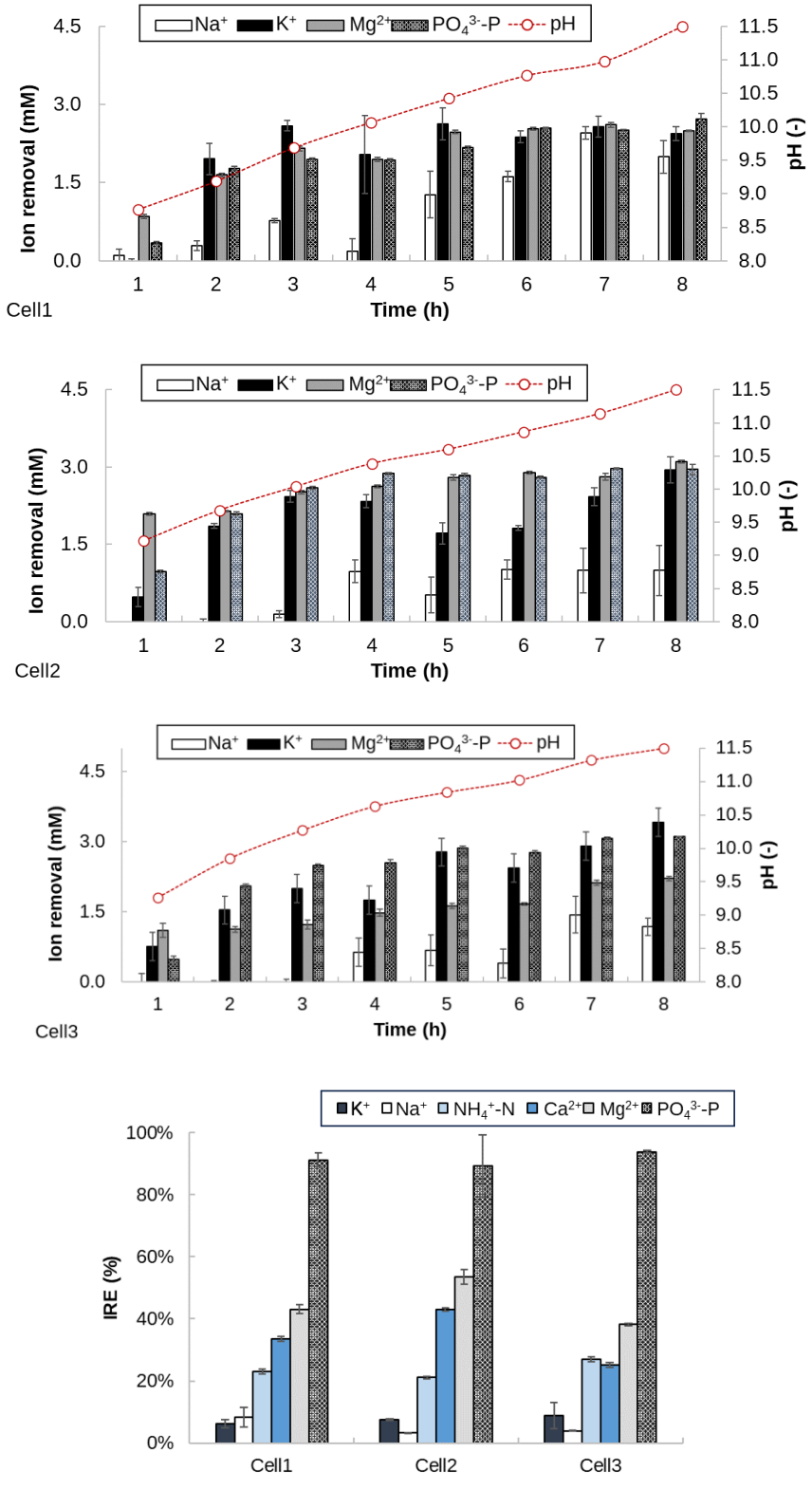

Figure 5.3 – *Top:* Evolution of the ions removal from the liquid phase and the pH measured in the crystalliser during the 8 hour batch precipitation tests using Cell1, Cell2, and Cell3. *Bottom:* Ions removal efficiency (IRE) once reached pH 11.5 for Cell1, Cell2, and Cell3.

5.3.2.2 Energy consumption and operational costs

The energy cost is a critical aspect for evaluating the feasibility of an electrochemical technology used for phosphate precipitation, and to compare its competitiveness with respect to conventional chemical precipitation. In this work, the attempt to reduce the energy costs was made by taking into account the cathode surface, electrode distance, and precipitation inside the electrochemical cell. Particularly, increasing the cathode surface and reducing the interelectrode distance allow for reducing the cell potential needed to reach the required current intensity. Testing the three electrochemical cell configurations, the characteristics of Cell3 (Table 5.1) resulted in the lowest specific energy consumption (i.e., 134 ± 22 kWh kg^{-1} P) (Table 5.3). While the difference in the average cell potential ($\Delta V_{average}$) between Cell1 (largest cathode surface) and Cell3 (closest electrodes) was not significant, the inherent characteristics of Cell2 led to an increased energy consumption. Promisingly, the related operational costs for Cell1 (43.7 € kg^{-1} P) and Cell3 (26.8 € kg^{-1} P) fitted in the range of the chemical precipitation cost (18.9-61.1 € kg^{-1} P) proposed by (31).

Table 5.3 – Energy consumption related parameters for the three electrochemical cell configurations tested in the batch precipitation experiments.

			Electrochemical system		
Parameter	**Units**		**Cell1**	**Cell2**	**Cell3**
CD	A m^{-2}		**11.0**	**80.1**	**36.5**
$\Delta V_{average}$	V	AV	**13.5**	**27.4**	**10**
		SD	1.0	5.5	1.0
sEC	kWh m^{-3}	AV	**9.2**	**17.6**	**6.4**
		SD	0.9	2.1	1.0
sEC_P	kWh kg^{-1} P	AV	**218**	**387**	**134**
		SD	21	46	22
Operational cost	€ kg^{-1} P	AV	**43.7**	**77.4**	**26.8**
		SD	4.1	9.1	4.3

AV, average; SD, standard deviation; CD, current density; $\Delta V_{average}$, average cell potential; sEC, specific energy consumption; sEC_P, specific energy consumption in relation to the P removal from the liquid phase.

Results are also promising if considering the switch of the precipitation system towards continuous-flow operation (results will be discussed onwards). In fact, the highest operational cost will be linked to the achievement of pH 11.5 in the process start-up, whereas the maintenance of a pH set-point once

the system is running in continuous implies switching the power supply on and off, thus decreasing the energy-related expenses. Furthermore, the eventual reduction in costs due to the approximation of the electrodes in the electrochemical cell can facilitate the development of a larger cathode surface within a smaller volume, offering an additional advantage from an engineering perspective.

5.3.2.3 Electrochemical impedance spectroscopy (EIS) tests

In the electrochemical cell-crystalliser integrated system, the precipitation of MPP is intended to occur within the crystalliser, as it facilitates more straightforward sludge recovery. Nevertheless, mineral deposition within the electrochemical cells (i.e., on the cathode surface and the membrane) was observed during the batch precipitation experiments. In fact, precipitation in the cathode surface is promoted by the elevated pH-values in the cathode proximity compared to the bulk liquid. To mitigate the cleaning-related costs and the consequent need to interrupt the treatment process, limiting mineral deposition in the cathodic compartment is critical. To monitor this phenomenon, the internal resistance for the different electrochemical cell configurations tested was measured by EIS before and after conducting the precipitation batch experiments (Figure 5.4). Particularly, the ohmic resistance (R_Ω) measured in the two-electrode EIS tests, represents the resistance offered by the membrane and the resistance of the two solution layers between the electrodes. An increase in the ohmic resistance (ΔR_Ω) was detected for all the systems tested. Since the solution used in the EIS tests was the same (i.e., denitrified effluent), such worsening in the electrochemical cell conditions can disclose mineral deposition on the membrane surface facing the cathodic compartment. The measured ΔR_Ω increase was 991 ± 9, 167 ± 5 and 28 ± 1 Ω m^2 for Cell1, Cell2 and Cell3, respectively. Thus, Cell1, which presented the larger membrane surface (Table 5.1), was prone to an intense precipitation resulting in a dramatic resistance increase if compared to the other two configurations. Three-electrode EIS tests were performed (results are not shown) to determine the contributions of each part of the equivalent circuit to their respective compartments, since it was possible to isolate the cathodic compartment influence on the EIS spectra. On the resulting two-electrode test Nyquist plots, diagonal lines with a slope of about 45° were identified (Figure 5.4). These were modelled using the Warburg impedance (W) in the equivalent circuit which is connected to high resistance in the diffusion layer. Since these lines did not appear in the 3-electrode EIS spectra, they were attributed to the anodic compartment. While R_1 and R_2 were attributed to the cathodic compartment, particularly, to the electrode and a possible not optimized connection which is generating a smaller resistance (R_2). An increase of R_1, which is considered the main cathode-related resistance, was detected in all the configurations, but the highest increase was again observed for Cell1 with a rise of

1.23 Ω m^2 against 0.10 and 0.01 Ω m^2 for Cell2 and Cell3, respectively. Precipitation on the electrode surface was almost inevitable due to the high pH, but depending on the configuration applied, the rise in the resistance was different. Considering the total resistance rise, the configurations with the smallest volume of the cathodic compartment, and particularly Cell3, which was characterized also by the highest $(S/V)_{CATHODE}$ ratio, showed the smallest increase. Based on these results, it was hypothesized that by reducing the cathodic chamber volume it was possible to reduce the time in which the solution is in contact with highest pH value, thus limiting deposition in the electrochemical cell.

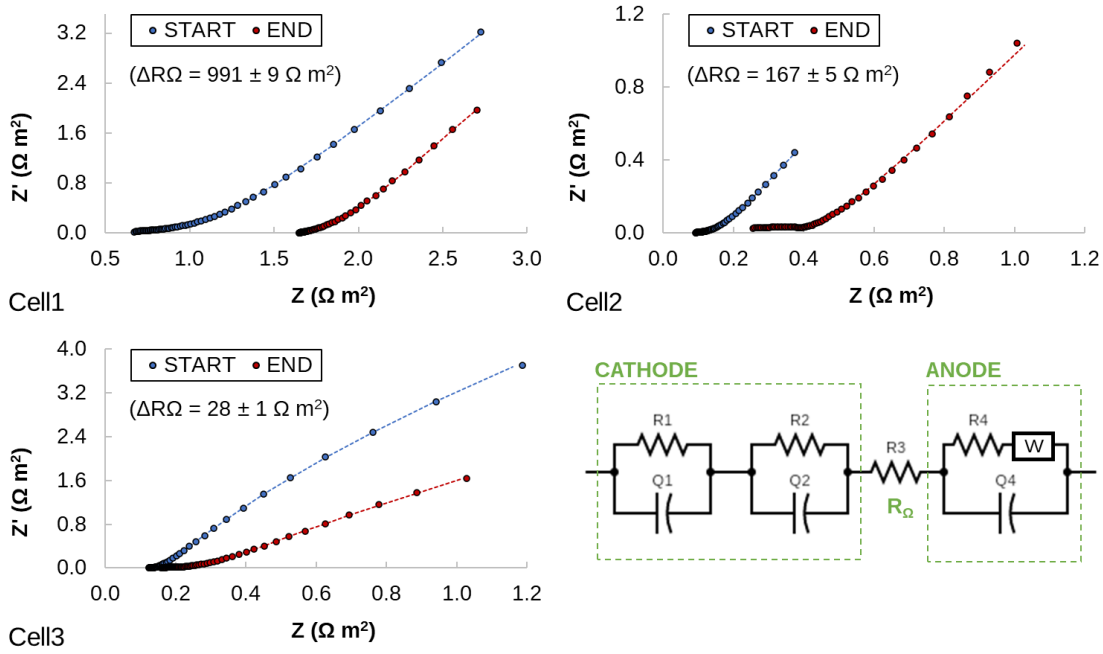

Figure 5.4 – Two-electrode EIS spectra (impedance real, and imaginary, components are Z, and Z', respectively) corresponding to the initial and final conditions in the precipitation batch experiments for Cell 1, Cell2, and Cell3, and the equivalent electric circuit used for fitting the EIS spectra. Dots represent experimental values and dashed lines the fittings achieved. The circuit consists of resistance (R), constant phase element (CPE, Q), and Warburg element (W). The EIS spectra intersection with the x-axis identifies the ohmic resistance (R_Ω).

5.3.2.4 Precipitate formed

Electrochemistry mediated precipitation has proven to be a viable technical alternative for MPP recovery from swine denitrified effluent (Figure S5.2, Table 5.4), thus avoiding the use of chemicals (e.g., NaOH) to raise the pH. Productivities reached were in the range of 0.7-0.8 g/L. Richness above 10% P, 10% K and 10% Mg (on dry weight basis) were achieved regardless the configuration of the electrochemical cell tested. Percentages for K and Mg were increased when compared with those

obtained in similar experiments with chemical precipitation (8). The higher concentration of cations such as K^+ and Mg^{2+} in the catholyte than in the denitrified effluent due to the migration of cations through the membrane of the electrochemical cell (Figure 5.2) could have favoured this fact. This also applies for Na^+ (increasing from 0.1% up to 0.4%) but not for Ca^{2+} (due to the low existing concentrations). Na^+ is a dispersing agent in soil and, when accumulated, it may lead to soil structure deterioration and affect crops production (31). Yet, the Na^+ content in the MPP recovered does not appear as a matter of concern for fertiliser applications. The reported values are slightly different from the theoretical percentages for MPP, confirming the production of a non-pure mineral as a multi-nutrient product.

Table 5.4 – Elemental composition (%) of the precipitates formed in the batch experiments with the electrochemical cell-crystalliser system. Results are given on dry weight basis (at 37ºC).

	This work			Company et al. (8)	
	Electrochemical system			NaOH dosage	Theoretical
Element	**Cell1**	**Cell2**	**Cell3**	**TEST CC5**	MPP
Phosphorus	11.2	11.0	10.5	11.8	11.6
Potassium	12.1	12.0	10.1	7.7	14.7
Magnesium	10.4	10.7	10.7	7.3	9.1
Sodium	0.3	0.2	0.4	0.1	0.0
Calcium	1.3	1.3	2.2	3.0	0.0

5.3.3 Continuous-flow precipitation experiments

According to the results presented above, Cell3 was selected to constitute the electrochemical cell-crystalliser combined system that operated under continuous-flow mode. When precipitating MPP, a high-alkaline catholyte is produced (pH 11.5), thus making it necessary a neutralisation step before its discharge. In this context, the neutralisation of the catholyte by circulating through the anodic compartment appears as an interesting alternative to the dosage of chemicals (e.g., H_2SO_4).

The electrochemical cell-crystalliser system was started up in batch, and when the pH in the crystalliser reached 11.5, the operational mode was switched to continuous-flow (HRT of 8 hours). Fresh denitrified effluent was fed to the crystalliser, and its content was recirculated through the cathodic compartment to keep the high pH value. Part of this catholyte was pumped to the anodic compartment before final discharge to neutralise the pH. The settled sludge was withdrawn from the bottom of the crystalliser. An on/off power supply control based on the pH measured in the crystalliser was used to maintain the pH at a constant value. The combined system ran under these conditions for 3 days.

Since the pH-value was controlled to 11.5 in the crystalliser, the pH in the cathodic compartment was sometimes higher or lower than the targeted value depending on the performance of the power supply. Thus, when the power supply was turned on, the maximum measured value in the outlet of the cathode compartment was pH 13.6. Otherwise, when the power supply was turned off, the minimum pH measured was 10.5. Probably due to the high cathodic pH values, especially in the first 38 hours (1.6 HRT), the cell potential was higher than the one measured during the start up with the same configuration (i.e., 20 V vs 12.5 V), then it dropped into range of 16.6 – 17.6 V (Figure 5.5). Similarly, the pH and the EC of the final effluent widely varied depending on the working conditions of the power supply. When the power supply was turned on, the pH and EC of the effluent remained into the range 5.5-6.5 and 5.0-6.5 mS cm^{-1}, respectively. On the contrary, when the power supply was turned off, the value of these two parameters increased up to 11.5 and 9.7 mS cm^{-1}, respectively, which were indeed the values reached in the crystalliser. Feasibility for neutralising the catholyte before discharge was thus demonstrated, although dependence on the performance of the power supply was also found. This situation could potentially be overcome following two different strategies: equalising the effluent in a buffer tank before discharge and reducing the current intensity applied to the system in order to minimize the on/off alternance of the power supply control to neutralise uninterruptedly the effluent.

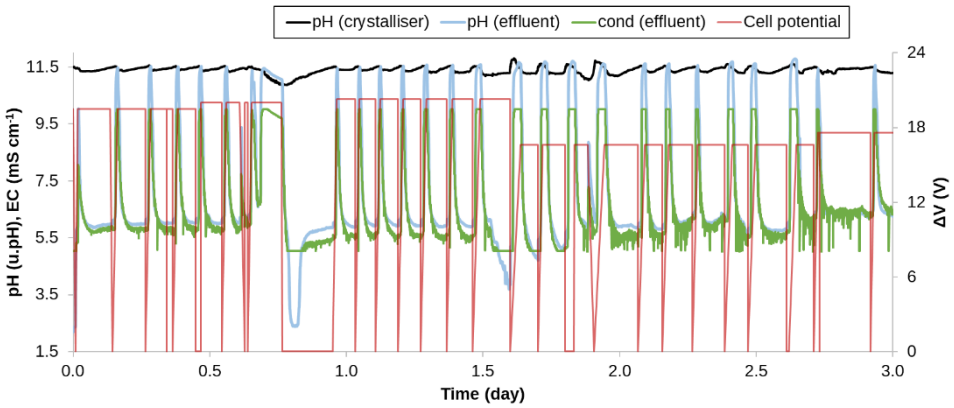

Figure 5.5 – Crystalliser and final effluent pH profile, final effluent conductivity profile, and cell potential (ΔV) profile over time following the power supply on/off (set point pH 11.5 in the crystalliser) during the continuous-flow operation test.

The removal of PO_4^{3-}-P and Mg^{2+} remained quite stable during the continuous-flow operation with an efficiency of 85 ± 3% (8.4 ± 0.3 mmol $(L \cdot d)^{-1}$) and 82 ± 6% (14.2 ± 1.0 mmol $(L \cdot d)^{-1}$), respectively. On the contrary, K^+ removal decreased from 30% (34.42 mmol $(L \cdot d^{-1})$, once the system started operating in continuous-flow mode, to 15% (17.5 mmol $(L \cdot d)^{-1}$) by the end of the test. Such performance would be explained by an intense accumulation of K^+ in the catholyte during the start-

up phase in batch. Similarly, Na^+ showed an increase in the removal efficiency from 21% to 88%. As monovalent cations, K^+ and Na^+ were those ions that migrated the most through the membrane.

The sEC was calculated considering the average potential in the time that the power supply was turned on and the total volume fed to the combined system (13.6 kWh m^{-3}). Equivalently, the sEC_P was estimated as 132.9 kWh kg^{-1} P, corresponding to an operational cost of 26.6 € kg^{-1} P. A similar cost was calculated for the start-up of the system in batch, which only lasted 8 hours (Table 5.3). This result highlighted that the preliminary phase to increase the denitrified effluent pH was very energy intensive as it only lasted 8h but generating a comparable sEC value to the continuous operation with the on/off power supply control lasting 3 days. Thus, reducing the start-up energy consumption represents an opportunity to increase the process energy efficiency. However, even considering the start-up related cost, the total cost of the treatment (49.4 € kg^{-1} P) fitted in the commercial chemical phosphorus precipitation cost (i.e., 18.9 − 61.1 € kg^{-1} P) (34).

Chlorine gas (Cl_2) production was monitored according to its concentration in the effluent of the electrochemical cell. The high chloride levels (Cl^-) in the swine denitrified effluent combined with the use of a Ti-MMO anode opened the door to the recovery of chlorine in the anodic compartment. In fact, the Ti-MMO anode, with its metal coatings serving as catalysts, effectively can facilitate chlorine production (32). An anode of this nature, comprising a titanium base metal plate and one or more metal oxide coatings for electrocatalysis, is conventionally employed in the chlor-alkali industry for the production of chlorine via Re. 3 (33):

$$2Cl^- \rightarrow Cl_2 + 2e^- \qquad \text{(Re. 3)}$$

After running the electrochemical cell-crystalliser combined system for 3 HRT, a stable concentration of 44 ± 3 $mgCl_2$ L^{-1} (22 $mgCl_2$ $(L \cdot d)^{-1}$) was achieved. This result is promising compared to the literature (34,35) and provides an opportunity to enhance the process circularity by introducing the production of value-added chemicals to the recovery of MPP from swine denitrified effluent. Particularly, chlorine holds the potential to be a value-added product due to its disinfecting properties, making it suitable for applications in water treatment or potentially for direct use within the swine farm. Li et al. (13) had already showed the feasibility of simultaneously obtaining chlorine gas and MPP (through the addition of synthetic sources of Mg^{2+} and PO_4^{3-}-P) in a combined cation-exchange membrane electrolysis - MPP crystallisation process for the recycling of concentrates generated from treating landfill leachate.

5.3.3.1 Arrest and resume of the process

To evaluate the possibility of avoiding the need for a start-up in batch mode and to simulate a semi-continuous operation (e.g., considering an operational arrest for cleaning the electrochemical cell) an operation break test was performed. This test consisted in arresting the treatment for 4 days and, subsequently, to resume it again in order to evaluate if this can have an influence on the process performance. During the treatment break, the liquid volume was completely kept inside the electrochemical cell and the crystalliser. Owing to the power supply interruption for 4 days, the pH of the catholyte decreased from 11.5 to 10.7. After restoring the current applied to the system without modifying the control strategy (i.e., 34 A m^{-2} with an on/off control of the power supply at a pH set-point of 11.5 in the crystalliser), it took about 6 hours to reach the targeted pH. Beyond this, the evolution of the pH and EC were no longer influenced by the operation break. Considering P and Mg^{2+} removal from the liquid phase, no evident differences were found. Thus, a stable removal efficiency of 85 ± 3% P (8.4 ± 0.3 mmol $(L \cdot d)^{-1}$) and 81 ± 8% Mg^{2+} (13.8 ± 1.2 mmol $(L \cdot d)^{-1}$) was reached regardless the 4-days stop. The concentration of the monovalent ions in the crystalliser, particularly K^+ and Na^+, presented a slight decrease over time enduring the process interruption (Figure 5.6), being a possible residual effect of the over-accumulation during the start-up phase. Comparing the ions removal efficiencies of the third day of operation (i.e., after 24 HRTs) with those measured after the process break, the obtained values were similar Thus, the KRE was 18 ± 4% before the break while 17 ± 3% after the break, corresponding to 21.1 ± 5.0 mmol $(L \cdot d)^{-1}$ and 19.6 ± 3.0 mmol $(L \cdot d)^{-1}$, respectively. A similar result was found for Na^+, suggesting that the process stabilisation related to monovalent ions removal took longer compared to the other ions. As a conclusion, the treatment could be arrested for a few days and resumed again without the need of a new start-up phase in batch to increase the pH until 11.5 before starting to operate the system in continuous-flow mode.

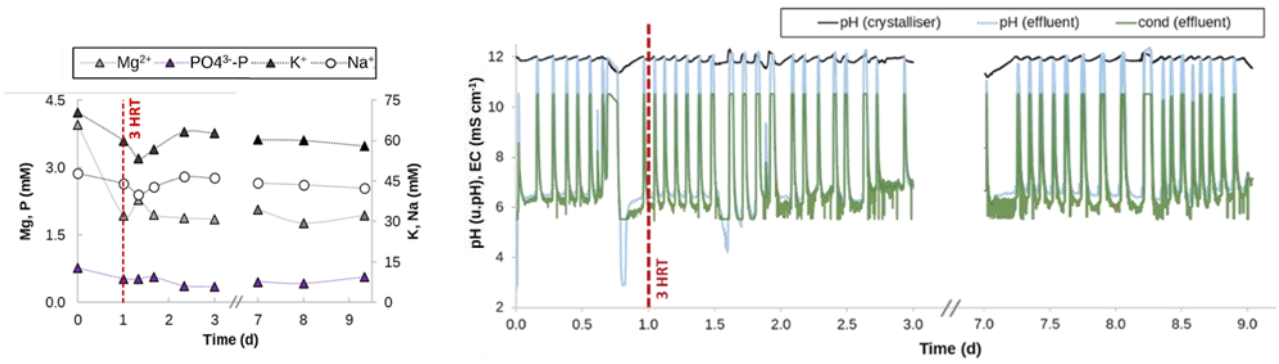

Figure 5.6 – *Left:* Evolution of the concentration of ions in the crystalliser. *Right:* Evolution of the pH and electrical conductivity in the electrochemical cell-crystalliser combined system. The continuous-flow operation was stopped at day 3 (i.e., after 9 HRTs) and resumed at day 7 until day 9.

5.3.3.2 Comparison with previous works

In this work, electrochemically driven precipitation is used to produce MPP with inert electrodes in an electrochemical cell-crystalliser combined system. This approach is different from other electrochemically driven precipitation experiences found in the literature which are mostly focused on electrocoagulation and the use of a sacrificial anode for the release of cations such as Mg^{2+} for the recovery of MPP (36) and MAP (15,37-39) from wastewater using a single-compartment electrochemical reactor. In this regard, the use of a sacrificial electrode requires regular replacement during long-term operation, introducing an additional operational cost to the process. As an example, Shan et al. (36) targeting P recovery as MPP from synthetic urine, using a sacrificial Mg^{2+} anode, and applying 35 A m^{-2} as current density found similar PREs than those obtained in this study (Table 5.5).

Table 5.5 - Comparison of the operating conditions used in this study and main results obtained in previous experiences involving electrochemically driven struvite precipitation (use of CD above 30 A m^{-2}).

Influent	CD (A m^{-2})	P_{inf} (mg L^{-1})	pH_{inf} (-)	pH_{target} (-)	PRE (%)	PRR	sEC_P	Process	Product	Ref.
swine denitrified effluent	37	103	8.0	11.5	83 - 90	8.41 mM d^{-1}	14 kWh m^{-3} 133 kWh kg^{-1} P	EMP	MPP	This work
simulated urine	35	140	8.0	12.0	88.5	n.m.	n.m.	Electr.coag.	MPP	[36]
synthetic source separated urine	160	256	9.0	12.0	90	n.m.	1320 kWh kg^{-1} P	Electr.coag.	MAP/MPP	[37]
synthetic urine	50	200	6.5	11.5	60	6.6 mgP cm^{-2} h^{-1}	3.7 Wh m^{-3}	Electr.coag.	MAP	[38]
urine	55	197	8.9	9.2	-	3.7 mgP cm^{-2} h^{-1}	1700 kWh kg^{-1} P	Electr.coag.	MAP	[39]

n.m.: not measured

5.3.3.3 Economical assessment

Assuming stable conditions under continuous-flow mode operation, treating denitrified effluent with an initial concentration of 1523 mgK L^{-1} (Table 5.2) and achieving 17% KRE, 30.24 t K-struvite y^{-1} is potentially produced. As a resource that has garnered recent attention, MPP market price is undisclosed but the price of struvite (i.e., literature price 100 € t^{-1} struvite (29)) can be considered as reference point for a preliminary economical evaluation. Thus, the economic benefit for the produced MPP would be 3024 € y^{-1} allowing to completely off-set the energy consumption for the power supply operation (228 € L^{-1} considering a stable value of 14 kWh m^{-3}, Table 5.5). Li et al. (10) reported an intense electricity consumption imputable to the electrochemical system configuration, but with a 10-times higher estimated economic benefit for K-struvite recovery (compared when assuming the same market price). However, since P is the limiting ion for MMP precipitation from denitrified effluent,

the K removal can be improved using a P-source as already described by Company et al. (8), allowing an optimistic perspective of improvement in the process performance.

5.4 Conclusions

Chemical-free MPP recovery from a swine denitrified effluent at pH 11.5 was successfully achieved using a crystalliser combined with a two-chambered electrochemical cell equipped with a CEM (total HRT: 8 hours; I: 2.65 A). Three different cell configurations were tested in batch to select the best one according to the ions removal, energy consumption and resistance increase. Next, the combined system was run in continuous-flow mode using the selected electrochemical cell. Finally, an operation break was imposed to assess its influence on the treatment performance. The main conclusions reached are as follows:

- Cell3 was selected as the best configuration since it allowed for ion removal efficiencies of 94 ± 1% for PO_4^{3-}-P (9.3 mmol $(L \cdot d)^{-1}$), 38 ± 1% for Mg^{2+} (6.6 mmol $(L \cdot d)^{-1}$) and 9 ± 4% for K^+ (10.2 mmol $(L \cdot d)^{-1}$) while achieving the lowest sEC_P (134 ± 22 kWh kg^{-1} P) and ΔR_Ω (28 ± 1 Ω m^2). The ion removal efficiency, and the solid productivity, slightly varied among configurations whereas sEC_P and ΔR_Ω were more influenced by the dimensional features.
- The main mineral phase recovered from the denitrified effluent was MPP regardless cell configuration (richness on dry weight was above 10% for P, K, and Mg). Compared to the chemical precipitation process, a higher Na^+ content was achieved due to intense cations migration through the CEM.
- Under continuous-flow operation, the measured ion removal efficiencies were 85 ± 3% for PO_4^{3-}-P (8.4 mmol $(L \cdot d)^{-1}$), 81± 8% for Mg^{2+} (13.9 mmol $(L \cdot d)^{-1}$) and 16 ± 2% for K^+ (19.9 mmol $(L \cdot d)^{-1}$). Through the power supply on/off control, the targeted pH (11.5) was successfully maintained in the crystalliser. The sEC_P was quantified as 122.9 kWh kg^{-1} P. Process arresting for a few days and starting up again was not a problem.
- Catholyte neutralisation in the anodic compartment was proven as feasible, leading to a decline in the pH-value down to 6.05 ± 0.71 when current was applied. Promising levels of chlorine (44 $mgCl_2$ L^{-1}) were measured in the outlet, which opens the door to combining MPP recovery with production of value-added chemicals such as free chlorine.
- Future work should explore the influence of operational parameters (e.g., HRT and CD) on the continuous-flow process performance with the aim of optimizing the energy consumption and MPP recovery. Since P is the limiting ion for MPP precipitation, the addition of different sources of P could be tested to increase Mg^{2+} and K^+ removal from the denitrified effluent.

Chlorine recovery should be investigated and implemented to increase the circularity of the treatment. These efforts have the potential to boost the practical implementation of this method as a sustainable wastewater treatment approach for the retrieval of value-added products.

References

1. Cordell D, White S. *Life's bottleneck: sustaining the world's phosphorus for a food secure future.* Annu Rev Environ Resour. 2014, 39: 161-188. https://doi.org/10.1146/annurev-environ-010213-113300.

2. Ciceri D, Manning DAC, Allanore A. *Historical and technical developments of potassium resources.* Sci Total Environ. 2015, 502: 590-601. https://doi.org/10.1016/j.scitotenv.2014.09.013.

3. Jena SK. *A review on potash recovery from different rock and mineral sources.* Mining Metall Explor. 2021, 38: 47–68. https://doi.org/10.1007/s42461-020-00286-7.

4. Perera MK, Englehardt JD, Dvorak AC. *Technologies for recovering nutrients from wastewater: a critical review*. Environ Eng Sci 2019, 36:511–529. https://doi.org/10.1089/ees.2018.0436.

5. Kabdaşlı I, Siciliano A, Limonti C, Tünay O. *Is K-struvite precipitation a plausible nutrient recovery method from potassium-containing wastes?-a review.* Sustainability 2022, 14: 11680. https://doi.org/10.3390/su141811680.

6. Yesigat A, Worku A, Mekonnen A, Bae W, Feyisa GL, Gatew S, Han J-L, Liu W, Wang A, Guardie A. *Phosphorus recovery as K-struvite from a waste stream: A review of influencing factors, advantages, disadvantages and challenges.* Environ Res. 2022, 214(P3): 114086. https://doi.org/10.1016/j.envres.2022.114086.

7. Shih K, Yan H. The crystallization of struvite and its analog (K-struvite) from waste streams for nutrient recycling. In: Prasad MNV, Shih K, (Eds.). *Environmental Materials and Waste: Resource Recovery and Pollution Prevention.* Academic Press, Amsterdam, The Netherlands, pp. 665–686, 2016. https://doi.org/10.1016/B978-0-12-803837-6.00026-3.

8. Company E, Farrés M, Colprim J, Magrí A. *Exploring the recovery of potassium-rich struvite after a nitrification-denitrification process in pig slurry treatment.* Sci Total Environ. 2022, 847: 157574. https://doi.org/10.1016/j.scitotenv.2022.157574.

9. Huang H, Zhang D, Wang W, Li B, Zhao N, Li J. *Alleviating Na^+ effect on phosphate and potassium recovery from synthetic urine by K-struvite crystallisation using different magnesium sources.* Sci Total Environ. 2019, 655: 211–219. https://doi.org/10.1016/j.scitotenv.2018.11.259.

10. Xu K, Li J, Zheng M, Zhang C, Xie T, Wang C. *The precipitation of magnesium potassium phosphate hexahydrate for P and K recovery from synthetic urine.* Water Res. 2015, 80: 71–79. http://dx.doi.org/10.1016/j.watres.2015.05.026.

11. Wang Y, Kuntke P, Saakes M, van der Weijden RD, Buisman CJN, Lei Y. *Electrochemically mediated precipitation of phosphate minerals for phosphorus removal and recovery: Progress and perspective.* Water Res. 2022, 209: 117891. https://doi.org/10.1016/j.watres.2021.117891.

12. Sciarria PT, Vacca G, Tambone F, Trombino L, Adani F. *Nutrient recovery and energy production from digestate using microbial electrochemical technologies (METs).* J Clean Prod. 2019, 208: 1022–1029. https://doi.org/10.1016/j.jclepro.2018.10.152.

13. Li X, Zhu W, Wu Y, Wang C, Zheng J, Xu K. *Recovery of potassium from landfill leachate concentrates using a combination of cation-exchange membrane electrolysis and magnesium potassium phosphate crystallisation.* Sep Purif Technol. 2015, 144: 1–7. http://dx.doi.org/10.1016/j.seppur.2015.01.035.

14. Li X, Zhao X, Zhou X, Yang B. *Phosphate recovery from aqueous solution via struvite crystallisation based on electrochemical-decomposition of nature magnesite.* J Clean Prod. 2021, 292: 126039. https://doi.org/10.1016/j.jclepro.2021.126039.

15. Bagastyo AY, Anggrainy AD, Khoiruddin K, Ursada R, Warmadewanthi IDAA, Wenten IG. *Electrochemically-driven struvite recovery: Prospect and challenges for the application of magnesium sacrificial anode.* Sep Purif Technol. 2022, 288: 120653. https://doi.org/10.1016/j.seppur.2022.120653.

16. Pintado T, Delgado-Pando G. *Towards more sustainable meat products: Extenders as a way of reducing meat content.* Foods 2020, 9: 1044. https://doi.org/10.3390/foods9081044.

17. Cândido D, Bolsan AC, Hollas CE, Venturin B, Tápparo DC, Bonassa G, Antes FG, Steinmetz RLR, Bortoli M, Kunz A. *Integration of swine manure anaerobic digestion and digestate nutrients removal/recovery under a circular economy concept.* J Environ Manage. 2022, 301: 113825. https://doi.org/10.1016/j.jenvman.2021.113825.

18. Schuiling RD, Andrade A. *Recovery of struvite from calf manure*. Environ Technol. 1999, 20: 765–768. https://doi.org/10.1080/09593332008616872.

19. Tarragó E, Ruscalleda M, Colprim J, Balaguer MD, Puig S. *Towards a methodology for recovering K-struvite from manure.* J Chem Technol Biotechnol 2018, 93: 1558–1562. https://doi.org/10.1002/jctb.5518.

20. Clauwaert P, De Paepe J, Jiang F, Alonso-Fariñas B, Vaiopoulou E, Verliefde A, Rabaey K. *Electrochemical tap water softening: A zero chemical input approach.* Water Res. 2020;169. https://doi.org/10.1016/j.watres.2019.115263.

21. Hasson D, Sidorenko G, Semiat R. *Calcium carbonate hardness removal by a novel electrochemical seeds system.* Desalination. 2010, 263: 285–289. http://dx.doi.org/10.1016/j.desal.2010.06.036.

22. De Paepe J, Clauwaert P, Gritti MC, Ganigué R, Sas B, Vlaeminck SE, Rabaey K. *Electrochemical in situ pH control enables chemical-free full urine nitrification with concomitant nitrate extraction.* Environmental Science Technology. 2021, 55: 8287–8298. https://doi.org/10.1021/acs.est.1c00041.

23. Díaz Nieto CH, Palacios NA, Verbeeck K, Prévoteau A, Rabaey K, Flexer V. *Membrane electrolysis for the removal of Mg^{2+} and Ca^{2+} from lithium rich brines.* Water Res. 2019, 154: 117–124. https://doi.org/10.1016/j.watres.2019.01.050.

24. Tarragó E, Puig S, Ruscalleda M, Balaguer MD, Colprim J. *Controlling struvite particles' size using the up-flow velocity.* Chem Eng J. 2016, 302: 819–827. https://doi.org/10.1016/j.cej.2016.06.036.

25. Romans-Casas M, Feliu-Paradeda L, Tedesco M, Hamelers HVM, Bañeras L, Balaguer MD, Puig S, Dessì P. *Selective butyric acid production from CO_2 and its upgrade to butanol in microbial electrosynthesis cells.* Environ Sci Ecotechnol. 2024, 17: 100303. https://doi.org/10.1016/j.ese.2023.100303.

26. Timmerman LR, Raghavan S, Borole AP. *Advancing microbial electrolysis technology via impedance spectroscopy and multi-variate analysis.* Front Energy Res. 2022, 10: 756900. https://doi.org/10.3389/fenrg.2022.756900.

27. APHA, AWWA, WEF. *Standard Methods for the Examination of Water and Wastewater.* American Public Health Association, American Water Works Association, Water Environment Federation. Washington DC (USA), 2017.

28. Vannecke TPW, Lampens DRA, Ekama GA, Volcke EIP. *Evaluation of the 5 and 8 pH point titration methods for monitoring anaerobic digesters treating solid waste.* Environ Technol. 2015, 36: 861-869. https://doi.org/10.1080/09593330.2014.964334.

29. Muys M, Phukan R, Brader G, Samad A, Moretti M, Haiden B. *A systematic comparison of commercially produced struvite: Quantities, qualities and soil-maize phosphorus availability.* Sci Total Environ. 2021, 756: 143726. https://doi.org/10.1016/j.scitotenv.2020.143726.

30. Lei Y, Remmers JC, Saakes M, Van Der Weijden RD, Buisman CJN. *Influence of cell configuration and long-term operation on electrochemical phosphorus recovery from domestic wastewater.* ACS Sustain Chem Eng. 2019, 7: 7362–7368. https://doi.org/10.1021/acssuschemeng.9b00563.

31. Ferretti G, Di Giuseppe D, Faccini B, Coltorti M. *Mitigation of sodium risk in a sandy agricultural soil by the use of natural zeolites.* Environ Monit Assess. 2018, 190: 646. https://doi.org/10.1007/s10661-018-7027-2.

32. Batlle-Vilanova P, Rovira-Alsina L, Puig S, Balaguer MD, Icaran P, Monsalvo VM, Rogalla F, Colprim J. *Biogas upgrading, CO_2 valorisation and economic revaluation of bioelectrochemical systems through anodic chlorine production in the framework of wastewater treatment plants.* Sci Total Environ. 2019, 690: 352–360. https://doi.org/10.1016/j.scitotenv.2019.06.361.

33. Dong H, Yu W, Hoffmann MR. *Mixed metal oxide electrodes and the chlorine evolution reaction.* J Phys Chem C. 2021, 125: 20745–20761. https://doi.org/10.1021/acs.jpcc.1c05671.

34. Puggioni G, Milia S, Dessì E, Unali V, Pous N, Balaguer MD, Puig S, Carucci A. *Combining electro-bioremediation of nitrate in saline groundwater with concomitant chlorine production.* Water Res. 2021, 206: 117736. https://doi.org/10.1016/j.watres.2021.117736.

35. Varigala S, Krishnaswamy S, Lohia CP, Hegarty-Craver M, Grego S, Luettgen M, Cid CA. *Optimal design of an electrochemical reactor for blackwater treatment.* Water Environ Res. 2021; 93: 148–158. https://doi.org/10.1002/wer.1374.

36. Shan J, Liu H, Long S, Zhang H, Lichtfouse E. *Electrochemical crystallisation for recovery of phosphorus and potassium from urine as K-struvite with a sacrificial magnesium anode.* Environ Chem Lett. 2022, 20: 27–33. https://doi.org/10.1007/s10311-021-01333-5.

37. Govindan K, Im SJ, Muthuraj V, Jang A. *Electrochemical recovery of H_2 and nutrients (N, P) from synthetic source separate urine water.* Chemosphere. 2021, 269: 129361. https://doi.org/10.1016/j.chemosphere.2020.129361.

38. Tan X, Yu R, Yang G, Wei F, Long L, Shen F. *Phosphate recovery and simultaneous nitrogen removal from urine by electrochemically induced struvite precipitation.* Environ Sci Pollut Res. 2021, 28: 5625–5636. https://doi.org/10.1007/s11356-020-10924-8.

39. Hug A, Udert KM. *Struvite precipitation from urine with electrochemical magnesium dosage.* Water Res. 2013, 47: 289–299. http://dx.doi.org/10.1016/j.watres.2012.09.036.

Supporting Information - Chapter 5

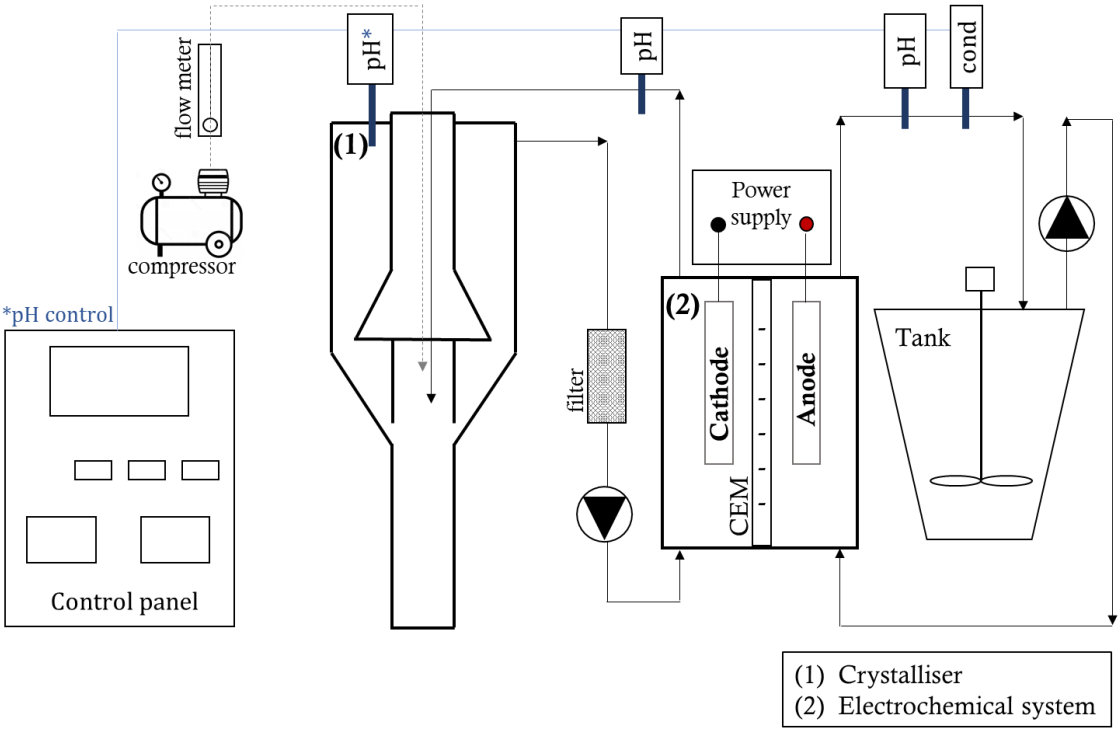

(A)

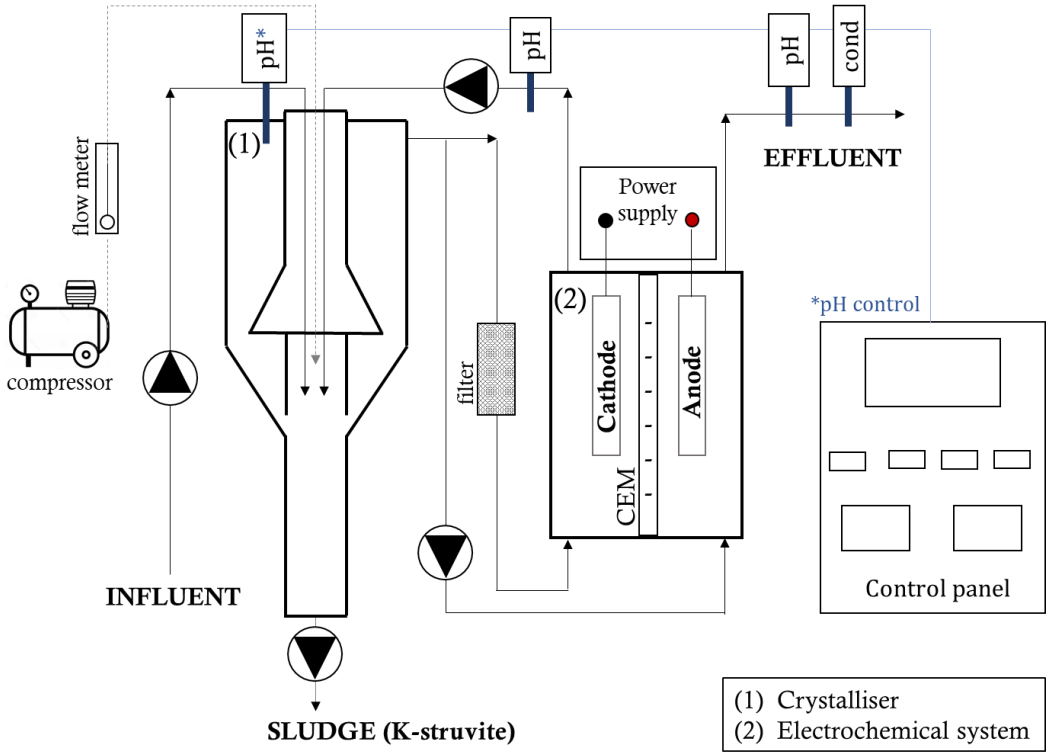

(B)

Figure S5.1 − Set-up of the combined system including the electrochemical cell and the crystalliser. Configuration in batch (A) and in continuous-flow mode (B).

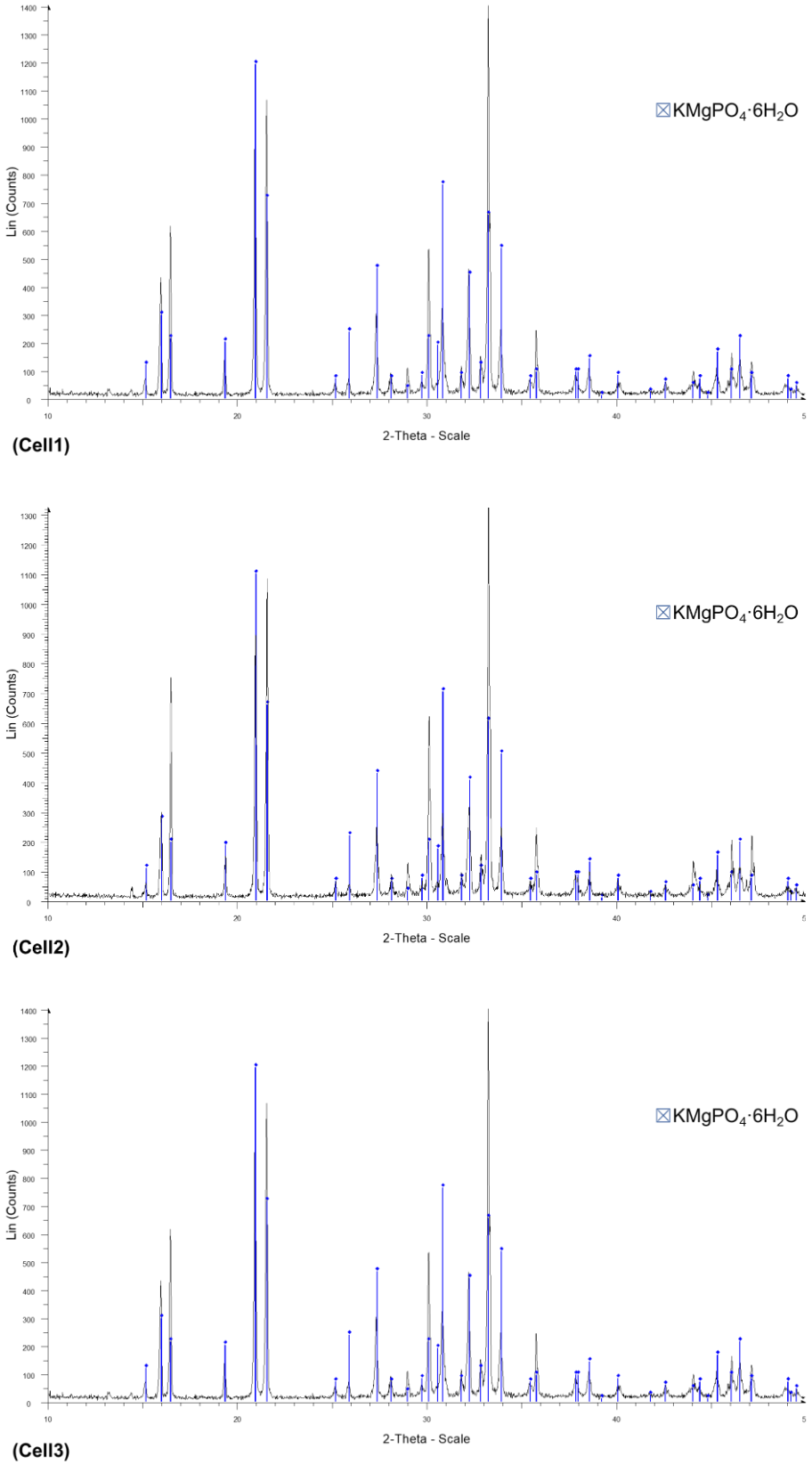

Figure S5.2 – XRD pattern for the solids collected from the crystalliser by the end of the precipitation batch experiments (pH 11.5) in Cell1, Cell2, and Cell3. Samples from the crystalliser were filtered, and the retained solids were dried at room temperature, and ground, before analysis.

CHAPTER 6: Implications and outlook

The present research aimed to enhance the base of knowledge concerning the applicability of different innovative technologies (i.e., Partial Nitritation/Anammox (PN/A), electrochemical induced precipitation (EMP)) to the treatment of nutrient-rich agro-industrial wastewater (Figure 6.1). This objective was pursued using a dedicated biological reactor (PN/A process) and different configurations of electrochemical systems (EMP process) fed with agro-industrial waste anaerobic digestion supernatant and swine denitrified effluent, respectively. The processes' performances were monitored, and multiple operating conditions were tested to achieve nutrient removal and recovery through a single or combined technique.

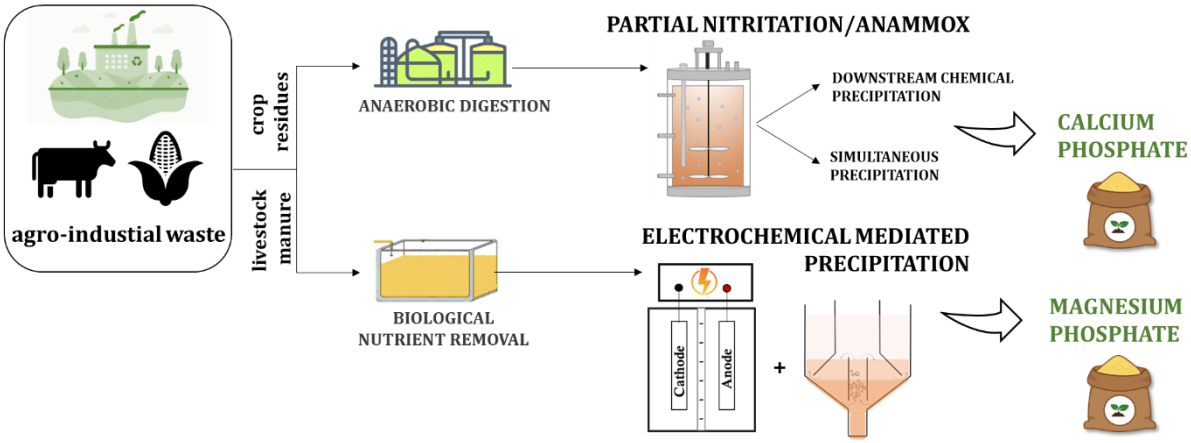

Fig.6.1 – Summary scheme of the general objectives of the present Ph.D. thesis.

6.1 This thesis's implications

Phosphorus (P) and potassium (K) are essential macronutrients for food production typically abundant in agro-industrial wastewater. These residues are receiving growing attention in nutrient recovery applications as sustainable alternatives to ore mining. PN/A process is a cost-effective process to remove ammonium-nitrogen (NH_4^+-N) from wastewater which can be combined with downstream chemical P precipitation or with concomitant P removal through biomineralisation. EMP process is a sustainable emerging alternative to chemical precipitation allowing a reagent-free P precipitation through hydroxyl production due to current application. These technologies' application allowed to precipitate calcium phosphate, magnesium phosphate and struvite-type minerals which can be used directly as slow-release fertilisers or can be used for fertiliser production.

Considering the results discussed in previous chapters, PN/A and EMP processes were proven to be sustainable and cost-effective alternatives for the treatment of nutrient-rich agro-industrial wastewater allowing P-minerals recovery (i.e., calcium phosphate, magnesium phosphate) with limited or zero-chemical inputs. The following considerations may be drawn:

- Ca/P ratio and the high Mg^{2+} levels in the influent of PN/A process treating anaerobic digestion supernatant likely affected calcium phosphate downstream (Chapter 2) and concomitant (Chapter 3) precipitation. Low solid crystallinity and effluent Ca/P ratio suggested that the main produced mineral was amorphous calcium phosphate rather than hydroxyapatite. Increased Ca^{2+} level is critical for boosting precipitation, thus Ca-rich agro-waste input in the anaerobic digestion step could allow avoiding external calcium sources which can potentially increase environmental pollution. Further studies are needed to improve the process selectivity and P recovery performance.
- Mineral-from-biomass separation is a key driver for the hydroxyapatite (HAP)-PN/A process scale-up and to evaluate the actual P recovery potential. This work explored sonication effect on biomass activity to evaluate a non-damaging method for recovering active biomass while disaggregating the granule structure (Chapter 3). Exposition time was proved to play a role in limiting the loss of anammox activity (i.e., 15 min corresponded to ca. 15% activity reduction), but the influence of different operating parameters should be studied to select optimal conditions. Particularly, sonication must be explored on formed HAP-granules to evaluate the release efficiency of inorganic solids and re-inoculated biomass long-term activity in the bioreactor.
- EMP process applicability for magnesium phosphate recovery from denitrified swine effluent is hindered by Ca^{2+} presence and unpreventable precipitation into the electrochemical system due to high local pH (≥11.5) in the cathode proximity (Chapter 4). Intense precipitation of carbonate compounds on the membrane surface could be prevented by introducing a pre-treatment targeting Ca^{2+} removal. Influencing P deposition into the electrochemical system, optimal configuration is a critical factor in limiting the increase of ohmic resistance with the consequent increase of energy consumption in long-term operation (Chapter 5). Lower cathodic volume can improve the electrochemical performances of the process allowing to reduce the time in which the bulk liquid is subjected to the high pH reached in the cathodic compartment.
- Catholyte neutralisation in the anode was achieved allowing to completely avoid the use of chemicals to adjust the pH (Chapter 4). Moreover, chlorine production in the anode was detected reaching promising levels (48 $mgCl_2\ L^{-1}$) in the outlook of implementing the recovery

of this value-added by-product (Chapter 5). K-struvite precipitation was successfully achieved through the combination of a 14.6L crystalliser with a double-chamber electrochemical system. These results can pave the way for further process optimisation aiming to process scale-up.

The findings of this work emphasize the importance of carefully selecting an appropriate approach for nutrient removal and recovery. The selection process should begin with an overall analysis of the wastewater characteristics, identifying possible products and by-products that can be recovered, while also considering the compounds that need to be eliminated for environmental protection purposes and treatment stability. Based on this information, it is likely that a combination of different processes will be necessary to achieve sustainable operation and recover valuable minerals and by-products.

6.2 Outlook (Future perspectives)

Despite the recent growing interest in implementing a nutrient recovery approach rather than removal in the emerging techniques applied to wastewater treatment, many aspects should be further explored. Future research directions in this area can have different perspectives.

Concerning fundamental comprehension, the interactions between constituent and competing ions and each compound's effect on the precipitation of the targeted mineral should be investigated in the different processes.

In the specific case of anammox-based technologies for calcium phosphate biomineralisation, it is crucial to consider the potential impact of competing cations such as Mg^{2+}, K^{+}, and Na^{+} on the mineral-biomass structure formation. This would help to boost the quality of the recovered product and thus its market value. For instance, the characteristics of the granular sludge might be affected by the affinity of the cations with other compounds such as extracellular polymeric substances and proteins (1). Besides, it would be important to investigate what kind of effect each cation may have on the activity of the already-formed mineralised sludge to ensure long-term process stability.

In the electrochemical method for struvite precipitation, exploring the influence of the competing cations (e.g., Ca^{2+}) on the internal resistance increase (e.g., due to membrane scaling), and consequently on the power consumption evolution, would contribute to effectively limiting energy costs which might hinder the process competitiveness. Moreover, improved operative conditions and system design balancing P precipitation with by-products' simultaneous generation (e.g., H_2, Cl_2) should be explored as they can consistently contribute to cost reduction (2).

From an engineering perspective, scaling up of PN/A and EMP technologies for nutrient recovery should be the clear objective in the upcoming years. With this aim, different operative factors need to be improved.

Hydroxyapatite (HAP) core in the PN/A sludge was proven to enhance the granules' properties, but there is a lack of experience with a non-damaging mineral recovery strategy to preserve active biomass from being wasted. Mineral-from-biomass separation is a key driver for the PN/A-HAP process to unveil the actual P recovery potential of the process and the resulting economic benefit. In this, testing recovered active biomass re-inoculation in the bioreactor in the long-term would be critical for the separation method selection. Besides, since PN/A process is limited by the presence of organic matter and due to nitrate production, exploring simultaneous denitrification for complete nitrogen and organic compounds removal would boost and widen the applicability of this process. Chen et al. (3) proposed a double-step process combining PN/A-HAP and Partial Denitrification (PD)/A-HAP to treat anaerobic digestion supernatant. However, achieving the combined process in a single reactor should be pursued to decrease the treatment costs in the future.

In EMP process the reproducibility of lab-scale results in pilot-scale plant located in the farm is a critical factor for the successful electrochemical system operation. The main limitation of long-term operation would be the precipitation inside the cathodic compartment, which can hinder the process stability. Due to the high pH in the cathode proximity, salts precipitation seems unpreventable. Thus, implementing a programmable and automatised cleaning strategy is a key driver for the future application of this process. To ease the mineral recovery some authors suggested polarity inversion to detach the solids from the cathode, as successfully tested by Takabe et al. (4). When electrodes polarity is reversed, the chemical reactions at the electrodes are reversed accordingly. The main advantage of this method is that the same equipment is needed, thus extra devices for cleaning purpose are not needed. Although, the prolonged exposure to this periodical shock may damage the electrodes depending on the materials.

PN/A and EMP processes have proven feasible for nutrient recovery with many advantages such as cost-effectiveness, higher sustainability and great flexibility compared to conventional techniques. Still some challenges are needed to face to improve the recovery efficiency and the long-term process stability, but an integrated approach will assist the technology progress. As an increasing interest in sustainability and resource conservation is rapidly raising, it is believed that in the coming years, significant advancements in coupling nutrient recovery technology will be experienced. Further operative factors improvement and higher recovery performance are likely to be achieved gradually, making these technologies an increasingly attractive choice for sustainable water treatment.

References

1. Magrí A, Company E, Gich F, Colprim J. *Hydroxyapatite Formation in a Single-Stage Anammox-Based Batch Treatment System: Reactor Performance, Phosphorus Recovery, and Microbial Community*. ACS Sustain Chem Eng. 2021; 9 (7): 2745–61. https://dx.doi.org/10.1021/acssuschemeng.0c08036.

2. Ren Y, Zheng W, Duan X, Goswami N, Liu Y. *Recent advances in electrochemical removal and recovery of phosphorus from water: A review.* Environ Funct Mater. 2022; 1 (1): 10–20. https://doi.org/10.1016/j.efmat.2022.04.003.

3. Chen Y, Guo G, Li YY. *A review on upgrading of the anammox-based nitrogen removal processes: Performance, stability, and control strategies.* Bioresour Technol. 2022; 364: 127992. https://doi.org/10.1016/j.biortech.2022.127992.

4. Takabe Y, Ota N, Fujiyama M, Okayasu Y, Yamasaki Y, Minamiyama M. *Utilisation of polarity inversion for phosphorus recovery in electrochemical precipitation with anaerobic digestion effluent.* Sci Total Environ. 2020; 706: 136090. https://doi.org/10.1016/j.scitotenv.2019.136090.

UNIONE EUROPEA
Fondo sociale europeo

REGIONE AUTÒNOMA DE SARDIGNA
REGIONE AUTONOMA DELLA SARDEGNA

ACKNOLEDGEMENTS

Emma Dessì expresses her sincere gratitude to her supervisors, Professor Carucci, Dr. Milia, and Dr. Magrí, for generously sharing their profound knowledge and experience. She appreciates their valuable advice and unwavering support during both the experimental activities and the writing phases of this thesis. Special recognition is extended to Professor Puig, Dr. Pous and Dr. P. Dessì for their comprehensive assistance in exploring electrochemical system technologies. The author acknowledges the analytical work conducted by technicians and researchers of the environmental engineering laboratory at DICAAR (Department of Environmental Civil Engineering and Architecture, University of Cagliari (Unica)) and at the LEQUIA (Laboratory of Chemical and Environmental Engineering, University of Girona (UdG)). Chapters 4 and 5 of this thesis are based on the work carried out at UdG-LEQUIA within the framework of the project ESPOTFER (REF: 56.30127.2021.5C), funded within the program of Demonstrative Activities 2021 by the Government of Catalonia–Department of Climate Action, Food and Rural Agenda. The collaborative effort with PhD student Emma Company (UdG) is duly recognized (Chapters 4 and 5), with equal contributions acknowledged, and genuine gratitude expressed for her understanding and supportive attitude.

Furthermore, sincere appreciation is extended to the entire group of Professors at Unica, to the welcoming LEQUIA family, and especially to all the PhD students and research fellows whose friendship deeply enriched the whole academic experience. Finally, the author wishes to express personal gratitude to her family, fiancé, and friends for sharing their enduring and invaluable support over the past years.

Emma Dessì also acknowledges the Italian Ministry of Education for the financial support provided through her PhD scholarship (Post lauream MIUR scholarship, D.M. n. 40 25/1/2018) and the Erasmus+ mobility program for funding her traineeships (PLACEDOC, A.Y. 2021-2022) at UdG-LEQUIA.

LIST OF PUBLICATIONS

Conference Proceedings

Dessì E., Milia S., Cara S., Carucci A., 2023. *Concomitant phosphorus and nitrogen removal from agro-industrial wastewater through Partial Nitritation/Anammox process.* 18th International Conference on Environmental Science and Technology (CEST2023). Athens, Greece, 30 August to 2 September 2023.

Dessì E., Company E., Milia S., Carucci A., Magrí A., Colprim J., 2023. *Reagent-free phosphorus recovery from a swine denitrified effluent in an electrochemical batch system.* 6th European Meeting of the International Society for Microbial Electrochemistry and Technology (EU-ISMET). Wagenigen, the Netherlands, September 6–8, 2023